Technical Letter Report

TLR-RES/DE/REB-2025-03

Reexamination of NUREG-1829 Loss-of-Coolant Accident (LOCA) Frequency Estimates

Date:

February 2025

Prepared in response to Research Assistance Request NRR-2024-008, by:

C. J. Sallaberry
Engineering Mechanics Corporation of Columbus

F. W. Brust
Engineering Mechanics Corporation of Columbus

E. Kurth-Twombly
Engineering Mechanics Corporation of Columbus

Robert E. Kurth
Engineering Mechanics Corporation of Columbus

Bengt Lydell
SIGMA-PHASE, Inc.
Vero Beach, FL

NRC Project Managers and Contributors:

Matthew Homiack
Materials Engineer
Reactor Engineering Branch

Christopher Nellis
Reactor Engineer
Reactor Engineering Branch

Division of Engineering
Office of Nuclear Regulatory Research
U.S. Nuclear Regulatory Commission
Washington, DC 20555–0001

EXECUTIVE SUMMARY

The NRC issued NUREG-1829, "Estimating Loss-of-Coolant Accident (LOCA) Frequencies Through the Elicitation Process," in April 2008 (ML082250436). The report provides LOCA frequency estimates based on an expert elicitation process for boiling water reactor (BWR) and pressurized water reactor (PWR) piping and non-piping passive systems as a function of effective break size and plant operating years. These LOCA frequency estimates reflect, in part, operating experience (OpE), probabilistic fracture mechanic (PFM) technology, and the state of knowledge in 2004. To determine the applicability of the Transition Break Size (TBS) in support of a proposal to allow increased enrichment of fuel in LWR plants, the NRC is reevaluating the NUREG-1829 LOCA frequencies while considering advances in PFM methodologies and learned OpE in time period after 2004.

As a first task, the more risk-significant base cases from NUREG-1829 were reexamined with updated PFM tools, data, and expertise. The base cases were BWR-1 (12- and 28-inch piping in the BWR recirculation system), PWR-1 (30-inch piping in the PWR hot leg), and PWR-2 (10-inch piping in the PWR pressurizer surge line) consistent with the definitions in NUREG-1829 Table 3.7. The BWR base cases are subject to intergranular stress corrosion cracking (IGSCC), and the PWR base cases are subject to primary water stress corrosion cracking (PWSCC).

The Extremely Low Probability of Rupture (xLPR), Version 2.3 PFM code was used to reanalyze the base cases. It was specifically developed to model the effects of PWSCC and, therefore, well-suited to reanalyze the PWR base cases. For the BWR-1 base cases, IGSCC was modeled using the assumption of an initial crack at the beginning of plant operation and used a generic stress corrosion cracking model with parameters adapted to match the IGSCC growth rate published in the 2023 Edition of the American Society of Mechanical Engineers Boiler and Pressure Code, Division 1, Section XI, Subsubarticle Y2310. To compare with the NUREG-1829 results, LOCA Categories 1 through 6 probabilities were generated considering the effects of leak detection and then converted into annual frequencies.

The PWR analyses were within the range of the NUREG-1829 base case results. The PWR-1 analysis was performed with both a generically representative welding residual stress (WRS) profile and a conservative WRS profile based on the hot leg pipe-to-reactor-pressure-vessel nozzle weld at Virgil C. Summer Nuclear Station, Unit 1, which developed a leak due to PWSCC in 2000. Neither WRS profile resulted in any category of LOCA. As a result, a 95 percent upper confidence bound was estimated for the annual LOCA frequencies. For both WRS profiles, the xLPR results were within the range of the NUREG-1829 base case results at 25 and 60 years of operation. For the PWR-2 analysis, a few realizations resulted in a LOCA with leak detection. The first was a small-break LOCA occurring around 35 years, and around 75 years there were medium- and large-break LOCAs. Nevertheless, the resulting annual frequencies were consistent with the NUREG-1829 base case results at 25 years of operation and generally less than the NUREG-1829 base case results at 60 years of operation.

The BWR analyses were also within the range of the NUREG-1829 base case results. The BWR-1 base case estimates in NUREG-1829 do not differentiate between the LOCA frequencies for the 12-inch and 28-inch piping in most cases. However, the xLPR code generated different LOCA frequency estimates for the two piping sizes due to their different loads and WRS profiles. In the 28-inch BWR-1 analysis, a few realizations resulted in small-break LOCAs with leak detection. Similarly, the 12-inch BWR-1 analysis had a few realizations with all LOCA categories. Nevertheless, the annual frequency estimates remained within or below the range of estimates from NUREG-1829. A few sensitivity studies were performed for the BWR analyses to evaluate the effects of different WRS profiles and water chemistries. The results were equivalent or lower than the initial analysis results.

The updated LOCA frequency results based on the xLPR simulations reflect the state of knowledge and PFM modeling capabilities in 2024 and are consistent with the NUREG-1829 base case results.

As a second task, the NUREG-1829 LOCA base cases were reevaluated and more generic LOCA frequency estimates were determined based on an analysis of OpE from 2005 through mid-2024 for the larger diameter (i.e., > 6”) piping systems. The database developed under the Nuclear Energy Agency’s Component Operational Experience, Degradation and Ageing Programme provided the source for the OpE data. The analysis consisted of four major steps:

(1) review applicable OpE
(2) calculate piping precursor failure frequencies
(3) calculate conditional probabilities of LOCA
(4) calculate LOCA frequencies

In the first step, domestic OpE applicable to the more risk-significant base cases from NUREG-1829 and studied in the xLPR PFM analysis was reviewed. Domestic OpE was also more generally reviewed for primary system piping branch connections greater than 6 inches in diameter (i.e., piping able to produce at least a Category 4 LOCA). The reviews covered the two distinct time periods (i.e., from before 1970 through approximately 2004 and from 2005 to mid-2024) and assessed differences and underlying factors of influence.

The results of the first step of the analysis were in the form of precursor failure frequencies per weld and reactor operating year for the period 1970 to 2004. In the second step, these piping precursor failure frequencies were updated using a Bayesian analysis approach using the post-2004 domestic OpE.

In the third step, the BWR and PWR conditional probability uncertainty distributions were developed from NUREG-1829 by first obtaining a geometric mean of the expert elicitation participant system-level results. This value represented a target LOCA frequency. Next, the geometric mean of the precursor failure frequency results of the respective system-level analyses were fit to lognormal distributions. Finally, the median conditional probability of LOCA was obtained by dividing the median target LOCA frequency by the median precursor rate. The resulting conditional probability of LOCA represents uncertainty in the 2004 state of knowledge when the NUREG-1829 expert elicitation was completed.

Lastly, in the fourth step, the uncertainty distributions developed in Steps 2 and 3 were convolved in a converged Monte Carlo uncertainty propagation to obtain the respective LOCA frequency uncertainty distributions.

The updated LOCA frequency results reflect the state of knowledge in 2024 and, relative to the NUREG-1829 results, indicate at least an order of magnitude reduction for LOCA Categories 4, 5, and 6. The significant reduction reflects the effectiveness of various material degradation mitigation processes that have been implemented for BWRs and PWRs, such as stress improvement processes, water chemistry changes, increased inspections, and more degradation resistant materials. The analysis methods included consideration of uncertainties in the state of knowledge regarding factors of improvement in reliability and integrity management and OpE.

In all evaluated base cases, LOCA frequencies calculated for the PFM analysis and the OpE evaluation had similar results to each other with variances that largely results from differences in assumptions. Both analytical approaches estimated LOCA frequencies at or below the estimates made in 2004 in NUEREG-1829. This outcome suggests the new understandings in probabilistic fracture mechanics or new OpE in the past 20 years has not identified a basis that increases the LOCA frequencies from the original NUREG-1829 estimates.

ACKNOWLEDGEMENTS

This study was performed in partnership with the NRC's Office of Nuclear Regulatory Research (RES) and the Office of Nuclear Reactor Regulation (NRR). The authors would like to thank Joey Messina and Ashley Smith of NRR Division of Safety Systems for sponsoring the work. The authors would like to thank Robert Tregoning, David Rudland, and Seung Min of the NRC for their valuable comments and insights in both the planning and production of this work. The authors benefited from their expertise and knowledge.

CONTENTS

LIST OF TABLES

LIST OF FIGURES

ACRONYMS

BWR	boiling water reactor
CDF	cumulative distribution function
CE	Combustion Engineering
CFP	conditional failure probability
CFR	*Code of Federal Regulations*
COD	crack opening displacement
DEGB	double end guillotine break
DMW	dissimilar metal weld
EFPY	effective full-power years
EPRI	Electric Power Research Institute
GDC	general design criterion
gpm	gallons per minute
HAZ	heat affected zone
ID	inner diameter
IGSCC	intergranular stress corrosion cracking
ISI	in-service inspection
LBB	leak-before-break
LCB	95% lower confidence bound
LD	leak detection
LHS	Latin hypercube sampling
LOCA	loss-of-coolant accident
lpm	liters per minute
Mid	mid-point (Median) in a distribution
NRC	Nuclear Regulatory Commission
OD	outer diameter
OpE	operating experience
PFM	probabilistic fracture mechanics
PWR	pressurized water reactor
PWSCC	primary water stress corrosion cracking
TLF	target LOCA frequency
UCB	95% upper confidence bound
VCIO	VC Summer weld with the assumption of Inner-to-Outer welding
WRS	welding residual stress
xLPR	Extremely Low Probability of Rupture

1 INTRODUCTION

1.1 Background

In response to the Staff Requirements Memorandum to SECY-02-0057, the U.S. NRC developed 10 CFR 50.46a, a proposed voluntary alternative to the emergency core cooling system requirements in 10 CFR 50.46. This proposed rule would have divided the current spectrum of Loss-of-Coolant Accident (LOCA) break sizes into two regions. The division between the two regions was to have been delineated by the transition break size (TBS). The first region included small breaks, up to and including the TBS, that were subject to all the requirements associated with 10 CFR 50.46. The second region included breaks larger than the TBS, up to and including the double-ended guillotine break (DEGB) of the largest reactor coolant system pipe.

A best estimate treatment of hypothetical breaks within this second region was allowed by relaxing certain conservative assumptions within 10 CFR 50.46. The TBS was based, in part, on LOCA frequencies developed in NUREG-1829. NUREG-1829 used expert elicitation to merge insights from operating experience (OpE) and PFM codes. The NUREG-1829 approach developed well-defined hypothetical base case scenarios and used these to anchor the expert opinion which was convolved to determine LOCA frequency distributions as a function of break size.

The originally proposed 10 CFR 50.46a rule was not finalized and the NRC decided not to pursue this rulemaking in 2016. However, this rulemaking concept was renewed in 2024 to facilitate, in part, use of increased enrichment fuels and allow higher fuel burnup. NUREG-1829 was published in 2008 and both PFM and OpE knowledge have evolved significantly since then. This current effort was initiated to evaluate the continued applicability of NUREG-1829 to determine if the proposed TBS concept remains viable.

1.2 Objectives of this Study

The goal of the present study is to reexamine the results in NUREG-1829 with updated tools, data, and expertise.

The review is decomposed in the following actions:

- Rerun selected bases cases from NUREG-1829 with updated data and PFM code: this section reassesses the inputs used for the PWR-1, PWR-2, and BWR-1 (split into two cases: BWR-1a and BWR-1b) cases, and then runs the xLPR code with those inputs.
- Reassess the OpE analysis for the bases cases PWR-1, PWR-2 (split into two cases: PWR-2a and PWR-2b), and BWR-1 (split into two cases: BWR-1a and BWR-1b) by incorporating the past 20 years (i.e., 2004 to 2024) of plant operating history.
- Reassess piping LOCA frequency estimates for systems greater than 6” in diameter and convolve these results into plant-level LOCA frequency estimates for comparison with the author’s NUREG-1829 elicitation results.
- Update selective non-piping LOCA frequency estimates.

- Compare results obtained with PFM and OpE for the base cases reanalyzed by both of the two approaches.

2 PROBABILISTIC FRACTURE MECHANICS

2.1 Approach

2.1.1 Welds Considered in the Analysis

For the elicitation work performed in NUREG-1829 [1], a set of base cases were developed to be assessed by panel members with clearly defined conditions and assumptions to improve the accuracy of each member's assessment and to better quantify and compare their results. The resulting base cases are listed in Table 3.7 of [1]. Four of the base cases were selected to be run using xLPR. The conditions analyzed in this report are summarized in Table 1.

Table 1: Welds Considered for the xLPR Rerun

Case #	Weld location	Plant type	Degradation mechanisms
PWR-1	Reactor Vessel Outlet Nozzle	PWR	PWSCC
PWR-2	Surge Line	PWR	PWSCC
BWR-1a	Recirculation (28 inches OD[1])	BWR	IGSCC
BWR-1b	Recirculation (12.75 inches OD)	BWR	IGSCC

The criterion for selecting which base cases to analyze was the type of degradation mechanism. The base cases involving stress corrosion cracking were screened in and the ones involving fatigue were screened out. Three observations supported this decision:

- Prior xLPR analyses [2, 3] have demonstrated the lower impact of fatigue mechanisms.
- The PFM code used in the analysis of the base cases for NUREG-1829 also shows a lower annual frequency of adverse events when only fatigue is considered (see for instance Figure 4.1 of [1]).
- The development of a generic set of fatigue transients that would be representative of the fleet is complex and would require several additional assumptions.
- Flow accelerated corrosion is not a mechanism which is associated with piping systems that are larger than the proposed transition break size.

[1] Outer Diameter

2.1.2 Procedure to Run the Cases

The latest version of xLPR available (xLPR v2.3) was used to perform the runs. This version of xLPR was run using GoldSim 14. The xLPR code is described in NUREG-2247, “Extremely Low Probability of Rupture Version 2 Probabilistic Fracture Mechanics Code,” issued in August 2021 (ML082250436). It was specifically developed to model the effects of PWSCC and, therefore, well-suited to reanalyze the PWR base cases.

The inputs for PWR base cases mostly came from the “xLPR Group Report—Inputs Group, Version 1.0,” issued December 19, 2017 (ML19337B876) and the “xLPR Models Subgroup Report—Welding Residual Stresses, Version 1.0,” issued October 5, 2016 (ML16341B049). The material properties and some other inputs for the BWR base cases also largely came from the xLPR inputs group report, except for the crack growth rate model parameters. For the BWR-1 base cases, IGSCC was modeled using the assumption of an initial crack at the beginning of plant operation, and a generic stress corrosion cracking model available in the xLPR code was used with parameters adapted to match the IGSCC growth rate published in the 2023 Edition of the American Society of Mechanical Engineers Boiler and Pressure Code, Division 1, Section XI, Subsubarticle Y2310. The normal operating loads were selected to match the corresponding values from the NUREG-1829 PFM analyses, and the welding residual stress (WRS) profiles were created using finite element analysis with the geometries and welding parameters published in Electric Power Research Institute Technical Report NP-1743, “Effect of Weld Parameters on Residual Stresses in BWR Piping Systems,” issued March 1, 1981. Details of the inputs for xLPR base case runs are detailed in Section 7.1 and development of WRS profiles for the BWR base case are further detailed in Section 7.2.

2.1.3 Sample Size Selection

For the PWR-1 and PWR-2 cases, the new crack initiation optimization module added to version 2.3 of xLPR was used, reducing the computational time required (from 10 hours down to 30 minutes). For BWR-1a and BWR-1b, the initial flaw model (i.e. crack occurring at time zero on the area of the weld with largest tensile stress) was used.

The minimum number of xLPR realizations is based on the estimated sample size needed to capture two estimates, for which the smallest value can be used. The first estimate comes from the often used theoretical 10^{-6} /yr annual frequency limit (which requires a sample of 100,000 to have a 10^{-6} accuracy in 10 years). The second estimate comes from the original estimates for the Category 1 LOCA probabilities that were reported in Table 4.1 of NUREG-1829 (Piping Base Case Frequency Results by Participant). The column DH (Dave Harris) is considered as most of the input and comparison is performed against these specific PFM analyses performed in NUREG-1829:

2.1.3.1 PWR sample size selection

In Table 4.1 of NUREG-1829, the PWR-1 annual frequency values for column DH are 3.2×10^{-8}, 3.8×10^{-11}, and 1.1×10^{-12} for Categories 1,2, and 3 of LOCAs both at 25 years and 60 years. For the Category 1 LOCA, this is equivalent to a sample of size 1.25 million at 25 years and 520,000 at 60 years.

For PWR-2, the column DH annual frequency values are 4.8×10^{-7}, 2.2×10^{-9}, and 1.5×10^{-10} for Categories 1,2, and 3 of LOCAs at 25 years, and 1.4×10^{-5}, 9.6×10^{-8}, and 1.4×10^{-8} for Categories 1,2, and 3 of LOCAs at 60 years. For the Category 1 LOCA, this is equivalent to a sample size of 84,000 at 25 years and 1200 at 60 years.

Crack initiation optimization allows for the reduction in the number of *realizations* for the xLPR model to achieve results equivalent to a given sample size. The crack initiation optimization allows for having one or more initiation(s) during the simulation time for each realization and associates a corresponding weight for this realization, to reflect the amount of samples with zero initiations that would be needed in order to create one with initiation.

It is a method that calculates the likelihood of having at least one crack during the simulation time for each realization. It samples one potential outcome within the range of those possibilities and estimates the corresponding weight. In essence, it counts the number of realizations without cracks and only runs the ones with cracks then corrects the probabilities accordingly with a weight associated with each realization.

$\bar{I}(T_{max})$ represents the probability of initiation at the end of the simulation time (T_{max}).

$\frac{1}{\bar{I}(T_{max})}$ represents the sample size required to have at least one realization with initiation occurring over the simulation time. For example, if $\bar{I}(T_{max}) = 10^{-2}$, it is expected that a crack initiation will occur every $\frac{1}{10^{-2}} = 100$ realizations. Since each realization has an initiation occurring when using the crack initiation optimization, the equivalent sample size n_{eq} to obtain this many realizations with an initiation would be $n_{eq} \cong \frac{n}{\bar{I}(T_{max})}$.

For instance, if the probability of having a crack initiated over an 80 year period is equal to 3×10^{-3}, it means that only 3 realizations out of 1,000 would have crack initiation. The 997 remaining would return a result of 0 for all outputs relative to cracks. Thus, to have an equivalent 300 realizations with a crack occurring (i.e. a sample of size 300 when crack initiation optimization is used), the total equivalent sample size n_{eq} would be around 100,000.

Due to the use of crack initiation optimization, the sample size n (realizations with an initiated crack) selected for both PWR-1 and PWR-2 was 5,000 as an initial benchmark since the probability of initiation is not known beforehand. Additional runs of 5000 would be performed if greater accuracy was found to be needed after the initial run. However, results for PWR-1 and PWR-2 in Section 2.3.1 and 2.3.2 respectively showed these additional runs were not needed. More information on the crack optimization module can be found in the xLPR documentation [4].

2.1.3.2 BWR sample size selection

Only one set of data was reported in the DH column (Table 4.1 of NUREG-1829) for the BWR-1 base case, which represents rupture in the 12” pipe lines since these have a high rupture probability: the annual frequency values are 9.2×10^{-3}, 6.8×10^{-3}, and 4.8×10^{-3} for Categories 1,2, and 3 of LOCAs at 25 years, and 5.7×10^{-4}, 5.0×10^{-4}, and 5.0×10^{-4} for Categories 1,2, and 3 of LOCAs at 60 years. Thus, for BWR-1a and b, the probabilities recorded in Table 4.1 of NUREG-1829 indicate that even a low sample size (in the 100’s) would be sufficient to capture the same level of accuracy than what was recorded in NUREG-1829.

For BWR-1a and BWR-1b, it was expected to have some LOCA occurrences with leak rate detection given the NUREG-1829 results. The sample size was kept at 5,000 to be consistent with PWR-1 and PWR-2. The crack initiation optimization was not used in this case and an initial flaw was considered at time zero. The reason behind not using crack initiation (with or without optimization) was that the initiation model was based on PWSCC and not IGSCC and that input parameters to fit an IGSCC initiation model were not readily available as it was the case for the IGSCC growth. This assumption is considered conservative.

2.1.4 Quantities of Interest

2.1.4.1 Outputs saved in xLPR

To estimate the quantities of interest for this study, the following outputs were saved from the xLPR simulations:

- Initiation indicator (I) time history for each realization (set to 0 before crack initiation occurs and to either 1 or a weighted value after crack initiation). This is a unitless parameter. The weighted value represents the likelihood of having a crack occurring during the simulation time for this particular realization.
- Rupture indicator (R) time history for each realization (set to 0 before rupture occurs and to either 1 or a weighted value after crack initiation). This is a unitless parameter.
- Total leak rate (L) time history for each realization expressed in cubic meters per second (m^3/s).
- Probability of non-repair (N) time history for each realization. This is a unitless parameter.
- Crack opening area (C) time history for each realization expressed in square millimeters (mm^2).

2.1.4.2 Quantity of interest and estimation procedure

The quantity of interest is the annual LOCA frequencies, as defined in Section 2 of NUREG-1829 [1].

Six LOCA categories are defined in Table 3.2 of NUREG-1829 [1] by increasing flow rate. Those are listed in Table 2. The LOCAs are cumulative, meaning that a larger LOCA will also be considered as a lower category LOCA. Similarly, a rupture is considered as a LOCA.

Table 2: LOCA Category Definitions

LOCA Category	Name	Flow Rate Threshold (gpm)	Classification Acronym
1	Small Break LOCA	> 100	SB-LOCA
2	Medium Break LOCA	$> 1{,}500$	MB-LOCA
3	Large Break LOCA	$> 5{,}000$	LB-LOCA
4	Large Break LOCA Type a	$> 25{,}000$	LBa-LOCA
5	Large Break LOCA Type b	$> 100{,}000$	LBb-LOCA
6	Large Break LOCA Type c	$> 500{,}000$	LBc-LOCA

In addition, the impacts of leak detection (LD) and ISI were considered.

The probability of a given size LOCA can be estimated from the selected saved outputs listed in Section 2.1.4.1. The only additional information needed is the Leak Rate value at which a LOCA is reached (e.g., $L_{SBLOCA} = 100$ gpm) as well as the Leak Rate Detection Limit (L_{th}).

The following approach was used to estimate the quantities of interest at each time step, using SBLOCA as an example (some additional potential outputs of interest are also described for completeness). The equations for MBLOCA and LBLOCA are conceptually similar:

- Probability of crack initiation: $\bar{I} = \sum_{i=1}^{n} I_i$
- Probability of rupture: $\bar{R} = \sum_{i=1}^{n} R_i$
- Probability of 1st leak:
  - $Leak_i = if\ (L_i > 0)\ then\ I_i, else\ 0$
  - Then $\overline{Leak} == \sum_{i=1}^{n} Leak_i$
- Probability of SBLOCA:
  - $SBLOCA_i = if\ (L_i \geq L_{SBLOCA}\ or\ R_i > 0)\ then\ I_i, else\ 0$
  - Then $\overline{SBLOCA} = \sum_{i=1}^{n} SBLOCA_i$

- Time of Leak detection (LD)[2]: $t_{LRD,i} = \min(t_k | L_i > L_{th})$

- Time of SBLOCA: $t_{SBLOCA,i} = \min(t_k | L_i > L_{SBLOCA})$

- Time between LD and SBLOCA: $t_{lapse,i} = t_{SBLOCA,i} - t_{LRD,i}$

- Probability of SBLOCA with LD:
  - $If\ (t_{lapse,i} > 0\ then\ LRDSBLOCA_i = 0)$ (Cases detected before LOCA)
  - $Else\ LRDSBLOCA_i = I_i\ for\ t_k \geq t_{SBLOCA,i}$
  - Then $\overline{LRDSBLOCA} = \sum_{i=1}^{n} LRDSBLOCA_i$

- Probability of SBLOCA with ISI:
  - $ISISBLOCA_i = SBLOCA_i \times N_i(t_{SBLOCA,i})$
    - Probability of non-repair = N_i
  - Then $\overline{ISISBLOCA} = \sum_{i=1}^{n} ISISBLOCA_i$

- Probability of SBLOCA with LD and ISI:
  - $LRDISISBLOCA_i = LRDSBLOCA_i \times N_i(t_{SBLOCA,i})$
  - Then $\overline{LRDISISBLOCA} = \sum_{i=1}^{n} LRDISISBLOCA_i$

Where i represents the realization number and n the sample size.

For cases with initial flaw or direct initiation (BWR-1a and BWR-1b), the results are conditional on having an existing crack at time zero, and the sample size is used directly to determine probabilities.

For cases using crack initiation optimization (PWR-1 and PWR-2), an equivalent sample size (n_{eq}) was used as shown in Section 2.1.3.1. The crack initiation optimization allows for having one or more initiation(s) during the simulation time for each realization and associates a corresponding weight for this realization, to reflect the number of realizations with zero initiations that would be needed in order to create one with initiation.

Results in NUREG-1829 [1] are presented as annual frequencies. The probability of having at least one event of annual frequency λ over Y years can be approximated with $p = 1 - e^{-\lambda Y}$

An inversion can be used to express annual frequency λ as a function of probability and the equation is:

---

[2] The nomenclature $\min(t_k | L_i > L_{th})$ is the minimum time in the realization when the leak rate is greater than the threshold value. Similar nomenclature has an analogous interpretation.

$$\lambda = -\frac{\ln(1-p)}{Y} \qquad \text{Eq. (1)}$$

For low values of probability p, $\ln(1-p) \cong -p$ and the equation can be simplified as

$$\lambda \cong \frac{p}{Y}. \qquad \text{Eq. (2)}$$

For p values lower than 10^{-2}, the error in estimation is less than 1% of the estimated value (so less than 10^{-4} difference).

In the types of problems considered using xLPR so far, none of the realizations have seen leak rates equal or larger than 25,000 gpm. Rupture occurs long before such a leak rate is reached. As a result, the last 3 LOCAs (i.e., Categories 4, 5, and 6) are simply represented with the rupture output.

2.1.4.3 Post-Processing of the data

Post-processing was used instead of directly developing the outputs of interest within xLPR. The reason was the 2GB memory limitation when running the xLPR code. As a result, it was necessary to reduce the amount of data generated by the code so that more realizations could be performed. The data saved by the xLPR code was reduced to only the five outputs listed in Section 2.1.4.1 from which the quantities of interest could be calculated using the methods described above. The post-processing of the data was performed using a Python script. An independently developed Fortran code was written to validate the results from the Python script.

2.1.4.4 Estimate when no event occurs.

Usually, the inclusion of LD produces no LOCA in any of the realizations. Following the method presented in [5] , an upper bound is used for the LOCA considered, set to $\frac{3}{n}$, which represents the 95% confidence interval upper bound. The derivation of the upper bound can be found in [6]. For PWR-1 and PWR-2, the equivalent sample size n_{eq} is used in lieu of n to estimate the upper bound.

2.2 Analysis Assumptions

2.2.1 xLPR software

The PFM calculations were performed with the xLPR software. The xLPR code introduces assumptions and biases in the development of software modules for crack initiation, growth. etc. The developers of xLPR (NRC and EPRI) released a technical report to assess the impact of assumptions made in the development of these software modules [7]. The conclusions of the treatment of uncertainties and the potential biases in [7] are as follows:

1. All of the modules contained within xLPR V2 are best estimate or slightly conservatively biased. It is believed that the problem scope is conservatively characterized such that failure probabilities (e.g., leak or rupture) will tend to be over-predicted. The bias in outcomes predicted by xLPR V2 due to how the problem was defined cannot be readily quantified at this time due to a lack of alternative models.
2. The uncertainties in module development are accounted for by using the sampling strategy implemented within the Framework. In many cases, the user has the option of influencing input variable and model parameter distributions for the purposes of conducting sensitivity studies to better understand the implications of model calibration efforts.
3. Validation testing demonstrates that the PWSCC initiation, growth, and other models did well in predicting a high probability of occurrence for flaws or very small leaks when conditions representing plants in which flaws, or very small leaks, have been observed in both U.S. and international PWR plants were modeled.

This demonstrates that the modeling of Cases PWR-1 and PWR-2 using the xLPR code is acceptable.

2.2.2 Leak Rate model for the BWR Base Cases

The LEAPOR software is used to estimate leak rate from a through-wall crack in xLPR. The input parameters are set for a PWR environment, which is not appropriate when applied to a BWR. Since no parameterization has been performed for the LEAPOR input parameters, the model was still used as is.

However, in order to confirm that this approach did not introduce too strong a bias, Section 3.7 and Table 3.8 of NUREF-1829 [1] were used to estimate an equivalent crack opening area for each of the LOCA categories considered. From Table 3.8, the BWR Liquid column was used to correlate the flow rate flux with the effective break size as the recirculation line contains no steam at the beginning of a hypothetical break. The effective break size in Table 3.8 was translated into mm, then the area was estimated assuming a circular break area, following the same approach in Section 3.7 of [1].

The resulting threshold crack opening areas were 127 mm^2 for SBLOCA, 2,565 mm^2 for MBLOCA, and 9,152 mm^2 for LBLOCA.

Figure 1 (resp. Figure 2) shows the comparison between the small-break and large-break LOCA probabilities when a leak rate threshold or a crack opening area (COA) threshold is used for BWR-1a (resp. BWR-1b). Medium break LOCA comparison gave similar results but were on top of the large-break LOCA results, so they have been not depicted for clarity.

The LOCA probabilities are similar whether they are based on leak rate or COA. The slightly higher value of the SBLOCA probability estimated using COA is considered within the range of acceptability, as the results are plotted in a linear scale. As such, it was considered acceptable to use the LOCA estimates as a function of leak rate for BWR-1a and BWR-1b cases.

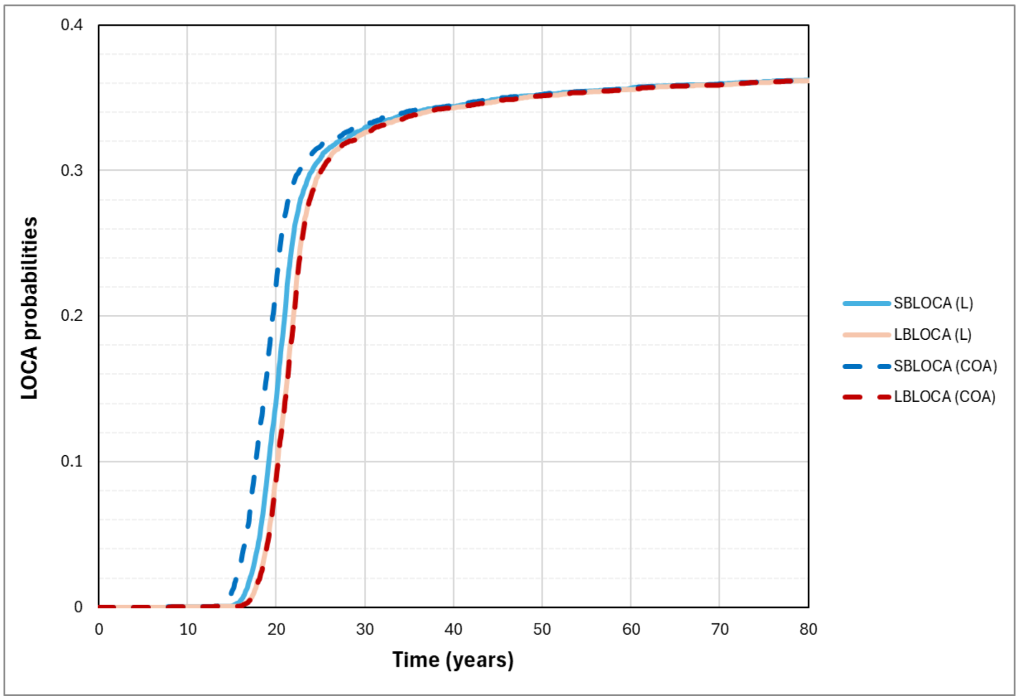

Figure 1: Comparison of LOCA probabilities when based on Leak Rate and COA for BWR-1a

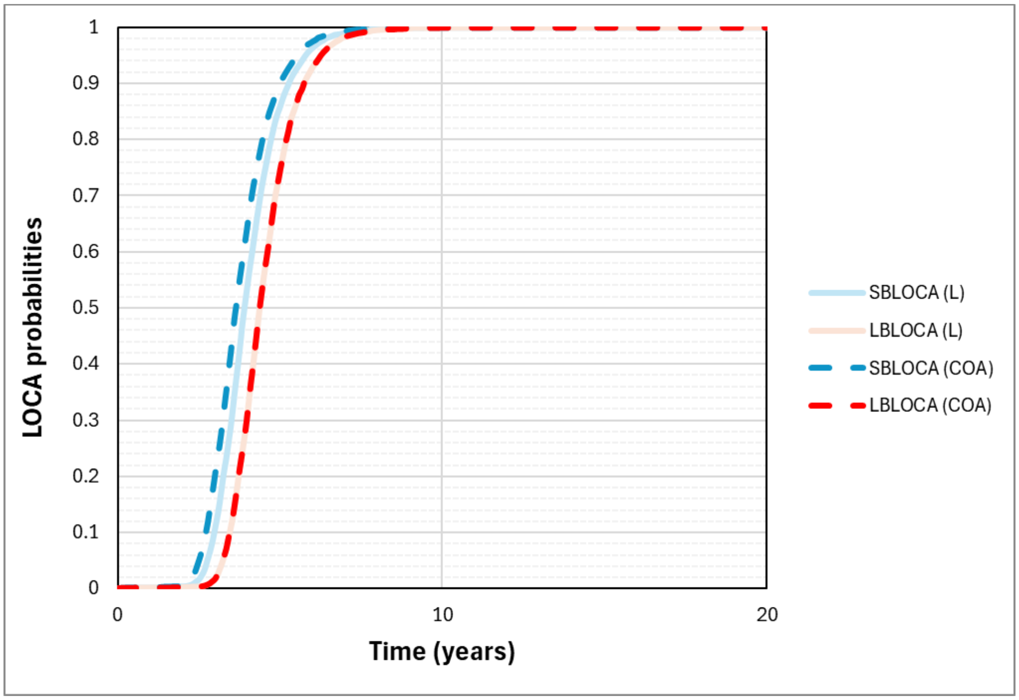

Figure 2: Comparison of LOCA probabilities when based on Leak Rate and COA for BWR-1b

2.2.3 Weld Residual Stresses

WRS is one of the most influential physical parameters in the considered analysis due to its impact on crack initiation and crack growth. Both the WRS profile and the uncertainty range play an important role.

For PWR-1, the selected WRS profile is the one derived from the V.C. Summer (VCS) reactor vessel outlet nozzle (RVON) weld that experienced leakage [8]. This profile is considered conservative due to higher mean value at the ID and low value at mid-thickness increasing the chances to create long thin cracks. The conservative aspect was confirmed by a sensitivity study in Section 2.4.1 using a generic RVON WRS profile.

The generic WRS profile for the surge line presented in [9] was considered representative for PWR-2, following the analyzes performed in [3].

New WRS profiles were generated for BWR-1a and BWR-1b. The location of the crack (in the weld or in the heat affected zone (HAZ)) as well as the weld condition (unrepaired or repaired) can have a significant influence on the results. Consequently, 4 WRS profiles were generated for BWR-1a and 4 WRS profiles for BWR-1b (as documented in Section 7.2) with the unrepaired-weld-centered WRS used as the generic case and the three other WRS profiles used as sensitivity cases in Sections 2.4.2 and 2.4.3 respectively for BWR-1a and BWR-1b.

2.2.4 Other assumptions

A 100 percent plant capacity factor (e.g., 80 effective full-power years) was assumed. This assumption is conservative because, due to outages, plants cannot practically achieve such a capacity.

The leak rate detection capability was assumed to be 3.78 lpm (1 gpm) for PWR-1 and PWR-2, and 18.93 lpm (5 gpm) for BWR-1a and BWR-1b. Plant leakage detection systems can reliably detect lower leak rates and much more quickly than the 1-month time step used in the xLPR code simulation.

The loads for PWR-1 and PWR-2 were equivalent to the ones considered in [2] and [3], respectively. Those loads were selected to be conservative.

The loads for BWR-1a and BWR-1b were taken from the DH base case inputs in NUREG-1829 [1]. They were compared to plant specific BWR loads [10], and confirmed to be higher.

Normal water chemistry was used to select the IGSCC parameters. This was considered conservative as it led to faster crack growth. A sensitivity case was run using hydrogen water chemistry on BWR-1b (section 2.4.4) to measure the impact of this assumption.

It is important to underline that the conservatism consideration in this study is toward higher initiation frequency and faster crack growth rate, which often translates to higher LOCA probabilities and frequencies without mitigation. This does not necessarily scale to LOCA probabilities and frequencies with leak rate detection: a slower growth (especially in the depth direction) may create long thin surface cracks that lead to rupture or large LOCAs occurrences undetected by LD.

2.3 <u>Results</u>

2.3.1 Case PWR-1: PWR RVON

None of the 5,000 realizations led to a LOCA of any category when leak rate detection is considered for the PWR-1 base case. Thus, the rule of 3 (presented in Section 2.1.4.4) was used to estimate a 95% confidence upper bound, with the use of the equivalent sample size.

The probability of initiation over 80 years of operation, when using the V.C. Summer RVON inside-outside (VCIO) axial WRS profile is estimated to be 1.747×10^{-2}. As a result, the equivalent sample size is equal to $n_{eq} \cong \frac{5{,}000}{1.747 \times 10^{-2}} \cong 286{,}164$.

As a result, the 95% upper bound probability of any LOCA over time is estimated around 1.04×10^{-5}, and the annual frequency after y years can be approximated by $\frac{1.04 \times 10^{-5}}{y}$.

Figure 3 shows a comparison of the 95% upper bound generated from the xLPR results with the range of data reported in NUREG-1829 Table 4.1 for the RVON base case at 25 years and 60 years. The xLPR results are on the upper bound at 25 years and logarithmically in the middle at 60 years. These results are within the expected range, especially considering the following:

- at 25 years, only one of the NUREG-1829 estimates is around 10^{-11} (the three others are in the 10^{-8} to 10^{-7} range).
- The VC Summer IO (VCIO) WRS was used for the reference case. It is quite conservative, especially when coupled with a 50 MPa standard deviation. The conservatism comes from the unique WRS profile starting with a high value at the ID (leading to higher probability of crack initiation) and a low value around 30% (slowing down the crack growth in the depth direction, leading to long thin crack). Coupled with the large standard deviation, it increases the chances to create a realization with a crack that will slowly growth through the depth in the compressive WRS region until a surface crack rupture or an early through-wall crack rupture occurs (thus not captured by leak rate detection).
- The upper bound estimate is conservative and there is a high probability that increasing the sample size would not lead to any additional realizations of even an SBLOCA with LD, which would reduce the annual frequency upper bound estimate. This is illustrated in one of the sensitivity study cases (Section 2.4.1).

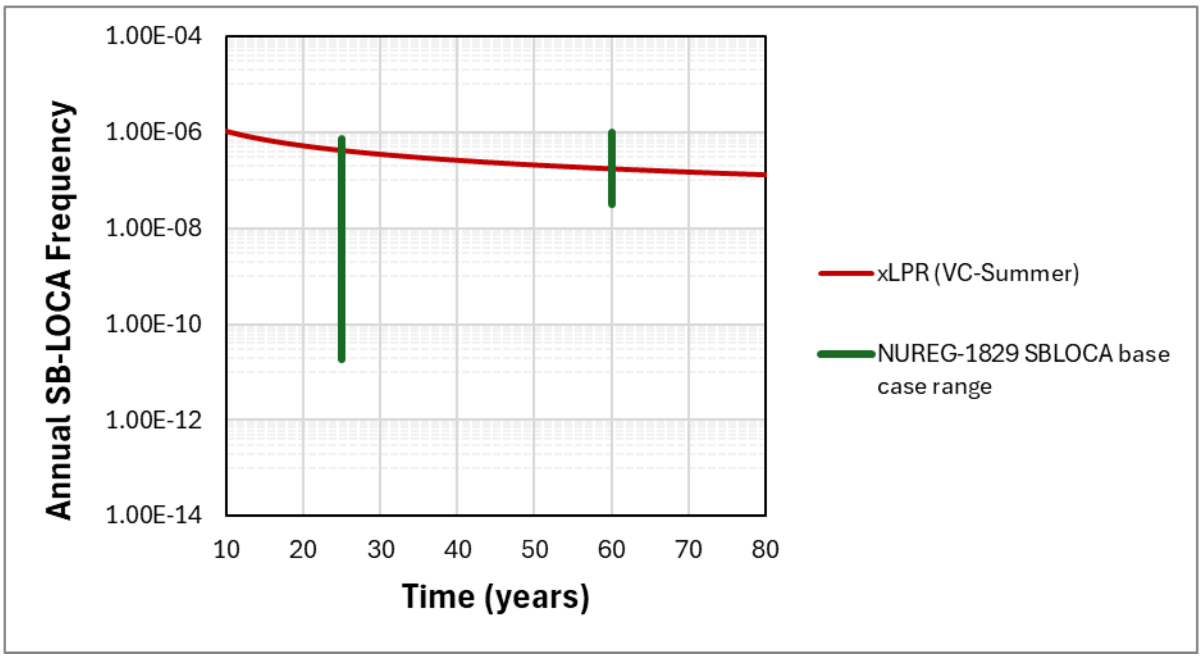

Figure 3: Comparison of xLPR upper bound estimate and NUREG-1829 range of data for the RVON base case.

2.3.2 Case PWR-2: PWR Surge Line

In the PWR-2 base case, there were a few instances of LOCAs recorded over the course of 80 years. During the time in which none of the 5,000 realizations had yet lead to a LOCA of any break size when leak detection is considered (i.e., < 35 years), the rule of 3 [6] is used to estimate a 95% confidence upper bound, with the use of the equivalent sample size.

The probability of initiation at 80 years when using the generic surge line WRS is estimated to be 2.10×10^{-3}. As a result, the equivalent sample size is equal to $n_{eq} \cong \frac{5{,}000}{2.1\times10^{-3}} \cong 2{,}376{,}735$.

For the period of time with no LOCA results, the 95% upper bound probability of any LOCA over time is estimated around 1.26×10^{-6}, and the annual frequency after y years can be approximated by $\frac{1.26\times10^{-6}}{y}$.

Figure 4 presents the comparison between the xLPR results and the NUREG-1829 results. As observed, no realizations have any LOCAs with LD for the first 25 years, and the upper bound falls within the middle of the range of the NUREG-1829 data logarithmically. Some SBLOCAs are observed after 35 years, and some MBLOCAs and LBLOCAs occur near the end of the simulation. However, as seen with the comparison at 60 years, the SBLOCA xLPR results are below the NUREG-1829 range, highlighting that the NUREG-1829 analysis is conservative.

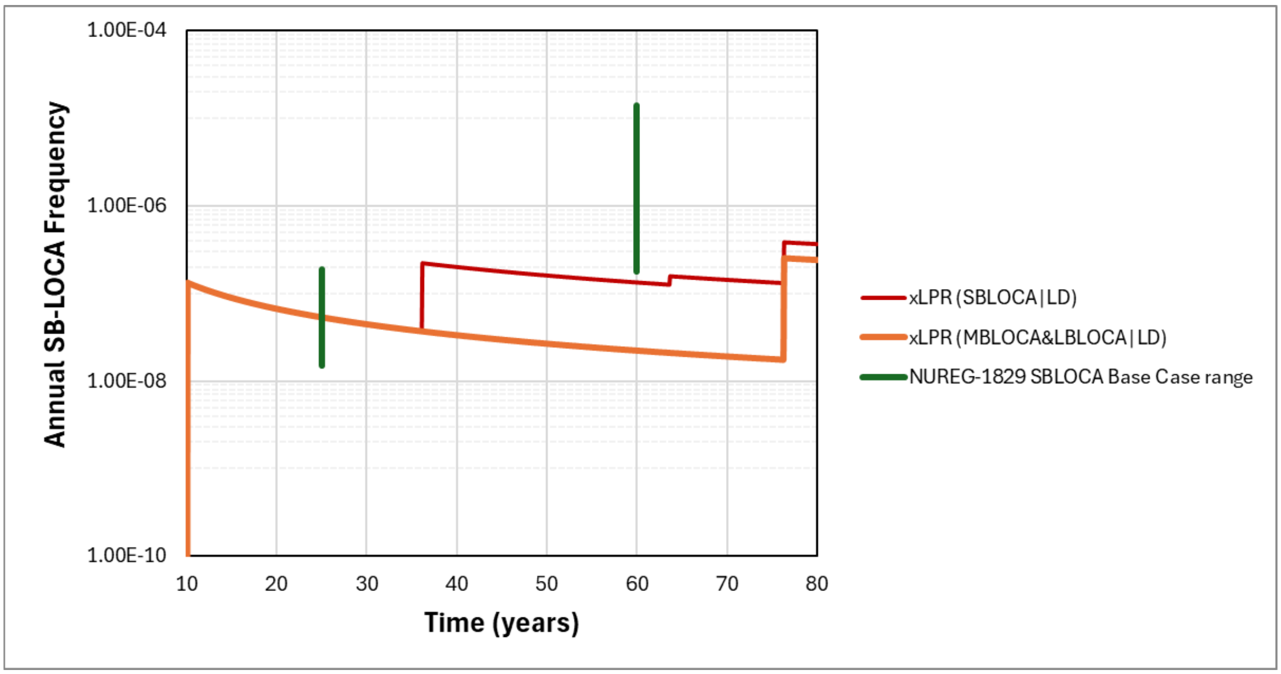

Figure 4: Comparison of xLPR reference results and NUREG-1829 range of data for the Surge Line base case

Since LOCA results with LD were observed, it was possible to adjust them to account for the impacts of ISI. Figure 5 shows the results when ISI with 10-year inspection intervals is implemented (blue curve in Fig. 5) and the frequencies are decreased by several orders of magnitude. Thus, showing once again that a direct comparison with the base case assumptions in NUREG-1829 compare favorably and confirm the conservative approach used in the NUREG report. Note that while the PFM SBLOCA results with only LD show three increases in value around 35 years, 64 years and 75 years (Figure 4 and 5), the addition of ISI shows an increase only at 35 years (Figure 5). The reason is that LOCAs which occur later in a plant lifetime tend to be associated with cracks with slower crack growth with a likelihood of experiencing multiple inspections such that they are unlikely to go undetected. The corrective term from multiple inspections is low enough to make the increase negligible and not visible on the log scale in Figure 45.

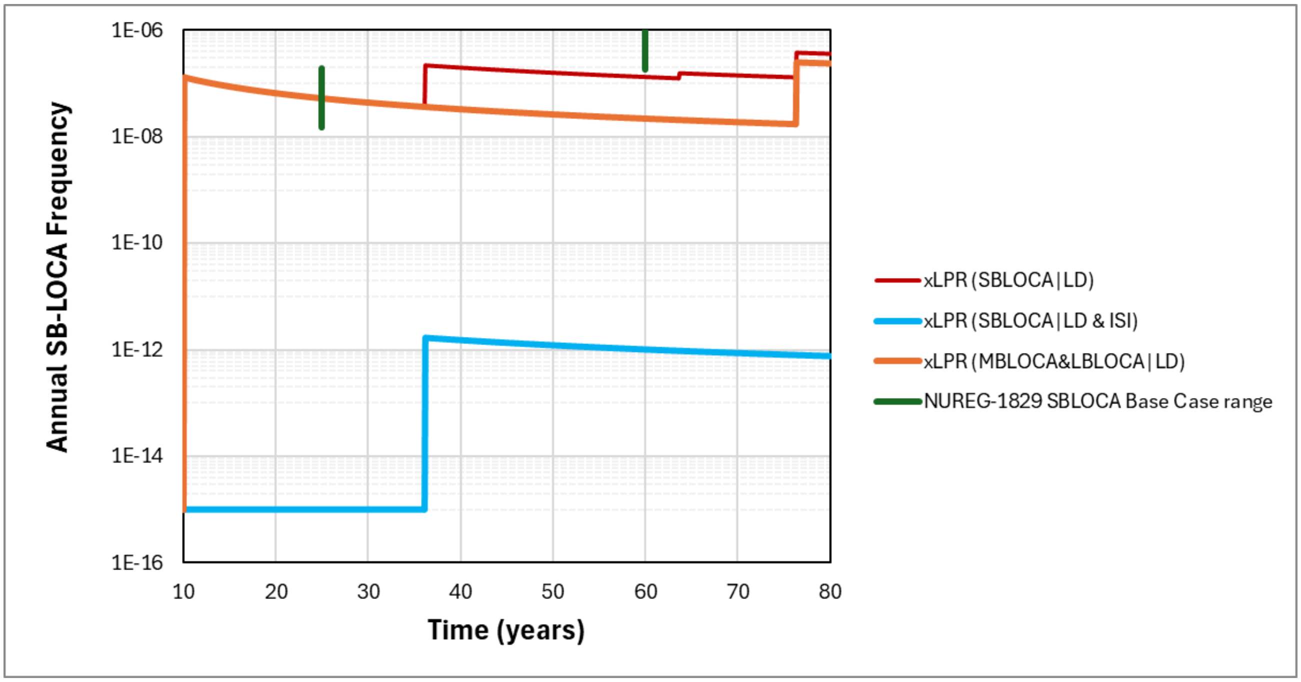

Figure 5: Impact of including the ISI for the Surge Line base case

2.3.3 Case BWR-1a: BWR 28" Recirculation Line

For the 28-inch recirculation line, some realizations generated LOCAs with LD for the base case. They occurred early on before the 20-year mark when the first ISI occurs and before application of mechanical stress improvement process (MSIP).

This result is nevertheless in range with the predictions from NUREG-1829. Dave Harris predicted an annual frequency of SBLOCA at 25 years using the PRAISE PFM code, which is more than 30 times higher than the xLPR prediction. For MBLOCA, the NUREG-1829 PFM prediction is in the same order of magnitude as the xLPR prediction. The LBLOCA frequency estimates from NUREG-1829 were slightly lower than the MBLOCA (a range of $[4.6 \times 10^{-7}$ - $4.8 \times 10^{-6}]$ for LBLOCA vs. $[1.2 \times 10^{-6} - 5.3 \times 10^{-6}]$ for MBLOCA at 25 years and a range of $[2.4 \times 10^{-6} - 4.2 \times 10^{-6}]$ for LBLOCA vs. $[9.2 \times 10^{-7} - 3.3 \times 10^{-6}]$ for MBLOCA at 60 years) though the difference is small enough that the same conclusion can be reached when comparing NUREG-1829 results and xLPR predictions.

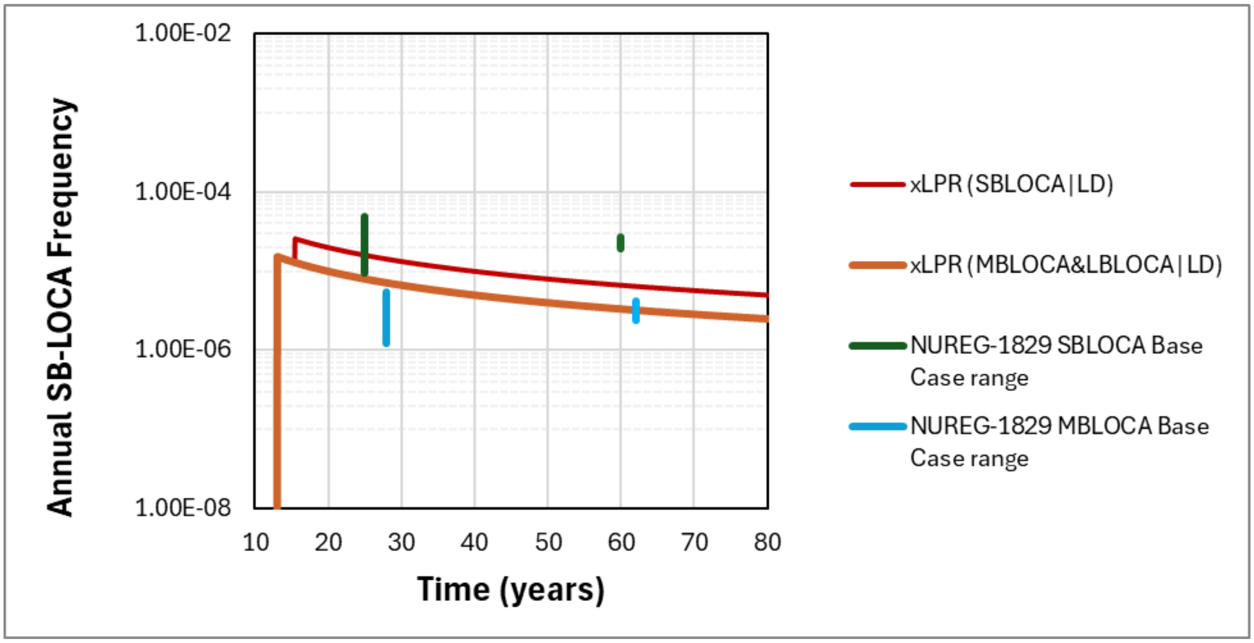

Figure 6: Comparison of xLPR reference results and NUREG-1829 range of data for the BWR 28in Recirculation line base case

2.3.4 Case BWR-1b: BWR 12" Recirculation Line

For the 12" BWR recirculation line, some realizations had a rupture in the first timestep. However, as seen in Figure 7, the resulting annual frequency at 25 years and 60 years is within the lower quartile of the NUREG-1829 predictions (from Table 4.1), confirming that the NUREG-1829 base case analysis was clearly conservative for the LOCA category considered. NUREG-1829 produces a single set of results for both the 12-inches and 28-inches recirculation lines, so a similar conclusion can be made when comparing the MBLOCA and LBLOCA results.

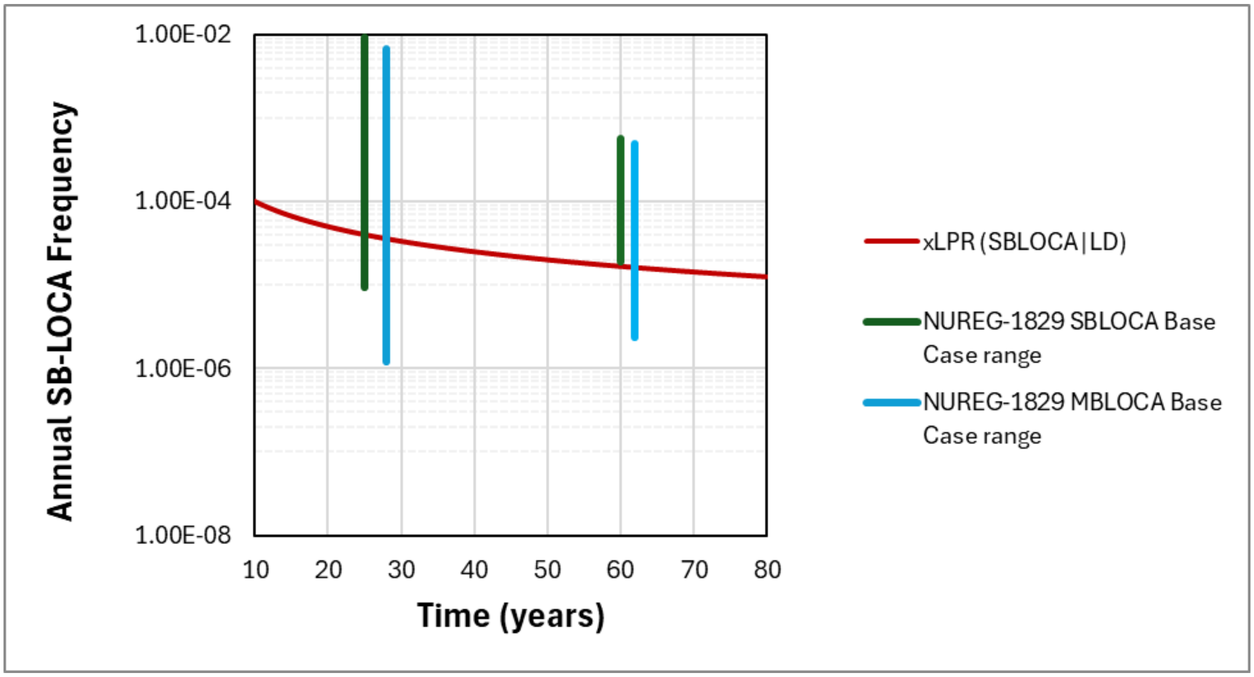

Figure 7: Comparison of xLPR reference results and NUREG-1829 range of data for the BWR 12in Recirculation line base case

While having some failures at the beginning of the simulation could be considered problematic, it is important to underline that this result is due to bias in the sampling of the crack depth and length as well as the material properties.

The distribution in crack depth is lognormal with a geometric mean of 1.5 mm and a geometric standard deviation of 1.42 mm. On a sample of size 5,000, it can create initial cracks whose depth is more than ¼ of the thickness. Similarly, the (total) crack length can vary from 7cm to 8cm.

The loads used were selected from the Dave Harris analysis for the Recirculation 12” base case and sum to 141.7 MPa (Table F.17 of [1]), which is relatively high for a pipe of this size. The ultimate strength of the base metal is represented by a normal distribution with a mean of 443 MPa, a standard deviation of 25.86 MPa, and truncated at a minimum of 386 MPa and a maximum of 507 MPa. The yield strength is represented by a normal distribution with a mean of 153.6 MPa, a standard deviation of 14.38 MPa, and truncated at a minimum of 123 MPa and a maximum of 190 MPa. This leads to a flow stress (taken as the average between yield and ultimate strength) following a normal distribution of mean 298.3 MPa and standard deviation 14.8 MPa. This leads to low critical bending moments which are used to estimate the crack stability.

The combination of large potential cracks, high loads and relatively low flow stress can create conditions that lead to instability at the first time step. The probability of such event, while likely to be non-physical, is in line with the predictions from NUREG-1829.

2.4 Sensitivity Studies

The base case reruns were complemented with selected sensitivity studies in order to estimate the impact of some of the conservatisms in the base cases. Sensitivity studies on both PWR welds studied in this report were previously performed and are documented in NRC Technical Letter Reports TLR-RES/DE/REB-2021-09, "Probabilistic Leak-Before-Break Evaluation of Westinghouse Four-Loop Pressurized-Water Reactor Primary Coolant Loop Piping using the Extremely Low Probability of Rupture Code," issued August 2021 (ML21217A088), and TLR-RES/DE/REB-2021-14-R1, "Probabilistic Leak-Before-Break Evaluations of Pressurized-Water Reactor Piping Systems using the Extremely Low Probability of Rupture Code," issued April 2022 (ML22088A006). These reports used xLPR to investigate the probability rupture before detectable leakage in selected systems and found this break-before-leak behavior was extremely unlikely. Selected sensitive studies considered the influence of various factors such as water chemistry, weld residual stress profile, temperature, etc. on the probability of leakage in the studied systems. The results found that the weld residual stress profile was one of the most impactful factors to consider when analyzing a weld's susceptibility to leakage.

Considering this outcome, this report also investigated the impact of the WRS profile where there is uncertainty. The first of those sensitivity runs was on the PWR-1 case and tested the impact of using the conservative VCIO WRS compared to the generic RVON WRS profile. A set of 4 WRS profiles were developed for each BWR-1a and BWR-1b, based on the location (center of weld or in the HAZ) and the status (unrepaired or repaired weld). The weld center unrepaired case was used as the base case as it was considered the most representative scenario. The other three weld profiles were covered with sensitivity runs. Finally, the IGSCC model selected included different parameters for water chemistry. The most conservative value was selected on the base case, and the more representative (hydrogen water chemistry) was used on BWR1-b as a sensitivity run.

2.4.1 PWR-1: Sensitivity on WRS Profile

Case 1.1.6a in [3] used a less conservative but more representative, generic WRS profile. The VCIO WRS profile is not only plant-specific, but it also has a 50 MPa standard deviation, which creates even higher tensile values at the ID for crack initiation.

The PFM analysis for PWR-1 was rerun in xLPR using the generic RVON WRS profile. While all 5,000 realizations performed for the PWR-1 case with the generic WRS profile also did not lead to any LOCAs when LD is considered, the fact that the probability of initiation is lower than when the VCIO WRS leads to a lower bound curve.

The probability of initiation at 80 years when using the generic RVON WRS is estimated to be 3.37×10^{-3}. As a result, the equivalent sample size is equal to $n_{eq} \cong \frac{5{,}000}{3.37\times10^{-3}} \cong 1{,}483{,}781$. While the base case (i.e. with VCIO WRS) had an equivalent sample size of $n_{eq} \cong \frac{5{,}000}{1.747\times10^{-2}} \cong 286{,}164$.

The factor of five difference between the two equivalent sample sizes is reflected when the upper bound of probability of LOCA and the corresponding annual frequencies at 25 years and 60 years are constructed as seen in Table 3 and Figure 8.

Table 3: Comparison of probability and annual frequency estimates of LOCA with LD, with two different WRS profiles

WRS Case	Upper Bound Probability of LOCA	Annual Frequency at 25 years (95% upper bound)	Annual Frequency at 60 years (95% upper bound)
VCIO RVON	1.05×10^{-5}	4.19×10^{-7}	1.75×10^{-7}
generic RVON	2.02×10^{-6}	8.09×10^{-8}	3.37×10^{-8}

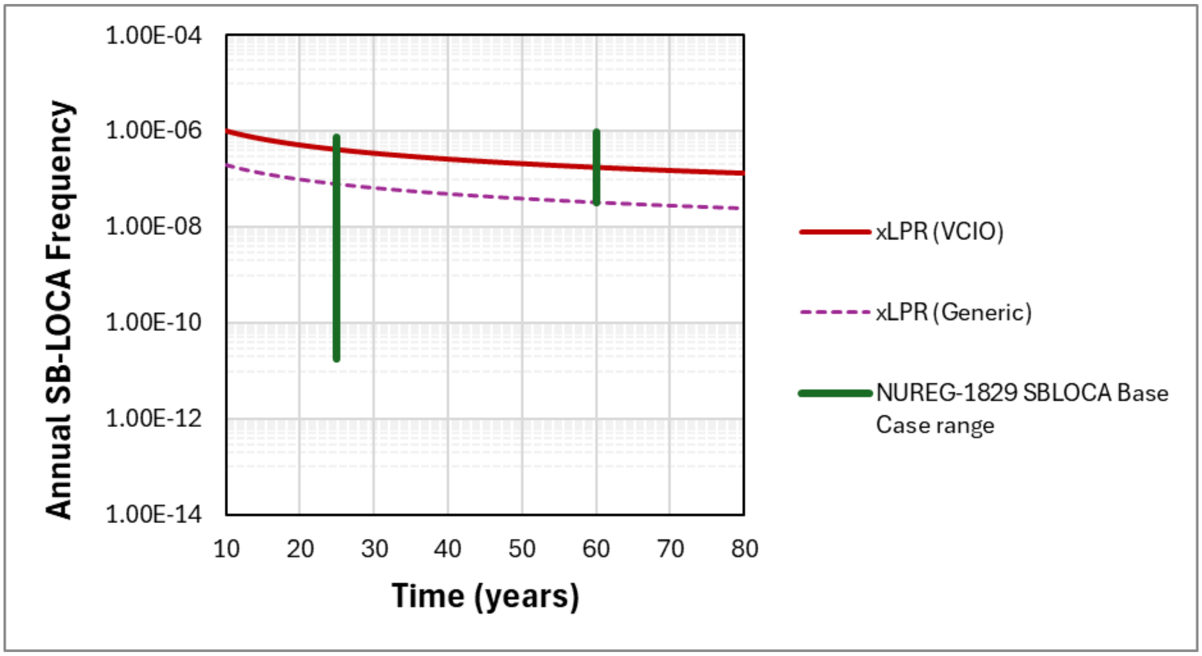

Figure 8: Sensitivity analysis on WRS profile for the RVON case on SBLOCA with LD.

2.4.2 BWR-1a: Sensitivity on the WRS Profile

In addition to the reference WRS profile (no repair at the weld centerline), three other profiles were generated both for the unmitigated and MSIP cases without LD and ISI: (1) weld centerline with a 10-percent repair depth, (2) HAZ with no repair, and (3) HAZ with a 10-percent repair depth. The BWR-1a PFM analysis was rerun in xLPR for the other three WRS profiles. As most of the LOCA results are zero when LD is considered, and since the few remaining realizations fail at the simulation time due to very rare sampling combinations, a comparison of the LOCA results with LD would not be meaningful. Instead, the probability of SBLOCA without LD and ISI has been used to compare the differences in results for the different WRS profiles for this section and in Section 2.4.3.

Figure 9 shows large variations in the probability of SBLOCA with the different WRS profiles. The unrepaired cases have a probability of SBLOCA less than 0.4 at 80 years. The repaired cases have quick increases in probability reaching 1 for the HAZ centered case around 12 to 15 years. The weld centerline case is slightly slower, resulting with a visible impact of MSIP mitigation after 20 years.

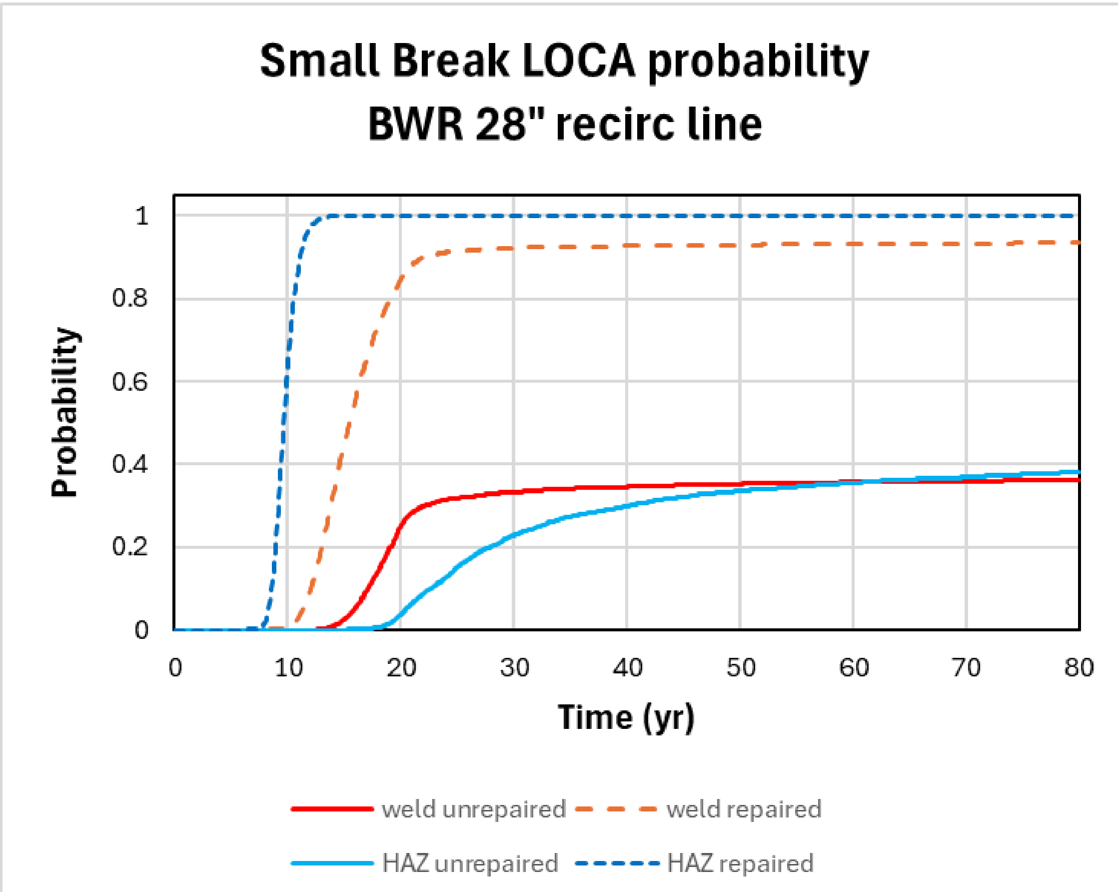

Figure 9: Sensitivity analysis on WRS profile for the BWR 28" recirc. Line

2.4.3 BWR-1b: Sensitivity on the WRS Profile

Like for BWR-1a in Section 2.4.2, the BWR-1b PFM was rerun in xLPR for the other three WRS profiles. The probability of SBLOCA without LD and ISI has been used for comparison.

Figure 10 shows a probability of SBLOCA equal to 1 (meaning all realizations have a SBLOCA when no LD and ISI is considered) within the first 10 years, which highlight the fast crack growth. The weld centerline results are nearly the same whether repair is considered. HAZ with a 10-percent repair depth gives faster growth, while HAZ with no repair leads to slower growth.

Because of such fast growth and considering that the first inspection is set at 20 years, there would be no impact if ISI was considered.

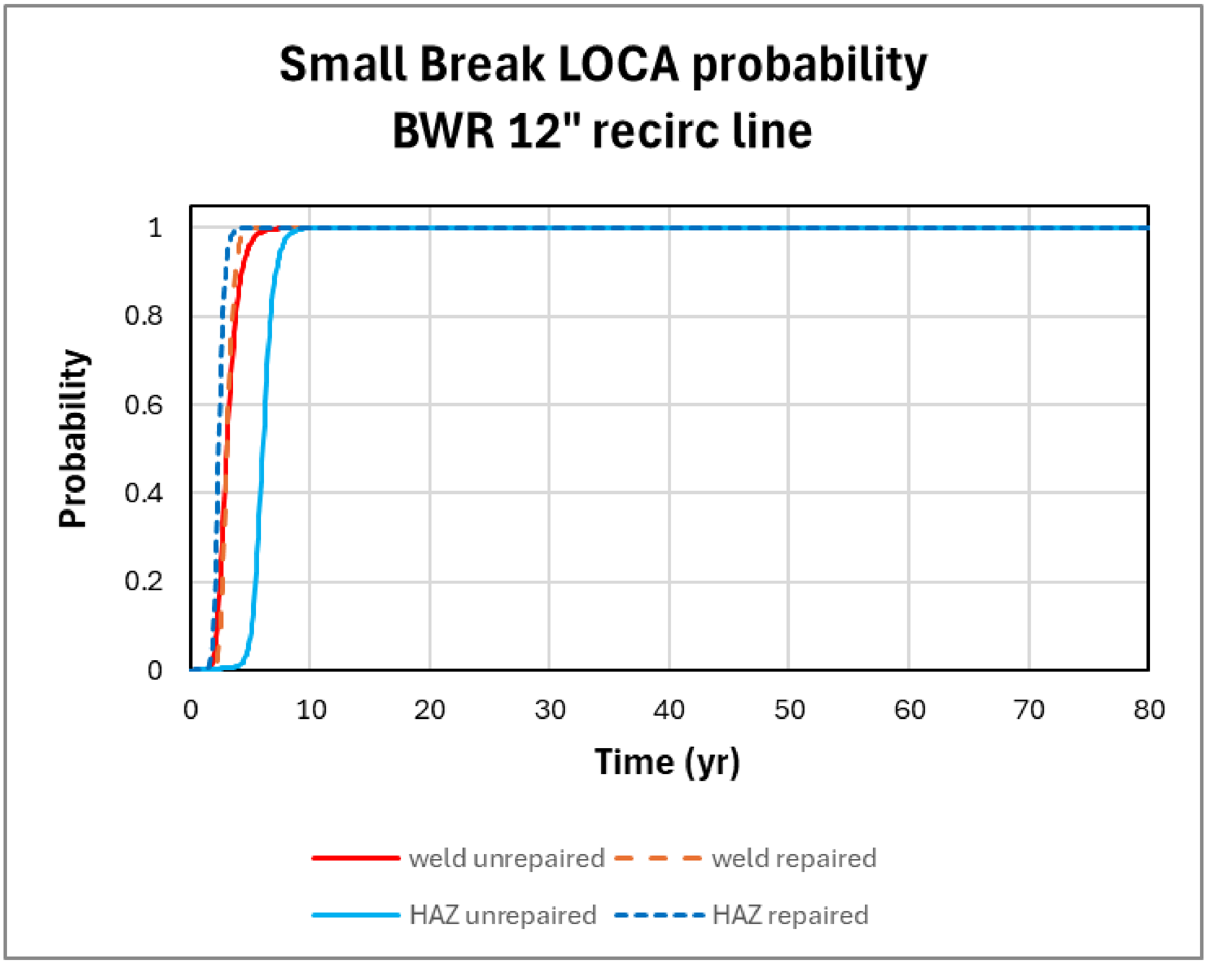

Figure 10: Sensitivity analysis on WRS profile for the BWR 12" recirc. Line

2.4.4 BWR-1b Sensitivity on the Water Chemistry.

The IGSCC growth rate model includes two parameters ($Cond$ and ECP in Eq. (4) in Section 7.1.3) on the crack growth factor depending on the water chemistry (normal water chemistry and hydrogen water chemistry). The values for normal water chemistry, which had the largest values of the two, was used for BWR-1a and BWR-1b.

Hydrogen water chemistry has a lower growth factor, α equal to *3.04E-14* (m/s)(MPa-m$^{1/2}$)^(beta). The reference BWR recirculation 12-inch line case was rerun with this growth factor to assess the impact of the water chemistry. The probability of SBLOCA without LD and ISI has been used for comparison.

As shown in Figure 11, the impact of hydrogen water chemistry is notable, with a delay of about a decade in the onset of SBLOCA when probabilities are compared to the base case that used normal water chemistry.

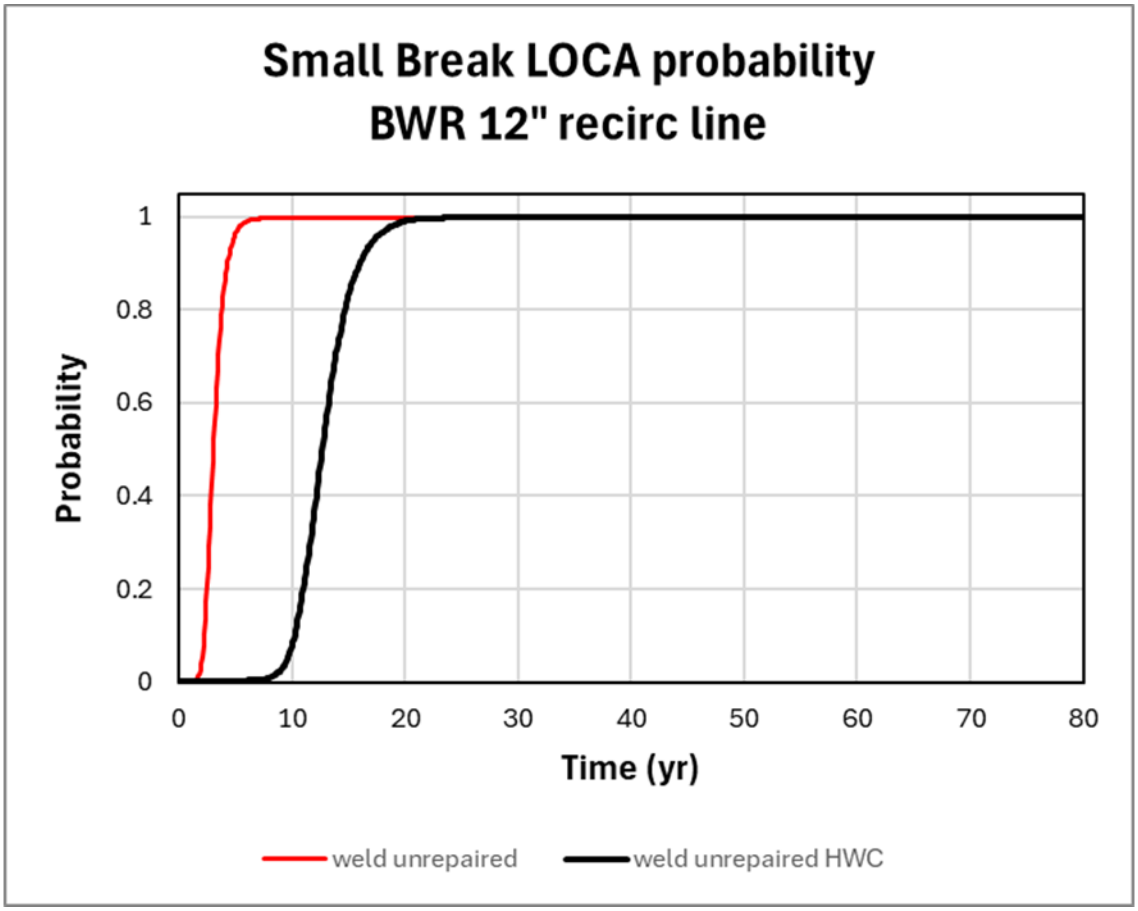

Figure 11: Sensitivity analysis on water chemistry for the BWR 12" Recirc. Line

3 OPERATING EXPERIENCE ANALYSIS

3.1 Approach and Methods

Section 3 documents the results of BWR and PWR piping LOCA frequency estimates based on an analysis of OpE data. The failure frequency estimates generated from the OpE data covered two distinct time periods from 1970 to 2004 and from 2005 to the present day. The scope of the analysis includes NUREG-1829 [1] base cases PWR-1, PWR-2, BWR-1a and BWR-1b as well as all other LOCA-sensitive piping of nominal pipe size greater than 6 inches. The implementation of the analysis format is summarized in Table 4 and Figure 13. The analysis consisted of four steps:

1. Review of the OpE applicable to NUREG-1829 base cases BWR-1a (Reactor Recirculation 28" diameter dissimilar metal weld), BWR-1b (Reactor Recirculation 12" diameter dissimilar metal weld), PWR-1 (Reactor Coolant System Hot Leg dissimilar metal weld) and PWR-2 (Pressurized Surge Line dissimilar metal weld and Hot Leg-to-Surge Line branch connection). This review covered two distinct periods, 1970 to 2004 and 2005-2024, differences and underlying factors of influence were assessed. The results were input to a "precursor" analysis in Step 2 to obtain updated piping component precursor rates. The database developed under the Nuclear Energy Agency's "Component Operational Experience, Degradation and Ageing Program" [11] provided the source for the domestic OpE data.

2. Calculation of piping component weld precursor rates. Expressed in units of failures per reactor operating year and the number of components exposed to a certain material degradation mechanism, the precursor rates were calculated using a Bayesian analysis approach. A constrained non-informative distribution (CNID) method was used to develop a prior precursor rate distribution representative of the state of knowledge in 2004. Next, the prior was updated using a Bayesian approach with data for the numerator (number of failures) and denominator (reactor operating years and number of components). A test for sensitivity to assumption used in developing the prior distribution is an intrinsic aspect of Bayesian reliability analysis. In this study, the prior precursor rate distribution was based on empirical data representing the OpE in the period 1970 to 2004. The underlying methodology is described in references [12, 13, 14, 15, 16, 17, 18, 19, 20]. The prior precursor rate distribution was updated using the 2005 to 2024 domestic OpE.

3. Calculation of conditional failure probabilities (CFP). The BWR and PWR base case CFP uncertainty distributions were developed from NUREG-1829 by first obtaining a geometric mean of the expert elicitation participant results for each component case. This value represented a "target LOCA frequency" (TLF), expressed as $Median_{TLF}$. Next the precursor failure frequency results of

respective analysis case were converted to fit a lognormal distribution, expressed as $Median_{Precursor}$. Finally, the median of the CFP was obtained by dividing the median TLF with the median precursor rate. The resulting CFP uncertainty distribution represents the CFP state of knowledge as of 2004 when the NUREG-1829 expert elicitation was completed. This CFP distribution is assumed to remain representative of today’s state of knowledge.

4. In a final step, the uncertainty distributions developed in Step 2 (precursor frequency) and Step 3 (conditional failure probability) were merged in a Monte Carlo uncertainty propagation to obtain LOCA frequency uncertainty distributions for each respective analysis case.

The implementation of the analysis approach is summarized in Table 4 and Figure 12. Additionally, an example calculation is provided in Section 7.3.

Table 4: Step-by-Step Analysis Approach to LOCA Frequency Quantification

Precursor Analysis: Weld Precursor rate (λ) Estimation	
1.1	Determine component and weld types - i
1.2	Perform data query domestic OpE for failure counts - n_{fail}
1.3	Estimate component exposure – T in terms of reactor operating years. Develop uncertainty distributions to account for plant-to-plant weld population variability. Using engineering judgment, assign a 50% probability that the best estimate of weld population is the correct value, 25% probability that the lower estimate is correct, and 25% that the upper estimate is correct.
1.4	Develop component informed precursor rate prior distributions for each degradation mechanism (DM), **1970 to 2004 OpE analysis.** Characterize the uncertainty using a constrained noninformative prior (CNID) prior distribution.
1.5	Perform Bayes' update for each exposure case (combination of weld count case and DM susceptibility (DMS) case) to account for the **2005 to 2024 OpE.**
1.6	Develop mixture distribution to combine results for different exposure hypotheses to yield conditional precursor rate distributions given plant-specific DM analysis.
1.7	Calculate total precursor rate over all applicable damage mechanisms.
Conditional Failure Probability (ρ) Development	
2.1	Select component evaluation boundaries to define conditional rupture probability (CRP) model categories. Differentiate ASME XI Category B-F from Category B-J welds.
2.2	Obtain NUREG-1829 Expert Elicitation LOCA distributions from the "BWR Piping Raw Data" and "PWR Piping Raw Data" files, NRC ADAMS Accession Nos. ML080560008 and ML080560011, respectively.
2.3	Determine geometric mean of expert distributions from Step 2.2 (lognormal). Obtain a single lognormal distribution for each system case and LOCA category by taking the geometric mean of the medians of the experts' lognormal distributions as the composite distribution median, and the geometric means of the range factors of the experts' lognormal distributions as the composite distribution range factor.
2.4	Determine precursor rate distribution for the Base Case Analyses in NUREG-1829, fit to lognormal distribution.
2.5	Apply formulas to calculate CFP distributions to be used as prior distributions for each valid combination of CFP category and component.

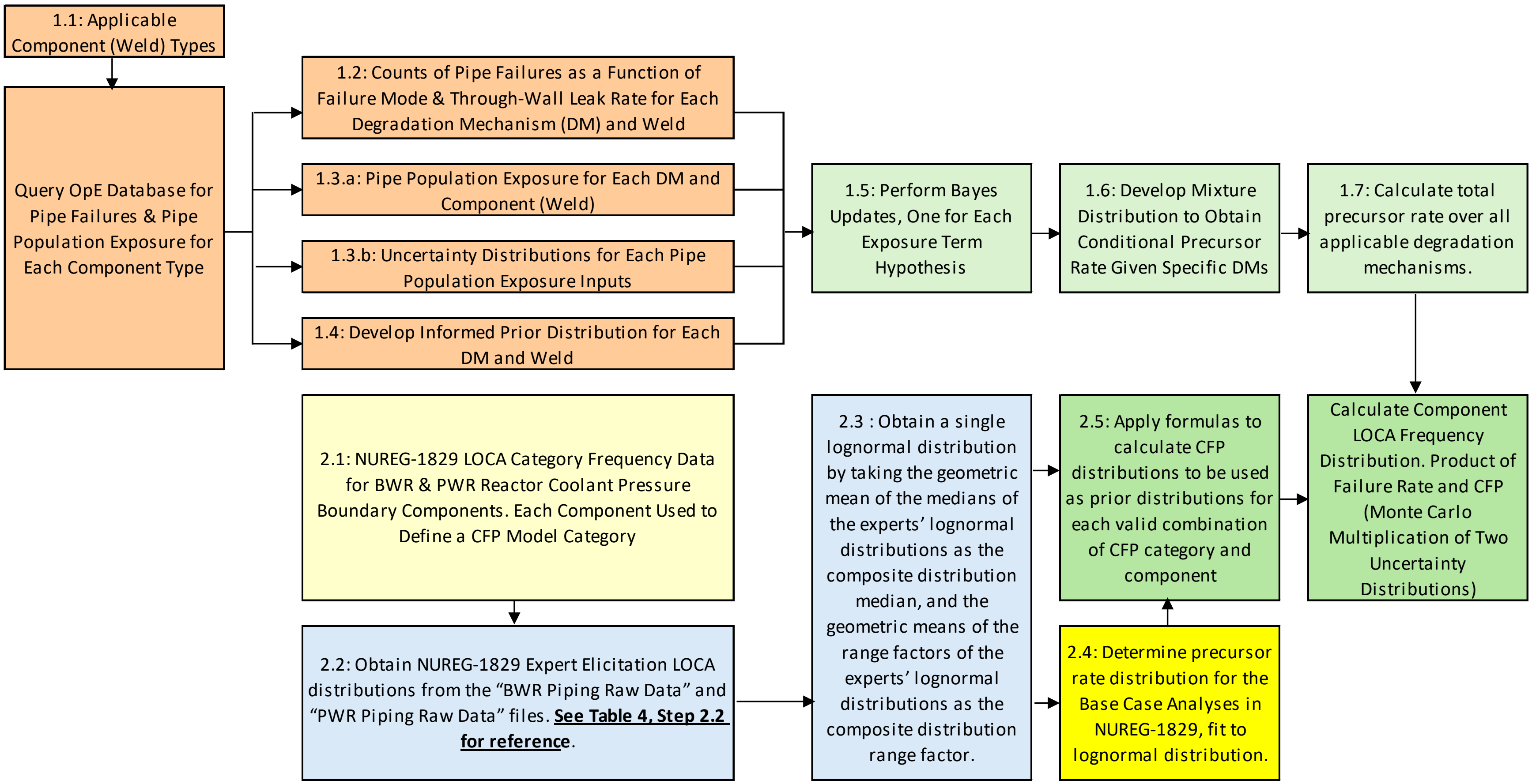

Figure 12: Step-by-Step Procedure for LOCA Frequency Quantification.

3.1.1 Welds Considered in the Analysis

The piping base case definitions in NUREG-1829 are summarized in Table 5. In addition to PWR-1, PWR-2, BWR-1a and BWR-1b, the scope of the OpE analysis included all LOCA-sensitive piping of nominal pipe size > 6 inches. The base case studies that supported the original expert elicitation were performed in the period 2003 to 2004. They accounted for the domestic OpE from 1970 until the 2003 to 2004 period. The updated LOCA frequency assessment accounts for the domestic OpE from 2005 to mid-2024.

Table 5: NUREG-1829 Base Case Definitions

Plant Type	NUREG-1829 Base Case	System	NPS[3] (inch)	ASME XI Weld Category	Degradation Mechanism
PWR	PWR-1	Reactor Coolant System Hot Leg	30	B-F, B-J	PWSCC
	PWR-2	Pressurizer Surge Line	10	B-F, B-J	PWSCC, TF
BWR	BWR-1a	Reactor Recirculation	28	B-F, B-J	IGSCC
	BWR-1b		12	B-F, B-J	
	BWR-2	Feedwater	12	B-J	FAC, IGSCC, TF

3.1.2 Analysis Procedure

In the OpE approach the probabilistic failure metrics of piping integrity are based on the "risk triplet idea," [12]. The analysis considers possible material degradation scenarios, and the likelihood that a piping pressure boundary failure occurs given a flaw in the material. Finally, the analysis assesses the consequences of a failure. An event tree, Figure 13, is used to illustrate the risk triplet concept. It illustrates what can go wrong, how likely it is to happen, and the consequences of a piping pressure boundary failure. Each element in the risk triplet is represented by a probability density function. The risk triplet representation is as follows:

$$\langle S_i, P_i, C_i \rangle \quad \text{Eq. (3)}$$

This model starts with an estimate of the weld precursor rate, next the model integrates the precursor rates, which are estimated using OpE data, by defining the conditional failure probability of a break of a given size given a pipe failure. Another way to look at this model is that pipe failures

[3] Nominal Pipe Size

are assumed to represent challenges to the piping system and that upon each challenge, there is a probability of experiencing a break of a given size.

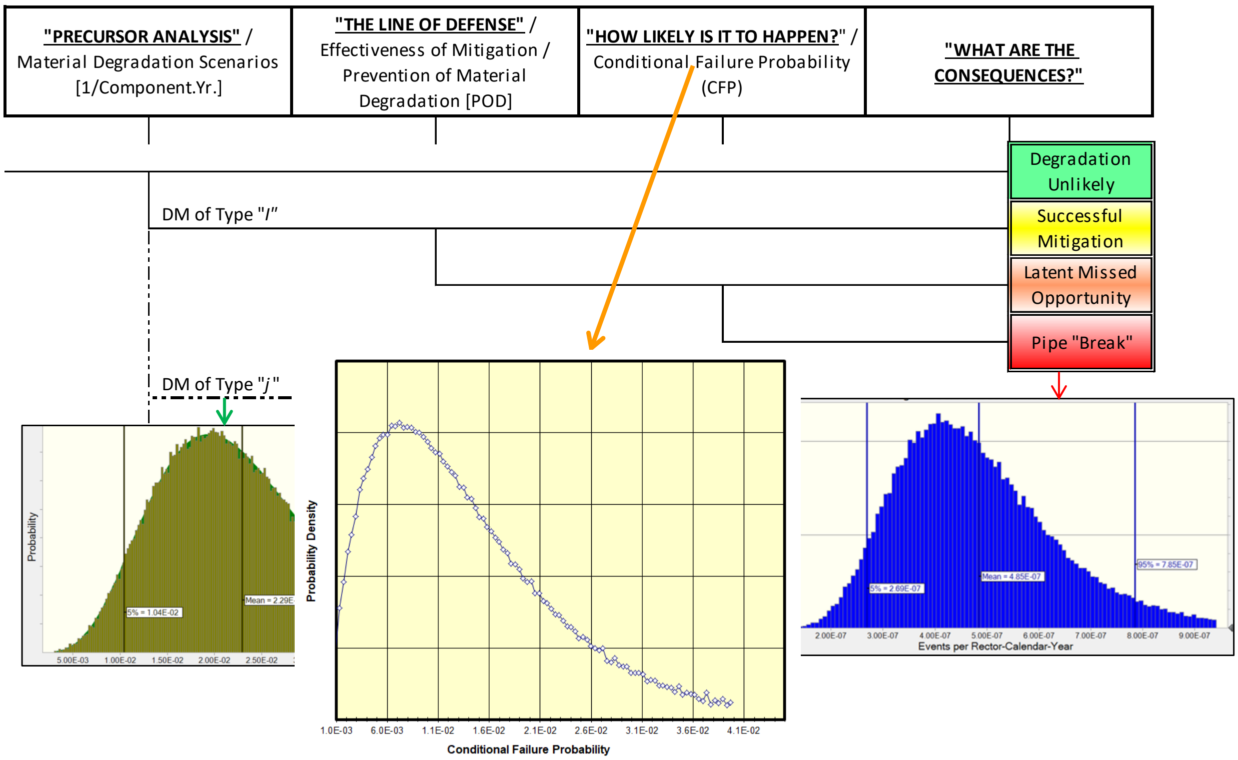

Figure 13: The Piping Integrity "Risk Triplet".

Parameter S_i represents the "precursor" to pipe failure and accounts for crack initiation and the potential for growth of a pipe flaw in the through-wall direction. This step produces a frequency of a degraded state. Next the analysis investigates the "line-of-defense" against a degraded pressure boundary integrity, i.e., the probability of detecting a degraded state before going through-wall producing a detectable leakage. This is followed by an assessment of the likelihood that a material degradation scenario propagates into loss of pressure boundary integrity, parameter P_i. Finally, the consequence, C_i, of a pipe is represented by the product of S_i and P_i.

The precursor analysis considers the incubation period and crack/flaw growth for different combinations of materials and degradation mechanisms. An incubation period refers to the total time that a certain piping pressure boundary goes through crack nucleation until the time the crack progresses to a critical degree such that there is an active crack growth in the through-pipe-wall direction. The quantitative assessment produces an estimate of the frequency of failure of a pressure boundary, i.e. precursor failure frequency. The definition of what constitutes a failure depends on the purpose of an analysis. Failure can be a crack or leak that results in repair without immediate effect on operations or shut down of the reactor. The input data comes from the OpE review.

The "Line-of-Defense" analysis considers the different strategies for early detection of a degraded piping pressure boundary so that a significant structural failure is prevented. Early detection encompasses reliability of a leak detection system and the probability of detecting (POD) crack before it penetrates a piping pressure boundary. Renewal theory gives a basis for analyzing the effect on the frequency of failure by, for example leak detection and non-destructive examination using ultrasonic testing or other techniques.

The analysis of the CFP considers how an undetected pipe flaw, or a minor through-pipe-wall leakage suddenly propagates to form a significant structural failure with dynamic effects on surrounding plant areas, structures, and equipment. This is represented by a conditional failure probability model that represents the margin to a major pressure boundary failure. The goal of the analysis is to establish a set of CFPs vs. break size for each piping system and non-piping component comprising each LOCA category in Table 6. For each category, the break sizes to be considered range from an equivalent break size of 0.5" to a break size corresponding to a double-ended guillotine break (DEGB) of the pipe.

Table 6: LOCA Categories in NUREG-1829

Plant Type	LOCA Category	Through-Wall Flow rate (kg/s)	Through-Wall Flow rate (gpm)	Equivalent Break Size (EBS) (mm \ Inch)
BWR	1	> 6.3	>100	12.7 \ 0.5
	2	> 100	>1,500	47.6 \ 1-7/8
	3	> 300	>5,000	82.5 \ 3-1/4
	4	> 1600	>25,000	177.8 \ 7
	5	> 6000	>100,000	457.2 \ 18
	6	> 32000	>500,000	1,041.2 \ 41
PWR	1	> 6.3	>100	12.7 \ 0.5
	2	> 100	>1,500	41.3 \ 1-5/8
	3	> 300	>5,000	76.2 \ 3
	4	> 1600	>25,000	177.8 \ 7
	5	> 6000	>100,000	355.6 \ 14
	6	> 32000	>500,000	787.4 \ 31

Two basic relationships are used to illustrate the types of input parameters that are needed to calculate probabilistic failure metrics that apply to piping systems:

$$\rho = \lambda \times CFP \qquad \text{Eq. (4)}$$

$$\lambda = \frac{n_{fail}}{\tau} \qquad \text{Eq. (5)}$$

These relationships appear next-to-trivial. A meaningful quantitative assessment requires a detailed breakdown of the physical factors that underlying piping pressure boundary degradation or failure, however. Parameter ρ corresponds to the consequence of a pipe failure and corresponds to C_i in the risk triplet. It is frequency of a pressure boundary failure of a certain magnitude "i". The “magnitude” corresponds to the volumetric through-pipe-wall flow rate, or it can be in terms of the dimensions of the opening in the pressure boundary, i.e. effective break size. Table 7 is a summary of how these parameters are estimated.

Parameter λ is referred to as the pipe failure, or precursor rate and is estimated from the number of “failures” (n_{fail}) that have been observed in a given period. Parameter τ is an exposure term, consisting of reactor operating years or equivalent full-power years of operation and number of piping components that produced the relevant OpE. The precursor rate is a simple maximum likelihood estimator described by a Poisson distribution with a single parameter, λ, which is the mean number of events over time. It is a representation of being in a certain degraded state of structural integrity, e.g. cracked, thinned, or leaking. The CFP represents the conditional probability that a pre-existing flaw in the pipe pressure boundary transitions from a stable to an unstable state.

Table 7: Piping Reliability Model Input Parameters

Parameter	Element in the Structural Integrity Risk Triplet	Formula	Description
ρ	C_i	Combination of probability density functions for l and CFP, respectively, using Monte Carlo simulation	Frequency of a pipe failure as a function of an equivalent break size (EBS) or through-wall mass or volumetric leak rate. The exact definition depends on the context of an analysis.
λ	S_i	$\lambda_{ik} = \frac{n_{fail,ik}}{\tau_{ik}} = \frac{n_{fail,ik}}{f_{ik} N_i T_i}$	Pipe precursor rate, which is the rate of being in a certain state, e.g., crack of certain dimension (through-wall depth as percentage of wall thickness, crack opening area, crack opening displacement, or through-wall leak). The precursor rate is calculated as the number of observed failures over an observation period.
CFP	P_i	$CFP = \frac{\alpha}{\alpha + \beta}$	The formula is symbolic, parameter α is the number of significant structural failures, and parameter β represents the number of challenges to the pressure boundary integrity.

To calculate the precursor rate, λ, one can start with a broad generic prior distribution. To address uncertainty in prior distribution, a CNID method can be used in which the mean value of a gamma distribution is anchored to the mean estimate of the precursor rate. The precursor rate is expressed in units of failures per reactor operating year and the number of components that are exposed to a certain material degradation mechanism. The generic prior is then updated with the 2005 to 2024 domestic OpE using a Bayesian approach with data for the numerator (number of failures) and denominator (reactor operating years and number of components). The parameters of CFP model were derived from the NUREG-1829 results to produce a table of CFP values versus effective break size for each relevant piping system and non-piping component.

3.1.3 Operating Experience Review

An OpE review was performed to generate input to the LOCA frequency update. This review covered two distinct periods, 1970 to 2004 and 2005 to 2024, differences and underlying factors of influence were assessed. The former period covers OpE that was available for the NUREG-1829 base case analyses. The accumulated OpE in terms of reactor operating years (ROYs) is given in Table 8, Table 9, and Table 10. The scope of the OpE review is given in Table 11 and Table 12. In these tables, the nominal pipe inside diameter and corresponding DEGB size used in the analysis are indicated. The range of nominal pipe size (NPS) for these systems is also indicated. The piping OpE is presented in terms of failure counts versus the period in which a failure was discovered is summarized in Table 13 and Table 14 for PWR and BWR plants, respectively. The failure counts were input to the Bayesian precursor analysis to obtain the updated pipe precursor rates.

Table 8: The Accumulated Reactor-Years of Operation

Scope of OpE Review	Plant Type	NUREG-1829 Expert Elicitation		TLR Expert Elicitation		ΔEFPY (2024 vs 2004)
		1970-2004		1970-2024		
		ROY	EFPY	ROY	EFPY	
Domestic Plants	BWR	987.8	839.6	1638.7	1393.9	553.3
	PWR-All	1615.4	1373.0	2735.4	2325.1	952.0
"PWR-All" includes B&W, CE and WE plants. All subsequent tables in Section 3 refer to WE reactor coolant system designs and the related domestic OpE.						

Table 9: PWR-1/PWR-2 Reactor Operating Years of Operation

NSSS Type	Westinghouse (WE) PWR International & US Reactor Operating Years				US Reactor Operating Years		
	1970-2004	2005-2024	1970-2024		1970-2004	2005-2024	1970-2024
WE-2	655.8	323.6	979.4	250.4	108.4	358.7	
WE-3	873.8	736.3	1610.1		350.9	260.0	610.9
WE-4	807.4	713.0	1520.4		679.4	580.3	1259.7
Totals:	2337.1	1772.8	4109.9		1280.7	948.6	2229.4

Table 10: BWR-1a/BWR-1b Reactor Operating Years of Operation

NSSS Type	No. NPS28 B-F Welds	No. NPS12 B-F Welds	BWR/US Reactor Operating Years		
			1970-2004	2005-2024	1970-2024
BWR/2	5	N/A	71.0	33.7	104.7
BWR/3	2	8	226.5	114.4	340.9
BWR/4	2	8	507.6	365.6	873.2
BWR/5	2	8	81.9	80.0	161.9
BWR/6	2	8	78.0	80.0	158.0
	Total Reactor Operating Years:		965.0	673.7	1638.7

Table 11: Scope of the PWR Operating Experience Review

PWR LOCA-Sensitive Piping		Pipe Inside Diameter (inch) Typical of WE 4 Loop	DEGB (inch)	Pipe Size (NPS) Range Across All PWR NSSS Designs
System	Pipe Segment(s)			
Reactor Coolant System (RCS)	RCS Cold Leg	27.5	38.9	30 - 44
	RCS Hot Leg	29	41.0	22 - 34
	RCS Cross-over Leg	31	43.8	22 - 34
	Pressurizer Surge Line	12.812	18.1	10 - 14
Residual Heat Removal System (RHR)	RHR Suction Line - off of RCS Hot Leg	10.126	14.3	6 - 12
	RHR Discharge to Cold Leg	8.5	12.0	6 - 12
	RHR Discharge to Cold Leg	6.813	9.6	
	RCS Hot Leg Recirculation	6.813	9.6	
Safety Injection System (SIS)	Accumulator Discharge to Cold Leg	10.126	14.3	10 - 12
	RCS Hot Leg Recirculation	6.813	9.6	6 - 12

Table 12: Scope of the BWR Operating Experience Review

BWR LOCA-Sensitive Piping		Pipe Inside Diameter (inch) - Typical of BWR/4	DEGB (inch)	Pipe Size (NPS) Range Across BWR/3/4/5/6 NSSS Designs
System	Pipe Segment(s)			
Reactor Recirculation System (RR)	RR Loop Piping	28	39.6	10 - 28
	RR Suction	10.75	15.2	
	RR Distribution Manifold	22	31.1	
Main Steam System (MS)	MS - inside containment	17.938	25.4	18 - 28
Feedwater System (FW)	FW - inside containment	15.25	21.6	12 - 24
	FW - inside containment	10.75	15.2	
Residual Heat Removal (RHR)/ Low-Pressure Coolant Injection (LPCI)	RHR influent lines from RR loops to containment penetration & LPCI injection line inside containment	14.312	20.2	8 - 24
		12.5	17.7	
High-Pressure Coolant Injection (HPCI)	HPCI discharge piping -	9.562	13.5	10 - 12
High-Pressure Core Spray (HPCS)	Discharge line inside containment – BWR5/6	9.562	13.5	10 - 12
Low-Pressure Core Spray (LPCS)	LPCS discharge piping	9.562	13.5	10 - 12
Reactor Water Cleanup System (RWCU)	RWCU from one RR loop to containment penetration	7.625	10.8	8 - 24

Table 13: Domestic PWR Operating Experience

SYSTEM	ASME Section XI Weld Category	Nominal Pipe Size (inch)	No. Precursor Failures		
			1970-2004	2005-2024	1970-2024
Prz-Surge Line	B-F	10 < NPS ≤ 22	0	2	2
RCS Cold Leg	B-J	6 < NPS ≤ 10	1	0	1
RCS Cold Leg	B-F	NPS > 22	0	2	2
RCS Hot Leg	B-F	NPS > 22	1	0	1
RCS Hot Leg @ S/G Inlet	B-F	NPS > 22	0	1	1
RHR	B-J	6 < NPS ≤ 10	0	1	1
RHR	B-J	10 < NPS ≤ 22	0	2	2
SIS	B-F/B-J	NPS > 8	0	0	0
		Total	2	8	10

Table 14: Domestic BWR Operating Experience

BWR SYSTEM	ASME Section XI Weld Category	Nominal Pipe Size (inch)	No. Precursor Failures	
			1970-2004	2005-2024
FW	B-J	10 < NPS ≤ 22	2	0
FW	B-F	10 < NPS ≤ 22	5	3
HPCI	B-J	6 < NPS ≤ 10	1	0
HPCI	B-J	10 < NPS ≤ 22	1	0
HPCS	B-J	6 < NPS ≤ 10	11	0
HPCS	B-J	10 < NPS ≤ 22	4	0
HPCS	B-F	6 < NPS ≤ 10	1	0
HPCS	B-F	10 < NPS ≤ 22	1	0
HPCS	B-F	NPS > 22	1	0
LPCI	B-J	10 < NPS ≤ 22	2	0
LPCS	B-J	10 < NPS ≤ 22	1	0
LPCS	B-F	6 < NPS ≤ 10	2	0
LPCS	B-F	10 < NPS ≤ 22	0	1
MS	B-J	10 < NPS ≤ 22	0	0
MS	B-J	NPS > 22	0	0
MS	B-F	10 < NPS ≤ 22	0	0
RHR	B-J	6 < NPS ≤ 10	3	0
RHR	B-J	10 < NPS ≤ 22	13	0
RHR	B-J	NPS > 22	27	0
RHR	B-F	10 < NPS ≤ 22	0	2
RHR	B-F	NPS > 22	0	1
RR	B-J	6 < NPS ≤ 10	4	2
RR	B-J	10 < NPS ≤ 22	271	1
RR	B-J	NPS > 22	192	0
RR	B-F	6 < NPS ≤ 10	11	0
RR	B-F	10 < NPS ≤ 22	63	10
RR	B-F	NPS > 22	16	8
RWCU	B-J	6 < NPS ≤ 10	16	0
		Totals:	648	28

Organized by severity level, the domestic and international BWR and PWR (combined) OpE from 1970 to 2024 is summarized in Table 15. Precursor failures are defined as degraded (DEG) or through-wall leakage (TWL) requiring repair or replacement per codes and standards. Significant structural failures (SSF) are characterized by an estimated or measured through-wall flow rate of greater than or equal to 100 gpm. The scope of the OpE analysis is limited to piping having nominal pipe size greater than 6 inches.

Table 15: The Domestic & International OpE by Severity Level

ASME III Safety Class	Nominal Pipe Size (NPS)	Precursors		SSF (≥ 100 gpm)
		DEG	TWL	
Light Water Reactor Class 1 - Primary Pressure Boundary	NPS ≤ 1	61	603	17
	1 < NPS ≤ 2	59	130	2
	2 < NPS ≤ 3	48	46	2
	3 < NPS ≤ 4	107	54	2
	4 < DN ≤ 6	92	21	1
	6 < NPS ≤ 10	213	19	0
	10 < NPS ≤ 22	706	73	0
	NPS > 22	395	16	0
	Totals:	1681	962	24

3.1.4 Conditional Failure Probability

The conditional failure probability uncertainty distributions were derived from the NUREG-1829 result. The LOCA frequency estimates in NUREG-1829 were based on an expert elicitation process which consolidated OpE and insights from PFM studies with knowledge of plant design, operation, and material performance. The elicitation required each expert panel member to qualitatively and quantitatively assess important LOCA contributing factors and quantify their uncertainty. Figure 14 provides an example of these estimates for Category 1 LOCAs in the BWR Recirculation System. The quantitative responses were combined to develop BWR and PWR total LOCA frequency estimates for each contributing panelist. The distributions for the six LOCA size categories and three time periods evaluated were represented by four parameters (mean, median, 5th and 95th percentiles). Finally, the individual estimates were aggregated to obtain group estimates.

As a basis for comparing the updated LOCA frequencies with the NUREG-1829 results, Table 16 and Table 17 were developed from NUREG-1829, Section 7, “Quantitative Results”, which provided the combined pipe and non-pipe LOCA frequencies. The piping and non-piping mean results were then derived from NUREG-1829 Section 7, “Quantitative Results” using the non-pipe-to-pipe frequency ratios provided in that report. Next, the derived pipe-only LOCA frequency uncertainty distributions were obtained using a CNID prior distribution to obtain the parameters of a gamma distribution which result in the intended mean value. This approach was used to best compare the updated OpE-based LOCA frequencies with those developed in NUREG-1829.

Table 16: NUREG-1829 BWR LOCA Frequencies at 25 years

LOCA Category	EBS (inch)	Total	Non-Pipe	Pipe			
		Mean	Mean	Mean	5%-tile	50%-tile	95%-tile
BWR @ 25 Years							
1	0.5	6.50E-04	1.26E-04	5.24E-04	1.77E-06	2.05E-04	1.73E-03
2	1.875	1.30E-04	3.71E-05	9.29E-05	3.09E-07	3.58E-05	3.02E-04
3	3.24	2.90E-05	2.87E-06	2.61E-05	8.51E-08	9.85E-06	8.32E-05
4	7	7.30E-06	4.13E-07	6.89E-06	2.80E-08	2.66E-06	2.25E-05
5	18	1.50E-06	9.81E-08	1.40E-06	4.05E-09	4.68E-07	3.95E-06
6	41	6.3E-09	6.3E-09	N/A	N/A	N/A	N/A

Table 17: NUREG-1829 PWR LOCA Frequencies at 25 years

LOCA Category	EBS (inch)	Total	Non-Pipe	Pipe			
		Mean	Mean	Mean	5%-tile	50%-tile	95%-tile
PWR @ 25 Years							
1	0.5	7.30E-03	7.08E-03	2.21E-04	8.70E-07	1.01E-04	8.50E-04
2	1.875	6.40E-04	5.22E-04	7.79E-05	3.06E-07	3.54E-05	2.99E-04
3	3.24	1.60E-05	4.24E-06	1.18E-05	4.63E-08	5.35E-06	4.52E-05
4	7	1.60E-06	8.38E-07	7.62E-07	3.00E-09	3.47E-07	2.93E-06
5	18	2.00E-07	6.67E-08	1.33E-07	5.24E-11	6.07E-09	5.12E-08
6	41	2.90E-08	1.69E-08	1.21E-08	4.75E-11	5.49E-09	4.64E-08

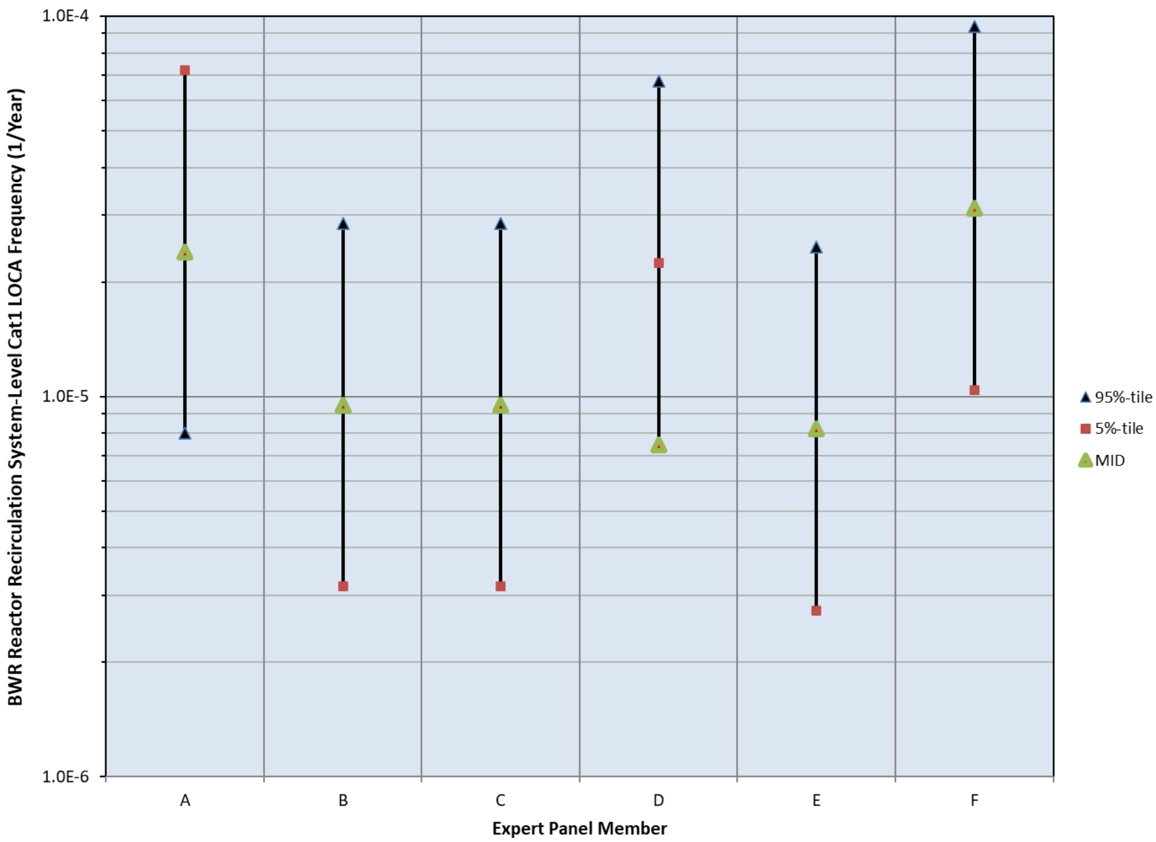

Figure 14: Expert Elicitation Input to System Level LOCA Frequency Assessment

This analysis uses the results of the expert elicitation as input to the development of CFP uncertainty distributions as a function of equivalent break size; it is a "reverse-engineering approach." Specifically, the expert elicitation results come from NUREG-1829 Expert Elicitation Response Sheets with LOCA frequencies provided for each system case. There were ten (10) PWR system cases, and fourteen (14) BWR system cases. Of these system cases, nine PWR system cases and 12 BWR system cases contributed to LOCA Category 4 or higher.

In a first step, lognormal geometric means of the expert elicitation participant results were developed for each system case of interest. Next, a single lognormal distribution for each system case and LOCA category was obtained by taking the geometric mean of the medians of the experts' lognormal distributions as the composite distribution median, and the geometric means of the range factors of the experts' lognormal distributions as the composite distribution range factor. Next the precursor failure frequency system level from NUREG-1829 Volume 2, Appendix D were converted to fit a lognormal distribution, i.e. the precursor frequency. Finally, the three equations below were used to calculate the CFP distributions to be used as prior distribution for each combination of precursor frequency and CFP. Since the use of lognormal distributions enables the LOCA frequency to be expressed as the product of a lognormally distributed precursor frequency and a lognormally distributed CFP, the parameters of the CFP distribution may be calculated using the following equations.

$$Median_{CFP(i)} = \frac{Median_{TLF(i)}}{Median_{Precursor}} \quad \text{Eq. (6)}$$

$$RF_{CFP(i)} = e^{1.645 \times \sigma_{CFP(i)}} \quad \text{Eq. (7)}$$

$$\sigma_{CFP_i} = \sqrt{\left(\frac{ln(RF_{TLF_i})}{1.645}\right)^2 + \left(\frac{ln(RF_{Precursor})}{1.645}\right)^2} \quad \text{Eq. (8)}$$

where

$Median_{CFP(i)}$ is the median of the lognormal distribution for the conditional failure probability in LOCA category i given a precursor failure.

$Median_{TLF(i)}$ is the median of the target LOCA frequency for category i.

$Median_{Precursor}$ is the median of the lognormal distribution for precursor frequency associated with an OpE, system-level analysis summarized in NUREG-1829, Appendix D.

$RF_{CFP(i)}$ is the range factor of the lognormal distribution for the conditional probability of pipe rupture in LOCA category i given pipe failure, equal to $SQRT(95^{th}/5^{th})$ of the lognormal distribution.

σ_{CFP_i} is the logarithmic standard deviation for the lognormal distribution for the conditional failure probability of pipe rupture in LOCA category i given pipe failure.

RF_{TLF_i} is the range factor of the lognormal distribution for target LOCA frequency for category i.

$RF_{Precursor}$ is the range factor for the lognormal distribution for the $Precursor$ frequency.

The medians and range factors of the CFP distributions were calculated from the medians and range factors of the target LOCA frequency distributions using the above formulas. Then, using the properties of the lognormal distribution, the remaining parameters of the distributions are calculated.

NUREG-1829 developed and applied base cases so that the panelists did not have to provide absolute frequencies during the elicitation. Instead, they chose appropriate base cases and provided a relative ratio to express the difference between the base cases and the important contributing variables that they identified. This technique was based on the premise that relative ratios are easier to assess, and therefore more accurate than absolute numbers. The decision to use and the application of these base cases was made by each individual panelist. Some panelists utilized them extensively, others considered the relative trends expressed by the base case estimates, and others chose not to utilize them at all. However, in general, the panelists using the base case estimates chose to anchor their responses to base case results based on OpE instead of the PFM results. Four-of-eight panelists based their BWR-specific responses on OpE, and three-of-nine panelists based their PWR-specific responses on OpE.

The BWR base cases assumed a BWR/4 plant type. The PWR hot leg and surge line base cases were modeled based on a three-loop Westinghouse plant while the high pressure injection (HPI) make-up line was representative of a Babcock & Wilcox (B&W) plant. The BWR base cases addressed IGSCC of dissimilar metal welds, the PWR base cases addressed PWSCC of dissimilar metal welds and thermal fatigue of branch connections between a Reactor Coolant System hot leg and pressurizer surge line and between a Reactor Coolant System cold leg and high-pressure safety injection line.

The model used to convert information on unconditional rupture frequencies to conditional failure probabilities makes use of the NUREG-1829 base case results. Each term in this model is subject to epistemic uncertainty, which is to be estimated. Next, this model and the base case analysis of the precursor rates are used to derive epistemic uncertainties for the CFPs in each LOCA category. This produces a set of TLF distribution parameters that have been selected to incorporate the epistemic uncertainties developed in NUREG-1829. This approach makes use of there being a technical basis for the precursor rate estimates from OpE data and a Bayes' uncertainty analysis method. These estimates were part of the information that was available to each NUREG-1829 expert. Since there have been no Category 1, 2, 3, 4, 5, or 6 LOCAs, the expert elicitation results of all the experts constitute an extrapolation from the OpE data. Therefore, the method simply assumes that the variability in the expert elicitation inputs for LOCA frequency represents the epistemic uncertainty in the LOCA frequency for each evaluation boundary. This epistemic uncertainty is then assumed to result from the combination of the epistemic uncertainty in the precursor rate and the epistemic uncertainty in the conditional probability of each LOCA category.

The expert elicitation that was performed for NUREG-1829 included a request for estimates of LOCA frequencies for specific piping components. Nine expert elicitation panel members provided input at this level. One set of numbers provided by the experts was LOCA frequencies by LOCA category in terms of a mid-value (Mid), an upper bound (UCB), and a lower bound (LCB), with the understanding that those would be interpreted as medians, 95%-tiles, and 5%-tiles of a lognormal uncertainty distribution. For symmetric inputs in the log scale (i.e., when UCB/Mid = Mid/LCB), which were provided in most cases, these distributions were assumed to be lognormal distributions.

In this step, the expert elicitation distributions were combined into a single composite distribution. NUREG-1829 discussed two approaches for developing expert composite distributions: the Mixture Distribution Method and the Geometric Mean Method. NUREG-1829 adopted the latter approach, and this approach was retained for this analysis.

When the geometric distribution method was used in NUREG-1829, it was oriented toward the calculation of the total LOCA frequency rather than the LOCA frequency for multiple locations. In this study, a single lognormal distribution for each base case component and each LOCA category was defined by taking the geometric mean of the medians of the experts' lognormal distributions as the composite distribution median, and the geometric means of the range factors of the experts' lognormal distributions for the LOCA frequencies as the composite distribution range factor. In this study the input lognormal distributions provided by the experts were fit to lognormal distribution by matching the 50th and 95th percentiles. A summary of the composite distribution parameters for the total hot leg LOCA frequencies, representing the PWR-1 base case, is given in Table 18.

Table 18: Derived Composite Distributions Results Based on Geometric Mean Method

Base Case PWR-1	Equivalent Break Size (in.)	LOCA Frequency (1/Year)				
		Mean	5%-tile	Median	95%-tile	Range Factor
Reactor Coolant System Hot Leg	≥ 0.5	4.08E-07	9.32E-09	1.21E-07	1.57E-06	13.0
	≥ 1.5	1.28E-07	2.25E-09	3.34E-08	4.95E-07	14.8
	≥ 3	6.51E-08	1.01E-09	1.59E-08	2.52E-07	15.8
	≥ 6.75	2.59E-08	2.49E-10	4.96E-09	9.88E-08	19.9
	≥ 14	1.50E-08	6.70E-11	1.90E-09	5.37E-08	28.3
	≥ 31.5	3.16E-09	4.84E-12	2.18E-10	9.78E-09	45.0

Next step in the analysis established inputs to the selection of target LOCA frequencies from the NUREG-1829 base case analyses. A secondary purpose was to establish the corresponding precursor rate and CFP distributions that are responsible for the base case results. The precursor rate distribution parameters were used to convert the target LOCA frequency distributions to CFP distributions.

The "risk triplet" model was applied to the precursor rate estimates derived and documented in Appendix D of NUREG-1829, assuming a lognormal distribution for the for each LOCA category. This resulted in lognormal parameters that reproduce the Appendix D results. The CFP distribution parameters were obtained by first developing the LOCA frequencies and then calculating the CFP distribution parameters using formulas for calculating the parameters for the product of two lognormal distributions. The underlying lognormal distribution parameters for the precursor and CFP distributions are shown in Table 19 for the PWR-1 base case. The uncertainty distribution parameters for the LOCA frequencies from this reconstruction of NUREG-1829 Appendix D results are shown in Table 20 for the PWR-1 base case. Table 19 and Table 20 are included for comparison.

Table 19: Precursor Rate and CFP Distributions Matching NUREG-1829 Appendix D

Base Case	LOCA Category	Break Size (in.)	Mean	5%tile	Median	95%tile	Range Factor
PWR-1 RCS Hot Leg	Precursor Rate (1/Year)		3.46E-04	1.01E-05	1.15E-04	1.32E-03	11.4
	1	≥ 0.5	1.67E-03	9.49E-05	7.55E-04	6.01E-03	8.0
	2	≥ 1.5	1.18E-04	5.38E-06	4.85E-05	4.37E-04	9.0
	3	≥ 3	4.73E-05	2.13E-06	1.93E-05	1.75E-04	9.1
	4	≥ 6.75	1.76E-05	7.71E-07	7.09E-06	6.52E-05	9.2
	5	≥ 14	6.59E-06	2.97E-07	2.69E-06	2.43E-05	9.1
	6	≥ 31.5	3.23E-06	1.38E-07	1.28E-06	1.20E-05	9.3

Table 20: LOCA Frequency Distributions from Benchmarking of Appendix D Results

Evaluation Boundary	LOCA Category	Break Size (in.)	Mean	5%tile	Median	95%tile	Range Factor
PWR-1 RCS Hot Leg	1	≥ 0.5	5.78E-07	3.53E-09	8.88E-08	2.13E-06	24.6
	2	≥ 1.5	4.08E-08	2.10E-10	6.15E-09	1.49E-07	26.6
	3	≥ 3	1.64E-08	8.33E-11	2.42E-09	5.95E-08	26.7
	4	≥ 6.75	6.09E-09	3.03E-11	8.93E-10	2.21E-08	27.0
	5	≥ 14	2.28E-09	1.16E-11	3.29E-10	8.29E-09	26.7
	6	≥ 31.5	1.12E-09	5.44E-12	1.58E-10	4.04E-09	27.3

In selecting the target LOCA frequencies, different options may be considered. A first option would be to only consider the base case results as documented in Appendix D of NUREG-1829. A second option would be to make use of the experts' geometric mean results. Parameters of the target LOCA frequency based on the second option are given in Table 21.

Finally, the CFP was obtained by dividing the median TLF with the median precursor rate. The medians and range factors of the CFP distributions were computed from the medians and range factors of the target LOCA frequency distributions. Then, using the properties of the lognormal distribution, the remaining parameters of the CFP distributions were calculated directly, Table 22 and Table 23.

Table 21: Parameters of the Target LOCA Frequency for PWR-1

Base Case	LOCA Category	Break Size (in.)	Target LOCA Frequency Distribution Parameters (1/Year)				
			Mean	5%-tile	50%-tile	95%-tile	RF
PWR-1	1	≥ 0.5	5.07E-07	6.31E-09	1.16E-07	2.15E-06	18.4
	2	≥ 1.5	8.22E-08	4.29E-10	1.49E-08	3.30E-07	27.7
	3	≥ 3	4.10E-08	1.68E-10	6.47E-09	1.60E-07	30.9
	4	≥ 6.75	1.57E-08	5.65E-11	2.09E-09	6.07E-08	32.8
	5	≥ 14	8.69E-09	2.09E-11	7.64E-10	2.93E-08	37.4
	6	≥ 31.5	2.11E-09	5.01E-12	1.79E-10	6.63E-09	36.4

Table 22: PWR Base Case CFP Distribution Parameters

Base Case	LOCA Category	Break Size (in.)	Mean	5%tile	Median	95%tile
PWR-1	1	≥ .5	1.61E-03	7.42E-06	7.54E-04	6.11E-03
	2	≥ 1.5	1.24E-04	2.90E-07	4.76E-05	4.44E-04
	3	≥ 3	4.49E-05	1.12E-07	1.89E-05	1.78E-04
	4	≥ 6.75	1.67E-05	3.89E-08	6.95E-06	6.62E-05
	5	≥ 14	6.25E-06	1.59E-08	2.64E-06	2.47E-05
	6	≥ 31.5	3.05E-06	6.47E-09	1.25E-06	1.22E-05
PWR-2	1	≥ .5	7.65E-03	7.07E-04	5.82E-03	2.02E-02
	2	≥ 1.5	6.63E-04	3.02E-05	4.51E-04	2.02E-03
	3	≥ 3	2.59E-04	1.17E-05	1.76E-04	7.88E-04
	4	≥ 6.75	9.68E-05	3.47E-06	6.34E-06	3.04E-04
	5	≥ 14	3.58E-05	1.78E-06	2.47E-05	1.08E-04

Table 23: BWR Base Case CFP Distribution Parameters

Base Case	LOCA Category	Break Size (in.)	Mean	5%tile	Median	95%tile
BWR-1a / BWR-1b	1	≥ 0.5	6.94E-03	2.74E-04	4.47E-03	2.21E-02
	2	≥ 1.875	1.68E-03	1.01E-05	8.22E-04	6.28E-03
	3	≥ 3.24	5.50E-04	5.11E-06	2.90E-04	1.98E-03
	4	≥ 7	1.67E-04	1.51E-06	8.73E-05	6.03E-04
	5	≥ 18	6.64E-05	3.18E-08	2.11E-05	2.86E-04

3.1.5 Probabilistic Failure Metrics of Interest

The OpE analysis develops probability density functions for each element in the risk triplet. The selected quantities of interest were obtained using Microsoft® Excel with two add-in programs, one for Bayesian reliability estimation to determine the updated precursor rates and another for a Monte Carlo multiplication procedure to combine S_i and P_i to produce results in the form of cumulative frequencies for each LOCA category.

3.2 Updated Base Case Results

Results are presented for the PWR and BWR component-level Base Case calculations, with evaluation boundaries corresponding those in Section 2.1.1. The component-level results include the updated precursor frequencies that are based on the 2005 to 2024 OpE and the frequencies for each LOCA category. The system- and plant-level LOCA frequencies are intended to be representative of a typical BWR3/4 plant and a typical 3-loop Westinghouse PWR plant. An example of calculation is given in Section 7.3.

3.2.1 Case PWR-1: PWR RVON

The selected evaluation boundary corresponds to that of Westinghouse PWR dissimilar metal weld (DMW) between the Reactor Pressure Vessel (RPV) outlet nozzle (stainless steel clad carbon steel) and the RCS hot leg pipe (austenitic stainless steel). The results are summarized in Table 24 and Table 25.

Table 24: PWR-1 Base Case Component-Level Results

Base Case	Category	Mean	5%-tile	50%-tile	95%-tile
PWR-1 PWR1: RC-HL @ RPV Outlet ASME XI Category B-F Weld	Precursor Frequency (1/B-F and Year)	1.28E-05	2.33E-08	1.81E-06	6.24E-05
	Cat1	1.77E-08	6.95E-11	8.04E-09	6.79E-09
	Cat2	4.06E-09	1.60E-11	1.85E-11	1.56E-08
	Cat3	2.05E-09	8.06E-12	9.32E-10	7.87E-09
	Cat4	7.26E-10	1.15E-11	3.30E-10	2.79E-09
	Cat5	3.17E-10	1.24E-12	1.44E-10	1.22E-09
	Cat6	7.47E-11	2.94E-13	3.40E-11	2.87E-10

Table 25: PWR-1 Base Case System-Level Results

Calculation Case	LOCA Category	System-Level LOCA Frequency (1/Calendar-Year)				Weld Population
		Mean	5%-tile	50%-tile	95%-tile	
PWR1: RC-HL @ RPV Outlet ASME XI Category B-F Weld	Cat1	5.31E-08	2.09E-10	2.42E-08	2.04E-07	WE 3-Loop Plant
	Cat2	1.22E-08	4.80E-11	5.55E-09	4.69E-08	
	Cat3	6.15E-09	2.42E-11	2.80E-09	2.36E-08	
	Cat4	2.18E-09	8.55E-12	9.89E-10	8.35E-09	
	Cat5	9.50E-10	3.74E-12	4.32E-10	3.65E-09	
	Cat6	2.24E-10	8.82E-13	1.02E-10	8.61E-10	

3.2.2 Case PWR-2a/PWR-2b: PWR Pressurizer Surge Line

The pressurizer surge line connects the bottom of the pressurizer to one of the reactor coolant system hot legs (RC-HL). Case 2 includes two evaluation boundaries, the dissimilar metal weld between the stainless steel surge line and the pressurizer nozzle (a B-F weld), and between the surge line and the RC-HL branch connection (a B-J weld). The results for both evaluation boundaries are summarized in Table 26.

Table 26: PWR-2 Base Case Results

Calculation Case	LOCA Category	LOCA Frequency (1/Weld-Year)			
		Mean	5%-tile	50%-tile	95%-tile
PWR-2a Pressurizer Surge Line ASME XI Category B-F Weld	Precursor frequency	5.12E-05	7.31E-08	6.06E-06	2.48E-04
	Cat1	7.06E-08	2.78E-10	3.21E-08	2.71E-07
	Cat2	1.62E-08	6.38E-11	7.39E-09	6.24E-08
	Cat3	8.19E-09	3.22E-11	3.73E-09	3.15E-08
	Cat4	2.90E-09	1.14E-11	1.32E-09	1.11E-08
	Cat5	1.26E-09	4.98E-12	5.76E-10	4.86E-09
PWR-2b Pressurizer Surge Line @ RC-HL Branch Connection	Precursor frequency	6.32E-06	2.63E-08	2.58E-07	2.24E-05
	Cat1	8.72E-09	3.43E-11	3.96E-09	3.35E-08
	Cat2	2.00E-09	7.86E-12	9.10E-10	7.68E-09
	Cat3	1.01E-09	3.97E-12	4.60E-10	3.88E-09
	Cat4	3.57E-10	1.40E-12	1.63E-10	1.37E-09
	Cat5	1.56E-10	6.13E-13	7.09E-11	5.98E-10

3.2.3 Case BWR-1a: BWR 28” Recirculation Line

The Reactor Recirculation system for BWR3/4/5/6 consists of two main piping loops external to the reactor vessel and 20 jet pumps which are internal to the reactor vessel. The BWR-1 base case evaluation boundary includes the dissimilar metal weld between the stainless steel main loop piping and the reactor pressure vessel nozzle. The Base Case BWR-1a results are summarized in Table 27 and Table 28.

Table 27: Component-Level BWR-1a LOCA Frequencies

Calculation Case	LOCA Category	LOCA Frequency (1/Weld-Year)			
		Mean	5%-tile	50%-tile	95%-tile
BWR-1a NPS28 B-F Weld	Precursor frequency	8.74E-05	3.84E-07	2.18E-05	4.01E-04
	Cat1	1.21E-07	4.75E-10	5.49E-08	4.64E-07
	Cat2	2.77E-08	1.09E-10	1.26E-08	1.07E-07
	Cat3	1.40E-08	5.51E-11	6.37E-09	5.38E-08
	Cat4	4.95E-09	1.95E-11	2.25E-09	1.90E-09
	Cat5	2.16E-09	8.47E-12	9.81E-10	8.28E-09

Table 28: System-Level BWR-1a LOCA Frequencies

Calculation Case	LOCA Category	System-Level LOCA Frequency (1/Calendar-Year)				Weld Population
		Mean	5%-tile	50%-tile	95%-tile	
BWR-1a B-F Weld	Cat1	2.41E-07	9.49E-10	1.10E-07	9.28E-07	2
	Cat2	5.54E-08	2.18E-10	2.52E-08	2.13E-07	
	Cat3	2.80E-08	1.10E-10	1.27E-08	1.07E-07	
	Cat4	9.90E-09	3.89E-11	4.50E-09	3.80E-09	
	Cat5	4.32E-09	1.70E-11	1.96E-09	1.66E-08	

3.2.4 Case BWR-1b: BW R 12” Recirculation Line

The Reactor Recirculation system for BWR3/4/5/6 consists of eight NPS12 risers off the NPS20 manifold. The Base Case-1b evaluation boundary includes the dissimilar metal weld between the stainless steel riser piping and the reactor pressure vessel outlet nozzle. The Base Case-1b results are summarized in Table 29 and Table 30.

Table 29: Component-Level BWR-1b LOCA Frequencies

Calculation Case	LOCA Category	LOCA Frequency (1/Weld-Year)			
		Mean	5%-tile	50%-tile	95%-tile
BWR-1b NPS12 ASME XI Category B-F Weld	Precursor frequency	3.20E-05	3.44E-07	1.24E-05	1.31E-04
	Cat1	4.41E-08	1.74E-10	2.01E-08	1.70E-07
	Cat2	1.01E-08	3.99E-11	4.61E-09	3.90E-08
	Cat3	5.12E-09	2.01E-11	2.33E-09	1.97E-08
	Cat4	1.81E-09	7.12E-12	8.24E-10	6.96E-09

Table 30: System-Level BWR-1b LOCA Frequencies

Calculation Case	LOCA Category	System-Level LOCA Frequency (1/Calendar-Year)				Weld Population
		Mean	5%-tile	50%-tile	95%-tile	
BWR-1b NPS12 ASME XI Category B-F Weld	Cat1	3.53E-07	1.39E-09	1.60E-07	1.35E-06	8
	Cat2	8.11E-08	3.19E-10	3.69E-08	3.12E-07	
	Cat3	4.09E-08	1.61E-10	1.86E-08	1.57E-07	
	Cat4	1.45E-08	5.70E-11	6.59E-09	5.57E-08	

3.3 Updated LOCA-Sensitive Piping Results

This section documents the component and system-level results for the LOCA-sensitive piping identified in Table 31. The results include the updated precursor frequencies that are based on the 2005 to 2024 domestic OpE and the frequencies for each LOCA category. The system- and plant-level LOCA frequencies are intended to be representative of a typical BWR3/4 plant and a typical 3-loop Westinghouse PWR plant.

Table 31: LOCA Sensitive PWR And BWR Piping > NPS6

PWR LOCA-Sensitive Piping		Pipe Inside Diameter (inch) Typical of WE 3 Loop
System	**Pipe Segment(s)**	
Reactor Coolant System (RCS)	RCS Cold Leg	27.5
	RCS Hot Leg @ Steam Generator Inlet	29
	RCS Cross-over Leg	31
	Pressurizer Surge Line	11.88
Residual Heat Removal System (RHR)	RHR Suction Line - off of RCS Hot Leg	10.126
	RHR Discharge to Cold Leg	8.5
	RHR Discharge to Cold Leg	6.813
	RCS Hot Leg Recirculation	6.813
Safety Injection System (SIS)	Accumulator Discharge to Cold Leg	10.126
	RCS Hot Leg Recirculation	6.813
BWR LOCA-Sensitive Piping		**Pipe Inside Diameter (inch) - Typical of BWR/4**
System	**Pipe Segment(s)**	
Reactor Recirculation (RR)	RR Loop Suction and Discharge piping	28
	RR Riser piping	10.75
	RR Distribution Manifold	22
Main Steam System (MS)	MS - inside containment	17.938
Feedwater System (FW)	FW - inside containment	15.25
	FW - inside containment	10.75
Residual Heat Removal (RHR) / Low-Pressure Coolant Injection (LPCI)	RHR influent lines from RR loops to containment penetration & LPCI injection line inside containment	14.312
		12.5
High-Pressure Coolant Injection (HPCI)	HPCI discharge piping	9.562
High-Pressure Core Spray (HPCS)	HPCS discharge piping – BWR-5 & BWR/6	12.5
Low-Pressure Core Spray (LPCS)	LPCS discharge piping	9.562
Reactor Water Cleanup System (RWCU)	RWCU from one RR loop to containment penetration	7.625

3.3.1 PWR Cold Leg & Cross-Over Leg

The RCS cold leg return line to the reactor vessel is 27-1/2 inches. The piping between the steam generator and the reactor coolant pump suction is 31 inches in inside diameter to reduce pressure drop and improve flow conditions to the pump suction. Precursor rates and LOCA frequencies are given for the RCS cold leg ASME XI Category B-F welds. In general, the PWSCC precursor frequency is strongly dependent on sufficiently high tensile surface stress, susceptible material, and the elevated temperature environment of the PWR. Based on OpE data it can be shown that the ratio of RCS cold leg to RCS hot leg PWSCC susceptibility is on the order of 6×10^{-2} or less (i.e., there was one event in the cold leg and 16 in the hot leg). This yields a precursor rate of about 8.0×10^{-7} per B-F weld and year. The component-level B-F weld LOCA frequencies are given in Table 32 and the corresponding estimated plant-level LOCA frequencies are given in Table 33 for a typical 3-loop Westinghouse PWR.

Table 32: RCS Cold Leg Component-Level Results

Analysis Case	Category	Mean	5%-tile	50%-tile	95%-tile
RCS Cold Leg B-F Weld	Precursor Frequency (1/B-F and Year)	8.00E-07	7.62E-09	1.52E-07	3.05E-06
	Cat1	1.29E-09	5.07E-12	5.86E-10	4.95E-09
	Cat2	9.92E-11	3.90E-13	4.51E-11	3.81E-10
	Cat3	3.59E-11	1.41E-13	1.64E-11	1.38E-10
	Cat4	1.34E-11	5.26E-14	6.08E-12	5.14E-11
	Cat5	5.00E-12	1.97E-14	2.28E-12	1.92E-11
	Cat6	2.44E-12	9.59E-15	1.11E-12	9.37E-12

Table 33: RCS Cold Leg Plant-Level LOCA Frequencies

Calculation Case	LOCA Category	System-Level LOCA Frequency (1/Calendar-Year)			
		Mean	5%-tile	50%-tile	95%-tile
RC-CL @ RPV Inlet, Steam Generator Outlet and Reactor Coolant Pump Inlet/Outlet Nozzles	Cat1	1.55E-08	6.09E-11	7.04E-09	5.95E-08
	Cat2	1.19E-09	4.68E-12	5.42E-10	4.57E-09
	Cat3	4.31E-10	1.70E-12	1.96E-10	1.66E-09
	Cat4	1.60E-10	6.30E-13	7.29E-11	6.16E-10
	Cat5	6.00E-11	2.36E-13	2.73E-11	2.31E-10
	Cat6	2.93E-11	1.15E-13	1.33E-11	1.12E-10

3.3.2 PWR Reactor Coolant System Branch Connections > 6”

The Class 1 portion of the RHR piping consists of the suction and discharge lines (also used as a low-head safety injection pathway during SIS actuation). The Class 1 portion of the SIS piping consists of all piping connecting the SIS to the RCS hot and cold legs. This piping includes the lines from the SIS pumps to the hot legs (for use during hot leg recirculation), and the lines from the accumulators to the cold legs. The component-level LOCA frequencies are given in Table 34 and the corresponding estimated plant-level LOCA frequencies are given in Table 35 for a typical 3-loop Westinghouse PWR.

Table 34: RHR & SI Component-Level LOCA Frequencies

Analysis Case	Category	Mean	5%-tile	50%-tile	95%-tile
RHR @ RC Hot Leg Branch Connection	Precursor Frequency (1/Weld and Year)	1.93E-05	4.37E-06	1.67E-05	4.33E-05
	Cat1	1.48E-07	5.80E-10	6.71E-08	5.67E-07
	Cat2	1.28E-08	5.03E-11	5.82E-09	4.91E-08
	Cat3	4.99E-09	1.97E-11	2.28E-09	1.92E-08
	Cat4	1.87E-09	7.34E-12	8.49E-10	7.17E-09
	Cat5	6.91E-10	2.72E-12	3.14E-10	2.65E-09
RHR & SI ASME XI B-J Welds	Precursor Frequency (1/Weld and Year)	9.85E-07	3.87E-09	4.48E-07	3.72E-06
	Cat1	7.54E-09	2.96E-11	3.25E-09	2.89E-08
	Cat2	6.52E-10	2.57E-12	2.97E-10	2.51E-09
	Cat3	2.54E-10	1.00E-12	1.16E-10	9.80E-10
	Cat4	9.53E-11	3.75E-13	4.33E-11	3.66E-10
	Cat5	3.53E-11	1.39E-13	1.60E-11	1.35E-10

Table 35: RHR & SIS Plant-Level LOCA Frequencies

Analysis Case	Category	Mean	5%-tile	50%-tile	95%-tile
RHR @ RC Hot Leg Branch Connection	Cat1	2.95E-07	1.16E-09	1.35E-07	1.14E-06
	Cat2	2.56E-08	1.00E-10	1.16E-08	9.80E-08
	Cat3	9.97E-09	3.92E-11	4.54E-09	3.83E-08
	Cat4	3.73E-09	1.47E-11	1.70E-09	1.43E-08
	Cat5	1.38E-09	5.43E-12	6.28E-10	5.31E-09
RHR & SI ASME XI B-J Welds	Cat1	7.01E-07	2.76E-09	3.19E-07	2.69E-06
	Cat2	6.07E-08	2.38E-10	2.76E-08	2.33E-07
	Cat3	2.37E-08	9.32E-11	1.08E-08	9.10E-08
	Cat4	8.86E-09	3.49E-11	4.03E-09	3.41E-08
	Cat5	3.28E-09	1.29E-11	1.50E-09	1.26E-08

3.3.3 BWR Primary Pressure Boundary Piping > 6”

This section includes a summary of the updated precursor rate analysis. The analysis considered the post-2004 OpE for dissimilar metal and similar-metal welds > 6” within the primary pressure boundary. The results of the analyses are given in Table 36 and Table 37.

Table 36: Updated BWR Primary System Precursor Weld Precursor Rates

BWR Category B-J Weld Precursor Rates						Weld Population
System	**NPS**	**Mean**	**5%-tile**	**50%-tile**	**95%-tile**	
FW	12	4.41E-07	1.96E-10	1.91E-08	1.62E-06	28
	18	3.93E-07	1.95E-10	1.89E-08	1.52E-06	41
HPCI	10	6.18E-06	1.28E-08	9.61E-07	3.00E-05	20
LPCS	10	8.51E-06	1.22E-08	1.01E-06	4.13E-05	10
MS	20	3.04E-07	1.92E-10	1.82E-08	1.30E-06	87
RHR	14	7.76E-06	1.61E-08	1.21E-06	3.76E-05	16
	16	4.89E-06	1.46E-08	9.70E-07	2.32E-05	35
RR	12	7.42E-05	2.75E-06	4.38E-05	2.49E-04	12
	22	1.84E-05	2.33E-08	1.98E-06	8.87E-05	4
	28	6.98E-06	1.84E-08	1.28E-06	3.35E-05	22
RWCU	8	7.76E-06	1.61E-09	1.21E-06	3.76E-05	16
BWR Category B-F Weld Precursor Rates						**Weld Population**
System	**NPS**	**Mean**	**5%-tile**	50%-tile	95%-tile	
FW Safe-end-to-RPV Nozzle	12	1.84E-05	2.33E-08	1.98E-06	8.87E-05	4
MS Safe-end-to-RPV Nozzle	26	3.96E-06	1.95E-09	1.89E-07	1.53E-05	4
RR Safe-end-to-RPV Nozzle	12	3.20E-05	3.44E-07	1.24E-05	1.31E-04	Base Case BWR-1a/1b
	28	8.74E-05	3.84E-07	2.18E-05	4.01E-04	

Table 37: BWR Plant-Level LOCA Frequencies

LOCA Category	Mean	5%-tile	50%-tile	95%-tile
Feedwater				
Cat1	7.08E-07	2.79E-09	3.22E-07	2.72E-06
Cat2	1.71E-07	6.73E-10	7.79E-08	6.58E-07
Cat3	5.61E-08	2.21E-10	2.55E-08	2.16E-07
Cat4	1.70E-08	6.71E-11	7.76E-09	6.56E-08
Cat5	1.07E-09	4.21E-12	4.87E-10	4.11E-09
High-Pressure Coolant Injection				
Cat1	8.58E-07	3.37E-09	3.90E-07	3.30E-06
Cat2	2.08E-07	8.16E-10	9.44E-08	7.97E-07
Cat3	6.80E-08	2.68E-10	3.10E-08	2.61E-07
Cat4	2.07E-08	8.12E-11	9.40E-09	7.94E-08
Low-Pressure Core Spray				
Cat1	5.90E-07	2.32E-09	2.69E-07	2.27E-06
Cat2	1.43E-07	5.62E-10	6.50E-08	5.49E-07
Cat3	4.68E-08	1.84E-10	2.13E-08	1.80E-07
Cat4	1.42E-08	5.59E-11	6.46E-09	5.46E-08
Main Steam				
Cat1	2.94E-07	1.16E-09	1.34E-07	1.13E-06
Cat2	7.11E-08	2.80E-10	3.24E-08	2.73E-07
Cat3	2.33E-08	9.15E-11	1.06E-08	8.93E-08
Cat4	7.07E-09	2.78E-11	3.22E-09	2.72E-08
Cat5	2.81E-09	1.11E-11	1.28E-09	1.08E-08
Reactor Water Cleanup				
Cat1	8.62E-07	3.39E-09	3.92E-07	3.31E-06
Cat2	2.09E-07	8.19E-10	9.48E-08	8.00E-07
Cat3	6.83E-08	2.69E-10	3.11E-08	2.62E-07
Cat4	2.07E-08	8.16E-11	9.44E-09	7.97E-09

3.4 Updated Non-Piping LOCA Frequencies

In addition to developing base case frequencies for piping systems, NUREG-1829 developed base case frequencies for a number of non-piping components. These studies included: a steam generator tube rupture (SGTR) frequency study, an overview of the pressurized thermal shock (PTS) re-evaluation effort, and BWR vessel rupture and PWR control rod drive mechanism (CRDM) ejection analyses. The results of the PTS re-evaluation are found in NUREG-1806 ("Technical Basis for Revision of the Pressurized Thermal Shock (PTS) Screening Limit in the PTS Rule (10 CFR 50.61)"). The scope of this "Operating Experience Analysis" included a task to update the SGTR frequency analysis and the CRDM ejection analysis.

3.4.1 Updated Steam Generator Tube Rupture Frequency Assessment

In NUREG-1829, the SGTR frequency assessment was based on domestic OpE. The base case assessment accounted for (4) ruptures in the period 1987 to 2002 that produced a loss of primary coolant in excess of 100 gpm. The analysis yielded a SGTR frequency of 3.5×10^{-3} per calendar year. These results were updated in two steps to include all reported SGTR events to date, Table 38. The results of the first step of the updated SGTR frequency analysis to reflect OpE up through 2024 are shown in Figure 15. In the second step, and to reflect an assumption that most, -if-not all plants have new steam generators, the PWSCC events were screened out to amplify the effect of going from Alloy 600 to 690 tube material. The Bayesian update of the prior SGTR results by excluding PWSCC events is shown in Figure 16.

Table 38: Summary of SGTR Events

Plant	Event Date	Through-Wall Leak Rate (l/s)	Rupture Characteristics
Point Beach-1	2/26/1975	7.9	Axially aligned bulges, the total length of which was less than 38 mm, neither of which exceeded about 20 mm in length and width.
Surry-2	9/15/1976	5.1	114.3 mm axial opening. PWSCC in U-bend
Doel-2	6/25/1979	15	100 mm axial opening. PWSCC in U-bend.
Prairie Island-1	10/2/1979	24.7	38 mm axial opening
Prairie Island-1	1/25/1982	21.2	Overpressure burst running 37.5 mm in the longitudinal direction of the tube with an opening width of 13 mm.
R.E. Ginna	5/16/1984	48.3	100 mm axial opening
Fort Calhoun	5/16/1984	7	32 mm axial opening. ODSCC at crevice.
North Anna-1	7/15/1987	40.2	360-degree rupture.
North Anna-1	2/25/1989	4.8	Failed mechanical plug severed at about 6 mm above expander portion of plug.
McGuire-1	3/7/1989	31.7	95 mm axial opening. ODSCC in the free span.
Mihama-2	2/9/1991	22.2	360-degree rupture.
Palo Verde-2	3/14/1993	15.1	65 mm axial opening. Caused by ODSCC.
Tihange-3	7/2/1996	11.1	35 mm axial opening
Indian Point-2	2/15/2000	9.5	63.5 mm axial opening. PWSCC in U-bend.
Ulchin-4	4/5/2002	35.4	75 mm axial and 10 mm circumferential opening. Caused by PWSCC at top of tube sheet.

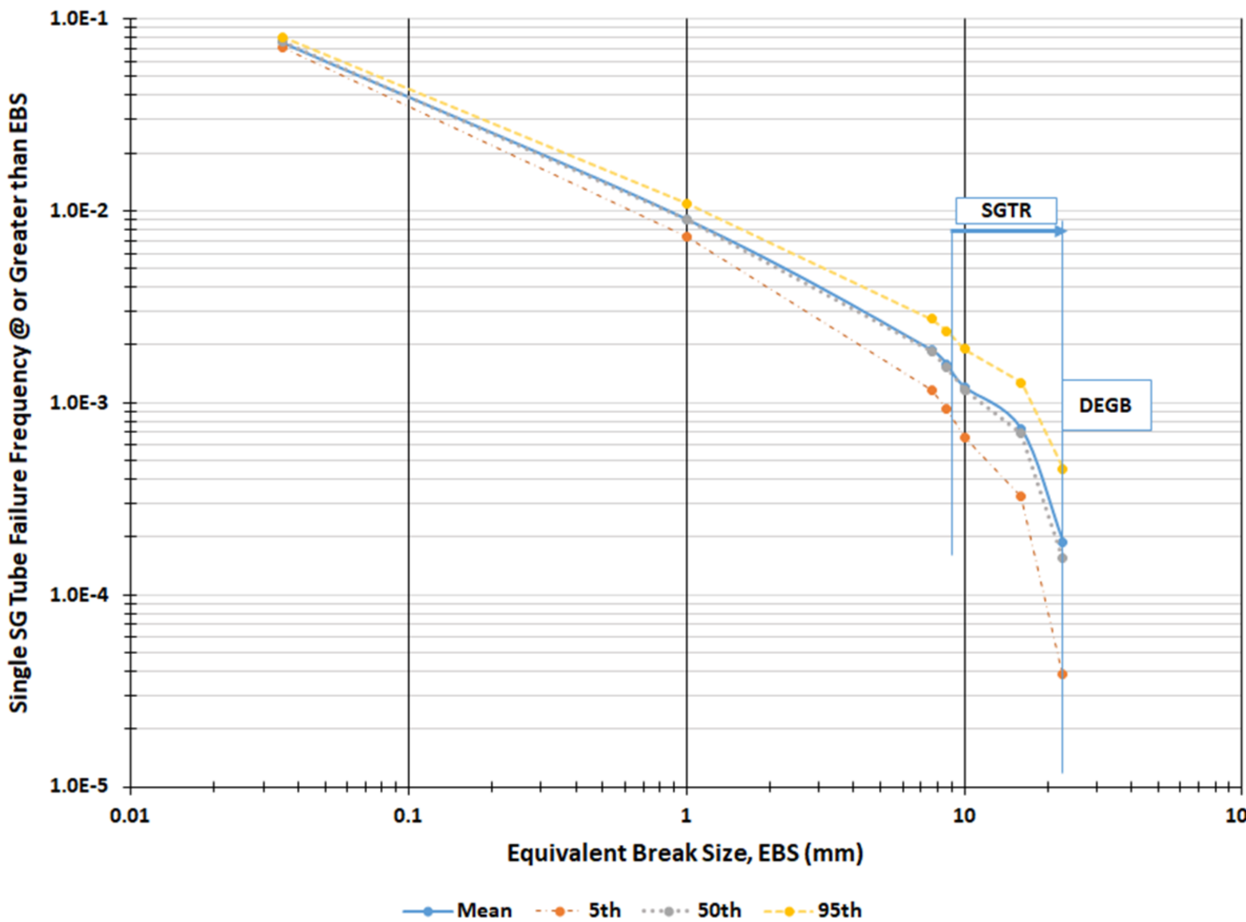

Figure 15: SGTR Frequency with No PWSCC Mitigation & No Loose Parts Monitoring

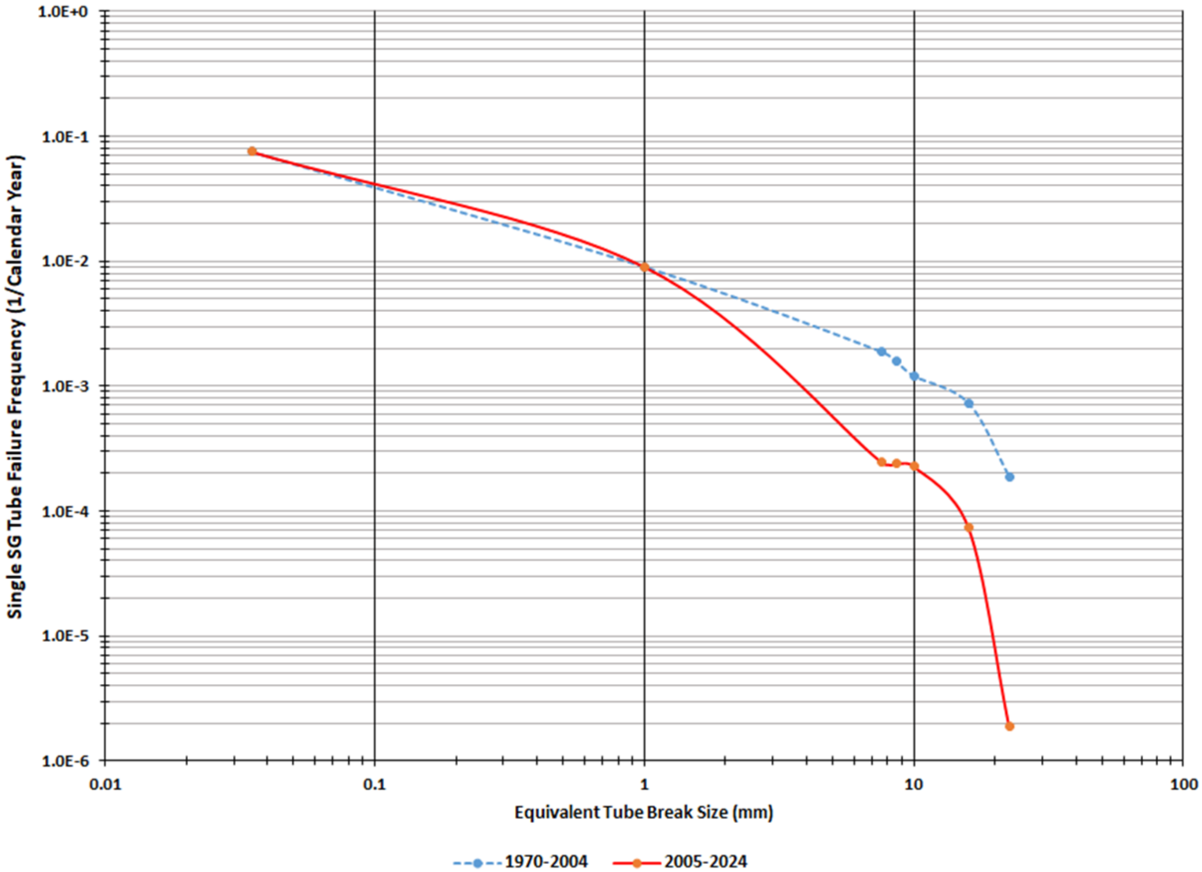

Figure 16: Updated SGTR Frequency with PWSCC Events Screened Out.

3.4.2 PWR Pressure Vessel Head Penetration Failure Frequency

The original base case LOCA frequencies attributed to PWR reactor pressure vessel head penetration (VHP) failures were estimated from a detailed analysis using a model that incorporated probabilistic fracture mechanics and a Weibull analysis of the frequency of nozzle cracking or leakage as a function of operating time and temperature. The VHP OpE is shown in Figure 17. The post-2004 OpE illustrated in Figure 17 comes from nine (9) reactor units. Several plants have replaced there susceptible VHP materials with more resistant materials or made repairs of affected nozzles using more resistant materials. In addition, increased inspection is performed to identify degradation before it becomes significant. Consequently, the precursor events have generally decreased since 2010. If it is assumed that these PWSCC mitigation measures have been fully effective, updated VHP LOCA frequencies can be developed assuming that no additional failures have occurred since 2004. The NUREG-1829 "average VHP frequencies" were converted to a CNID to produce a prior LOCA frequency which was updated assuming zero failures post-2004. These updated VHP LOCA frequencies are given in Table 39. Single VHP failures cannot lead to a LOCA above Category 3.

Table 39: Updated PWR VHP LOCA Frequencies

LOCA Category	Break Size		NUREG-1829 @ 25 Years	NUREG-1829 @ 40 Years	2024 Update (1/Year)			
	GPM	NPS	Avg. Frequency	Avg. Frequency	Mean	5%-tile	50%-tile	95%-tile
0	N/A	N/A	2.0E-02	5.0E-03	6.78E-05	2.67E-07	3.08E-05	2.60E-04
1	100	0.5	2.3E-03	2.8E-04	7.69E-06	3.03E-09	3.50E-06	2.96E-05
2	1500	1.5	2.5E-04	5.0E-05	8.48E-07	3.33E-09	3.86E-07	3.26E-06
3	5000	3.5	4.0E-08	2.0E-09	1.36E-10	5.33E-13	6.16E-11	5.21E-10

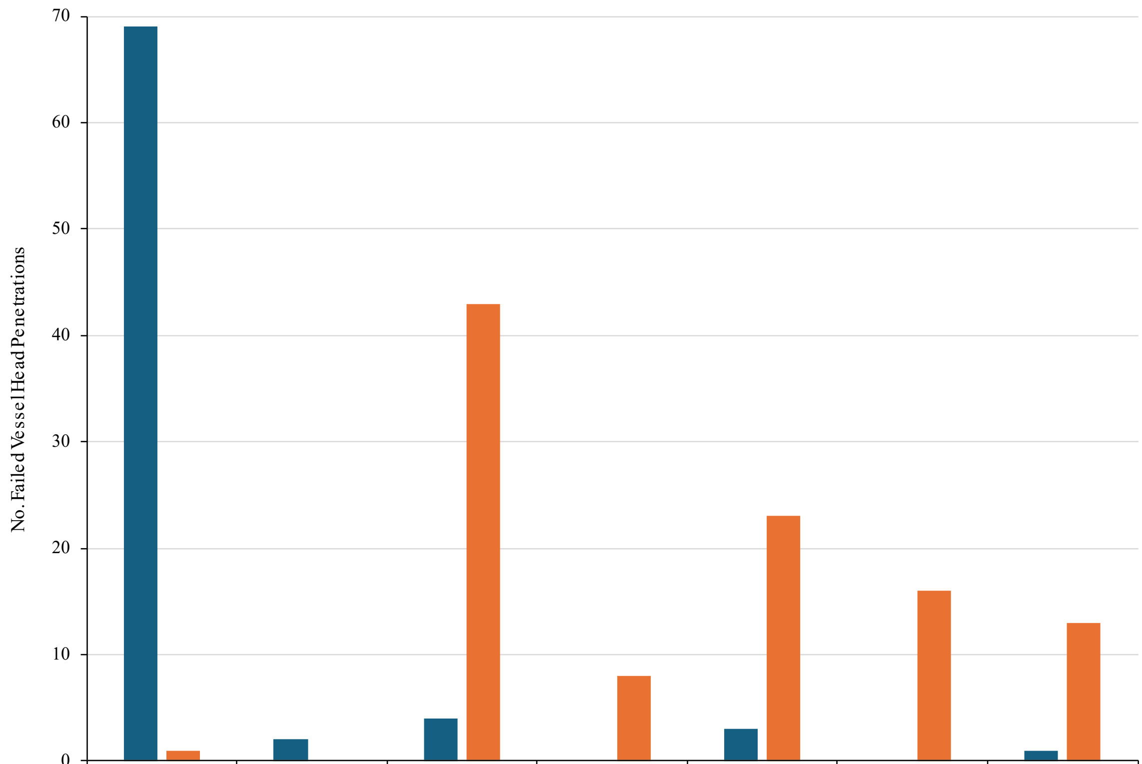

	1990-94	1995-99	2000-04	2005-09	2010-14	2015-19	2020-24
INT-OE	69	2	4		3		1
US-OE	1		43	8	23	16	13

Figure 17: PWR Vessel Head Penetration Operating Experience.

3.5 System- and Plant-Level Piping LOCA Frequencies

This analysis developed updated piping LOCA frequency distributions that accounted for the post-2004 OpE. Uncertainty distributions were developed at the component-, system- and plant-level, and a comparison was made against the NUREG-1829 results. As a general observation, relative to NUREG-1829 the updated, current-day (2024) BWR and PWR LOCA frequencies are lower by at least about an order of magnitude, Figure 18, Figure 19, Figure 20, and Figure 21. This reduction in LOCA frequencies is attributed to factors such as:

- Material changes such from stainless steel 304 to 316L/NG and nickel base material Alloy 600 to Alloy 690 and from Alloy 82/182 to 52/182.
- Application of full structural weld overlays and optimized weld overlays.
- Stress improvements through application of induction heat stress improvement (IHSI), mechanical stress improvement, cavitation/jet peening, shot peening, laser peening, in situ heat treatment, and improved welding preparations.
- Environmental changes such as BWR hydrogen water injection and noble metal chemical addition.

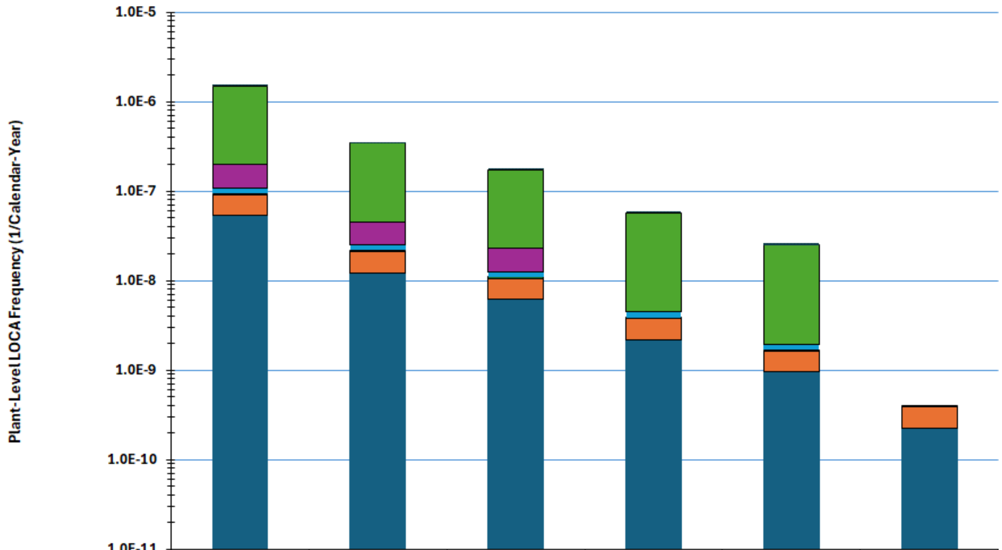

	Cat1	Cat2	Cat3	Cat4	Cat5	Cat6
SIS	6.03E-08	1.38E-08	6.99E-09	2.47E-09	1.08E-09	
RHR	1.29E-06	2.97E-07	1.50E-07	5.31E-08	2.32E-08	
PRZ-PORV & SRV Lines	8.91E-08	2.05E-08	1.03E-08			
PRZ-Surge Line	1.46E-08	3.35E-09	1.69E-09	5.98E-10	2.61E-10	
RC-CL	3.32E-09	7.62E-10	3.85E-10	1.36E-10	5.94E-11	1.40E-11
RC-HL @ SG Inlet	3.84E-08	8.82E-09	4.45E-09	1.58E-09	6.87E-10	1.62E-10
RC-HL RPV Outlet	5.31E-08	1.22E-08	6.15E-09	2.18E-09	9.50E-10	2.24E-10

Figure 18: System-Level PWR LOCA Frequencies.

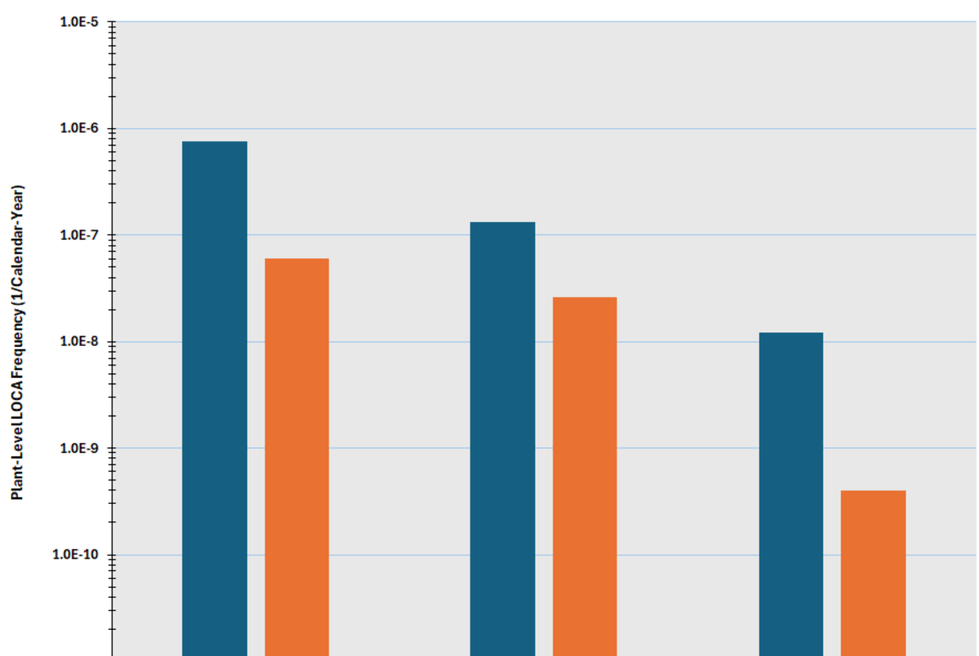

	Cat4	Cat5	Cat6
NUREG-1829	7.62E-07	1.33E-07	1.21E-08
PWR2024	6.00E-08	2.62E-08	4.00E-10

Figure 19: Plant-Level PWR LOCA Frequencies.

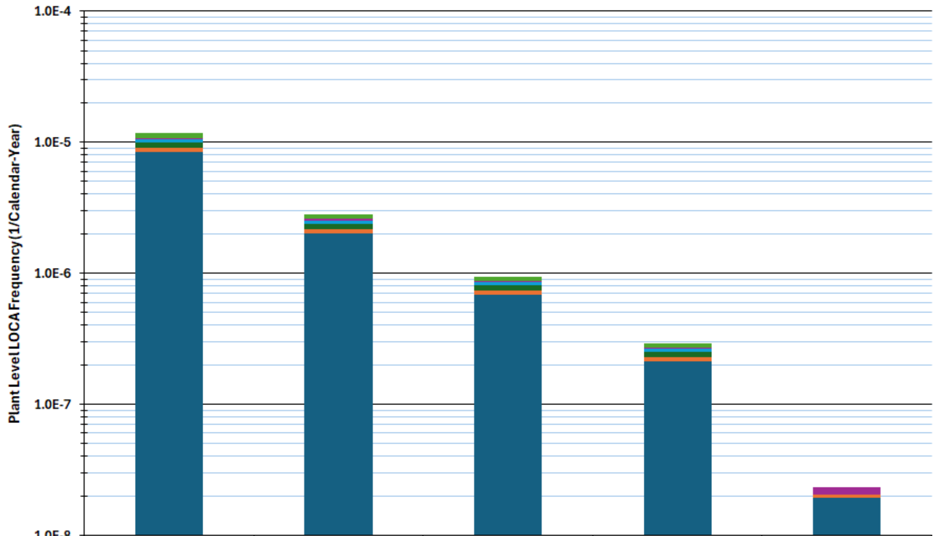

	Cat1	Cat2	Cat3	Cat4	Cat5
RWCU	8.62E-07	2.09E-07	6.83E-08	2.07E-08	
MS	2.94E-07	7.11E-08	2.33E-08	7.07E-09	2.81E-09
LPCS	5.90E-07	1.43E-07	4.68E-08	1.42E-08	
HPCI	8.58E-07	2.08E-07	6.80E-08	2.07E-08	
FW	7.08E-07	1.71E-07	5.61E-08	1.70E-08	1.07E-09
RR	8.35E-06	2.01E-06	6.84E-07	2.11E-07	1.94E-08

Figure 20: System-Level BWR LOCA Frequencies.

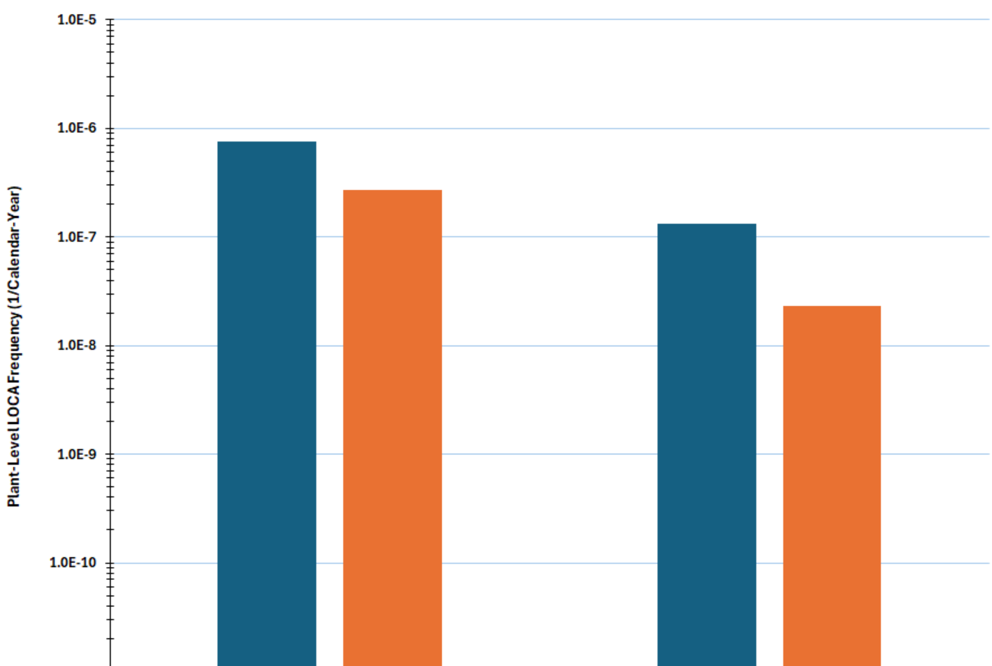

	Cat4	Cat5
NUREG-1829	7.62E-07	1.33E-07
BWR2024	2.70E-07	2.33E-08

Figure 21: Plant-Level BWR LOCA Frequencies.

3.6 Comparison of NUREG-1829 Appendix D and OpE-2024 Base Case Results

Volume 2 of NUREG-1829 includes the results of base case calculations performed by four of the expert elicitation panel members. A comparison of NUREG-1829 Appendix D base case results and the updated PWR-1 Base Case and BWR-1a Base Case (Section 3.2) is shown in Figure 22. The significant LOCA frequency reduction reflects the effectiveness of various material degradation mitigation processes that have been implemented for BWRs and PWRs, such as stress improvement processes, water chemistry changes, increased inspections, and more degradation resistant materials.

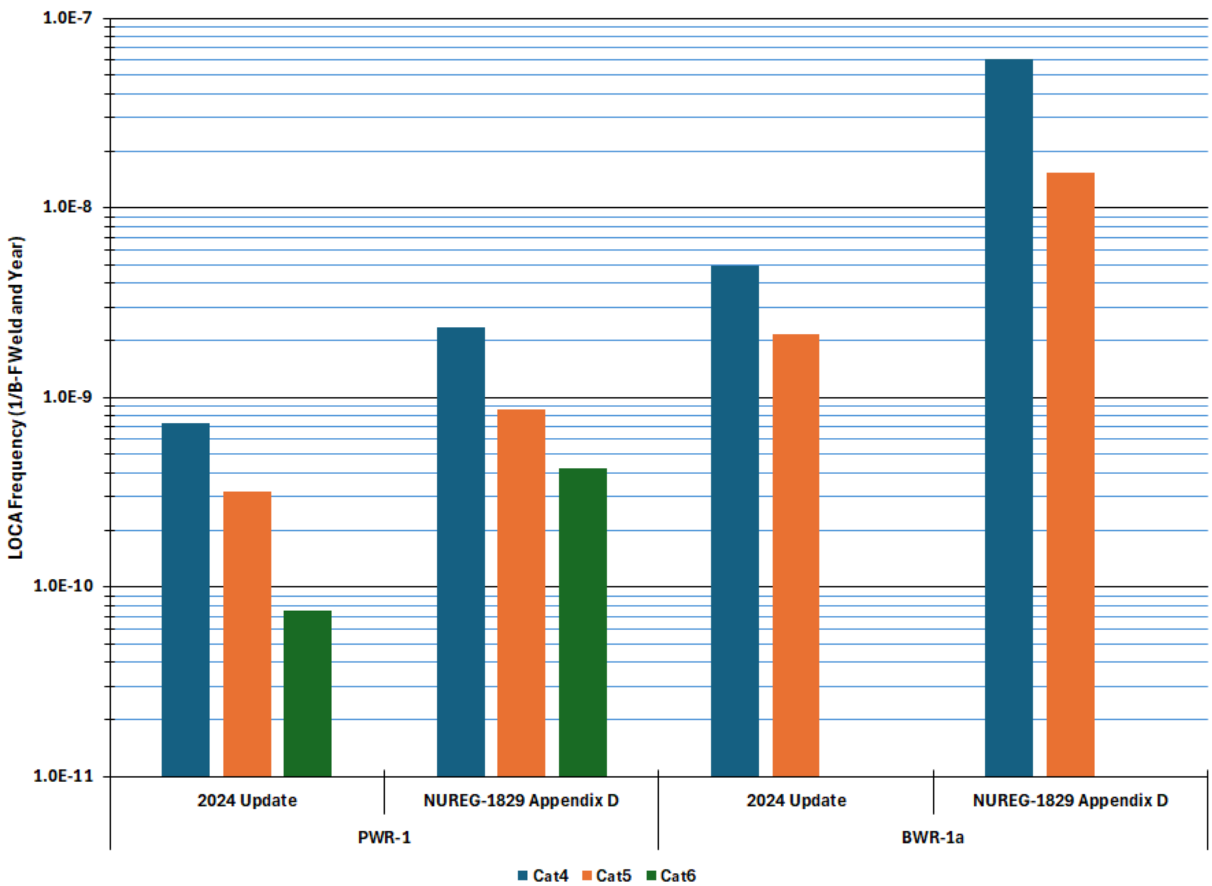

Figure 22: PWR-1 & BWR-1a Base Case Results Comparison.

3.7 Sensitivity Studies

Three sensitivity studies were performed to evaluate the impact of prior assumptions on the assessed precursor frequencies and LOCA frequencies. The basis for the selection of the PWR-1 and BWR-1 precursor frequencies is explained. The CFP parameters were derived from the NUREG-1829 expert elicitation and the impact of these parameters to the assumptions for determining precursor frequency and target LOCA frequency were evaluated.

3.7.1 PWR-1: Sensitivity on Prior Distribution

The analysis procedure is based on Bayesian reliability analysis in which a prior precursor frequency is updated with failure counts and exposure terms that apply to a particular base case analysis. In situations involving limited or no OpE data, it is not at all obvious which prior distribution is the most appropriate and the sensitivity of the results to the choice of the prior should always be examined. The international and domestic OpE appliable to Base Case PWR-1 is given in Table 40.

Table 40: OpE Applicable to Base Case PWR-1

PLANT	NSSS	COUNTRY	EVENT DATE	EVENT TYPE	% Through-Wall	PWSCC Confirmed?
Ringhals-3	WE-3	SE	16-Aug-00	Crack-Part	16	Assumed
Ringhals-3	WE-3	SE	16-Aug-00	Crack-Part	26	Assumed
Ringhals-4	WE-3	SE	31-Aug-00	Crack-Part	25	Yes
V.C. Summer-1	WE-3	US	07-Oct-00	P/H-Leak	100	Yes
Catawba-1	WE-4	US	20-May-05	Crack-Part	< 10	Assumed
Ohi-3	WE-4	JP	26-May-08	Crack-Part	20	Yes
Robinson-2	WE-3	US	01-Oct-08	Crack-Part	20	Assumed
Robinson-2	WE-3	US	01-Oct-08	Crack-Part	20	Assumed
Robinson-2	WE-3	US	01-Oct-08	Crack-Part	13	Assumed
Salem-1	WE-4	US	01-Nov-08	Crack-Part	24	Yes
Seabrook-1	WE-4	US	15-Oct-09	Crack-Part	21	Assumed
Tomari-1	WE-2	JP	17-May-11	Crack-Part	< 10	Assumed

A technical basis for prior distributions is found in Table 41. To examine the sensitivity on the prior distribution, three hypotheses are tested and identified as A1, A2 and A3 in Table 41. Assumptions 1 and 2 rely on OpE associated with the DMW between the RPV outlet nozzle and the RC hot leg. Assumption 3 assumes that the susceptibility to PWSCC is equal to a dissimilar metal weld at the RPV outlet nozzle and the steam generator inlet nozzle. The sensitivity of the posterior precursor frequence on the prior distribution is relatively small in comparison to the underlying uncertainties that have been quantified for the CFP estimates.

Table 41: Base Case PWR-1 Precursor Frequency Sensitivity on Prior Distribution

Hypothesis	1970 - 2004		2005 - 2024		Ratio A1/'A1+n'
	OpE	Precursor Rate	Domestic OpE	Precursor Rate	
A1	1 through-wall (TW) weld flaw (V.C. Summer) in 7163 weld-years	1.40E-04	0 TW weld flaws in 3371 weld years. Perform Bayesian update using the 1970-2004 OE as the prior state of knowledge ("Prior1").	1.28E-05	1 Corresponds to PWR-1 in Section 3.2.1
A2	1 TW weld flaw and 1 non-TW weld flaw in 7163 weld-years	2.79E-04	0 TW weld flaws in 3371 weld years. Perform Bayesian update using the 1970-2004 OE as the prior state of knowledge.	2.36E-05	1.84E+00
A3	RC-HL outlet & inlet nozzles: 1 TW weld flaw in 14,326 weld-years	6.98E-05	0 TW weld flaw in 6742 weld years. Perform Bayesian update using the 1970-2004 OE as the prior state of knowledge.	8.48E-06	6.62E-01

3.7.2 BWR-1a: Sensitivity on Prior Distribution

The BWR-1a prior precursor rate is based on a statistical analysis of IGSCC flaw data. The prior precursor rate was derived from an analysis of pre-1989 OpE flaw data and weld population data from ten BWR plants (in Appendix D of [1]). The weld precursor rate was estimated as a function of through-wall crack depth and years of operation at the time of flaw detection. This information was fitted to a lognormal distribution with the range factor fixed at 100. At the time of the NUREG-1829 base case analysis in 2004, this prior distribution was updated with new data from post-1988, Figure 23. For the 2005-2024 update, the output from the analysis performed in 2004 was updated with the post-2004 OpE. The BWR OpE is illustrated in Figure 24

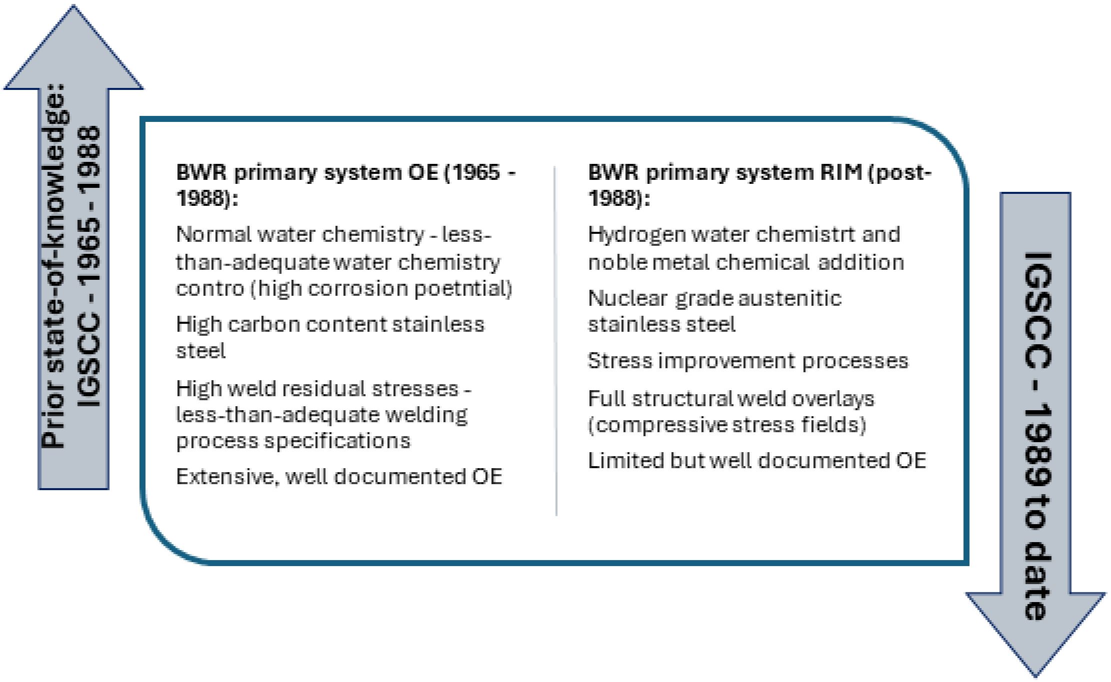

Figure 23: Basis for Defining Prior & Posterior Distributions.

For the period 2005-2024, the prior precursor rate was selected to be the “NPS28-Posterior” (Figure 24) from NUREG-1829, Appendix D. This produces an updated precursor rate of 4.6×10^{-5} per weld and per year. Using a prior distribution developed only using the “1965 to 1988” state of knowledge (Figure 24) produces an updated precursor rate of 9.5×10^{-5} per weld and year. The corresponding Cat4 and Cat5 LOCA frequencies associated with these failure precursor rates are given in Table 42. The increase in LOCA frequency is about a factor of 2, a change which is relatively small in comparison to the underlying uncertainties that have been quantified for the CFP estimates.

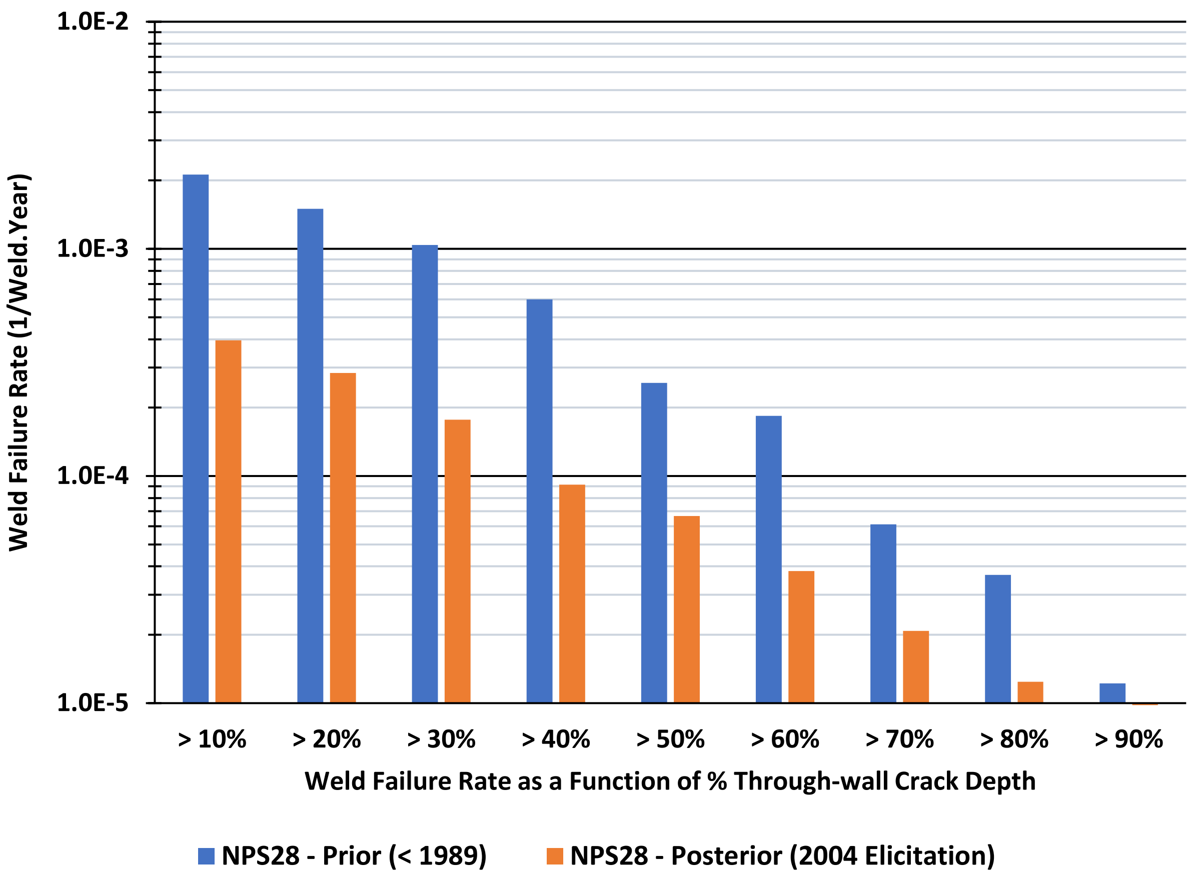

Figure 24: BWR-1a Prior and Posterior Precursor Weld Precursor rates.

Table 42: Effect of Prior Distribution on BWR1a LOCA Frequency Estimates

LOCA Category	Component-Level LOCA Frequency (1/Weld and Year)	
	2024 Single-Stage Bayesian Update	2024 Update Two-Stage Bayesian Update
Cat4	5.38E-09	2.62E-09
Cat5	2.35E-09	1.14E-09

3.7.3 CFP Parameter Sensitivity on Precursor Frequency

The CFP parameters are derived from NUREG-1829 using a "reverse-engineering" approach. A limited sensitivity analysis was performed to investigate the potential bias in the results by including NUREG-1829, Appendix D results; one of nine expert elicitation participants. To investigate the sensitivity of this issue on the results, the analysis documented in Section 3.1.2 in setting the target LOCA frequencies was repeated except that the geometric mean (GM) composite distribution in this case was developed excluding the NUREG-1829 Appendix D result. The results of this sensitivity analysis are shown in Table 43 for the PWR-1 Case. For this component there are small increases in the CFP range factors, however the changes in the mean values are generally less than 15% which is not significant in comparison with the CFP uncertainties.

Table 43: Results of Sensitivity Analysis to Address NUREG-1829 Appendix D Contribution to Experts Geometric Mean.

Case	LOCA Category	CFP Distribution Parameters				Ratio of means
		Mean	5%-tile	50%-tile	95%-tile	
PWR-1: Exclude NUREG-1829 Appendix D from GM	1	1.43E-03	1.78E-04	8.86E-04	4.42E-03	0.98
	2	3.45E-04	1.32E-05	1.30E-04	1.29E-03	1.04
	3	1.79E-04	4.87E-06	5.77E-05	6.84E-04	1.08
	4	6.19E-05	1.42E-06	1.84E-05	2.39E-04	1.08
	5	2.81E-05	4.31E-07	6.84E-06	1.09E-04	1.13
	6	6.43E-06	9.85E-08	1.57E-06	2.49E-05	1.10
PWR-1: Including Appendix D Results – (i.e., Table 22)	1	1.61E-03	7.42E-06	7.54E-04	6.11E-03	--
	2	1.24E-04	2.90E-07	4.76E-05	4.44E-04	--
	3	4.49E-05	1.12E-07	1.89E-05	1.78E-04	--
	4	1.67E-05	3.89E-08	6.95E-06	6.62E-05	--
	5	6.25E-06	1.59E-08	2.64E-06	2.47E-05	--
	6	3.05E-06	6.47E-09	1.25E-06	1.22E-05	--

4 BENCHMARK

4.1 Introduction

Four of the piping system base cases defined in NUREG-1829 have been reanalyzed using current computational tools and OpE data. The original base case calculations were completed in the period 2003 to 2004. A final step in the updated LOCA frequency calculations is to benchmark the xLPR LOCA frequency estimates against the estimates calculated using the domestic OpE from 2005 through mid-2024.The results of the benchmarking are documented in this section. 60 years of operation is chosen as the reference point for comparisons in this section because it coincides with the 60-year NUREG-1829 estimates. The xLPR frequency estimates at 80 years are not significantly different from the 60-year estimates.

4.2 PWR-1

The results of the annual Category 1 (Small-break) OCA frequency from the PFM analysis (Section 2.3.1) and the OpE evaluation (Section 3.2.1, Table 24) on the component are compared at 60 years of operation.

The annual frequency is estimated at 1.75×10^{-7} /yr by PFM when considering LD and 1.77×10^{-8} /yr by OpE. The PFM results are higher by an order of magnitude. However, when a generic RVON WRS is considered (Section 2.4.1), the annual frequency is estimated at $3.37 \times\ 10^{-8}$ /yr, which can be considered as equivalent (factor of two difference) in a probabilistic sense.

No LOCA occurred with leak rate detection for the two considered PFM runs, thus the result reported is an 95$^{\text{th}}$ percentile upper bound in both the VCIO and Generic cases: The difference between the two PFM runs comes from the change in the equivalent sample size. The generic WRS used in Section 2.4.1 is considered more consistent with the OpE approach and thus PWR-1 results are considered equivalent between OpE and PFM approach for Category 1 LOCA. Since there was no recorded SBLOCA with leak rate detection in the PFM results, there will also be no larger break LOCA and the larger LOCA frequencies will be estimated as the same upper bound as the SBLOCA. Therefore, no further comparison was made against OpE results.

4.3 PWR-2

The results of the annual Categories 1 and 2 LOCA frequencies from the PFM analysis (Section 2.3.2) and the OpE evaluation (Section 3.2.2, Table 26) on the component are compared at 60 years of operation. Case PWR-2a is used from the OpE evaluation to be consistent with the assumption of DMW used in the PFM analysis.

The annual frequency for the Category 1 LOCA is estimated at 1.32×10^{-7}/yr by PFM when considering LD and 7.06×10^{-8} /yr by OpE. The results are higher for the PFM by a factor of 2, though is still within the 95% upper bound calculated in Table 26 so the two frequencies can be considered very close.

The annual frequency for the Category 2 LOCA is estimated at 2.2×10^{-8} /yr by PFM when considering LD and 1.62×10^{-8} /yr for the OpE. The PFM results are higher by 36%, which can be considered equivalent in the probabilistic sense.

PWR-2 results are considered equivalent between OpE and PFM approach for the first two categories of LOCA. Since the PFM results will not change for larger categories LOCA with leak rate detection, no further comparison was made against OpE evaluation results.

4.4 BWR-1a

The results of the annual Categories 1 and 2 LOCA frequencies from the PFM analysis considering LD (Section 2.3.3) and the OpE evaluation(Section 3.2.3, Table 27) on the component are compared at 60 years of operation. For BWR-1a and BWR-1b, there were two divergent assumptions between the PFM and the OpE approaches with significant impact:

1 The OpE evaluation considers all the welds to have some mitigation technique applied: either mechanical stress improvement process (MSIP) or weld overlay (WOL). PFM considers no mitigation which is expected to increase the crack growth.

2 The loads used for the PFM analysis are the same used by Dave Harris in his PFM base case analysis. A separate benchmark performed at the time outlined that those loads were conservative and led to a factor of nearly two orders of magnitude difference between the OpE results and the PFM results for this base case in NUREG-1829.

As such, it was expected for the PFM results to be higher than the OpE results.

The annual frequency for the Category 1 LOCA is estimated at 6.67×10^{-6} /yr by PFM when considering LD and 1.21×10^{-7} /yr by OpE. The results are higher for the PFM by a little less than two orders of magnitude, which is consistent with the expected difference. The annual frequency for the Category 2 LOCA is estimated at 3.33×10^{-6} /yr by PFM when considering LD and 2.77×10^{-8} /yr by OpE. The results are higher for the PFM by a little more than two orders of magnitude, which is consistent with the expected difference.

The difference in BWR-1a results between the OpE and PFM approaches for the first two categories of LOCA is considered reasonable considering the different assumptions. Since the PFM results will not change for larger categories LOCA with leak rate detection, no further comparison was made against OpE results.

4.5 BWR-1b

The results of the annual Category 1 LOCA frequencies from the PFM analysis (Section 2.3.4) and the OpE evaluation(Section 3.2.4, Table 29) on the component are compared at 60 years of operation. The same differences in assumption described in Section 4.4 are applicable. As such, it was expected for the PFM results to be higher than the OpE results.

The annual frequency for the Category 1 LOCA is estimated as 1.67×10^{-5} /yr by PFM when considering LD and 4.1×10^{-8} /yr by OpE. The results are higher for the PFM by 2-3 orders of magnitude, which is within the range of the expected difference.

The difference in BWR-1b results between OpE and PFM approaches for the first category of LOCA is considered reasonable considering the different assumptions. It is important to note that the difference in estimates between BWR-1a and BWR-1b went *down* for the OpE approach, while it went *up* for the PFM approach (as expected with larger loads applied). Since the PFM results will not change for larger categories LOCA with leak rate detection, no further comparison was made against OpE results.

4.6 Conclusion

For the LOCA categories considered, the results between the OpE and PFM approaches were reasonably similar for the PWR-1 and PWR-2 base cases. There were differences in results between the OpE and PFM approaches for the BWR-1a and BWR-1b base cases. These differences observed for BWR-1a and BWR-1b align with the expected impact from the different assumptions used in the PFM and OpE analyses, especially the use of conservative loads in the PFM analysis.

5 SUMMARY AND CONCLUSIONS

The NRC issued NUREG-1829, “Estimating Loss-of-Coolant Accident (LOCA) Frequencies Through the Elicitation Process,” in April 2008 (ML082250436). The report provides LOCA frequency estimates based on an expert elicitation process for BWR and PWR piping and non-piping passive systems as a function of effective break size and plant operating years. The break sizes are organized into six LOCA categories, where Category 1 represents a small-break LOCA greater than 100 gallons per minute (gpm); Category 2 represents a medium-break LOCA greater than 1,500 gpm; and Categories 3, 4, 5, and 6 represent large-break LOCAs greater than 5,000 gpm, 25,000 gpm, 100,000 gpm, and 500,000 gpm, respectively. These LOCA frequency estimates reflect, in part, operating experience (OpE), PFM technology, and the state of knowledge in 2004.

As a first task, the more risk-significant base cases from NUREG-1829 were reexamined with updated PFM tools, data, and expertise. The base cases were BWR-1 (12- and 28-inch piping in the BWR recirculation system), PWR-1 (30-inch piping in the PWR hot leg), and PWR-2 (10-inch piping in the PWR pressurizer surge line) consistent with the definitions in NUREG-1829 Table 3.7. The BWR base cases are subject to IGSCC, and the PWR base cases are subject to PWSCC.

The Extremely Low Probability of Rupture (xLPR), Version 2.3 PFM code was used to reanalyze the base cases. It was specifically developed to model the effects of PWSCC and, therefore, well-suited to reanalyze the PWR base cases. For the BWR-1 base cases, IGSCC was modeled using the assumption of an initial crack at the beginning of plant operation, and a generic stress corrosion cracking model available in the xLPR code was used with parameters adapted to match the IGSCC growth rate published in the 2023 Edition of the American Society of Mechanical Engineers Boiler and Pressure Code, Division 1, Section XI, Subsubarticle Y-2310. For consistency with the NUREG-1829 results, LOCA Categories 1 through 6 probabilities were generated considering the effects of leak detection and then converted into annual frequencies.

The PWR analyses were within the range of the NUREG-1829 base case results. The PWR-1 analysis was performed with both a generically representative WRS profile and a conservative WRS profile based on the hot leg pipe-to-reactor-pressure-vessel nozzle weld at Virgil C. Summer Nuclear Station, Unit 1, which developed a leak due to PWSCC in 2000. Neither WRS profile resulted in any category of LOCA. As a result, a 95 percent upper confidence bound was estimated for the annual LOCA frequencies. For both WRS profiles, the xLPR results were within the range of the NUREG-1829 base case results at 25 and 60 years of operation. For the PWR-2 analysis, a few realizations resulted in a LOCA with leak detection. The first was a small-break LOCA occurring around 35 years, and around 75 years there were medium- and large-break LOCAs. Nevertheless, the resulting annual frequencies were within the range of NUREG-1829 base case results at 25 years of operation and below the range at 60 years of operation.

The BWR analyses were also within the range of the NUREG-1829 base case results. The BWR-1 base case estimates in NUREG-1829 do not differentiate between the LOCA frequencies for the 12-inch and 28-inch piping because the NUREG-1829 results are system estimates. However, the xLPR code generated different LOCA frequency estimates for the two piping sizes due to their different loads and WRS profiles. In the 28-inch BWR-1 analysis, a few realizations resulted in small-break LOCAs with leak detection. Similarly, the 12-inch BWR-1 analysis had a few realizations with all LOCA categories. Nevertheless, the annual frequency estimates remained within or below the range of estimates from NUREG-1829. A few sensitivity studies were performed for the BWR analyses to evaluate the effects of different WRS profiles and water chemistries. The results were equivalent or lower than the initial analysis results.

The updated LOCA frequency results based on the xLPR simulations reflect the state of knowledge and PFM modeling capabilities in 2024 and are consistent with the NUREG-1829 base case results.

As a second task, the NUREG-1829 base cases were reevaluated and more generic LOCA frequency estimates were determined based on an analysis of OpE from 2005 through mid-2024 for the larger diameter (i.e., > 6”) piping systems. The database developed under the Nuclear Energy Agency’s Component Operational Experience, Degradation and Ageing Programme provided the source for the OpE data. The analysis consisted of four major steps:

(1) review applicable OpE
(2) calculate piping precursor failure frequencies
(3) calculate conditional probabilities of LOCA
(4) calculate LOCA frequencies

In the first step, domestic OpE applicable to the more risk-significant base cases from NUREG-1829 was reviewed. Domestic OpE was also more generally reviewed for primary system piping branch connections greater than 6 inches in diameter (i.e., piping able to produce at least a Category 4 LOCA). The reviews covered the two distinct time periods (i.e., from before 1970 through approximately 2004 and from 2005 to mid-2024) and assessed differences and underlying factors of influence.

In the second step, the piping precursor failure frequencies were calculated using a Bayesian analysis approach. The initial results are expressed in units of failures per reactor operating year and per the number of components exposed to a certain material degradation mechanism, such as stress corrosion cracking. A constrained, non-informative distribution method was used to develop a prior piping precursor failure frequency distribution representative of the state of knowledge in 2004. The prior distribution was then updated using a Bayesian approach with the number of failures as the numerator and the number of reactor operating years and number of components as the denominator.

In the third step, the BWR and PWR system-level conditional probability uncertainty distributions were developed from NUREG-1829 by first obtaining a geometric mean of the expert elicitation participant results. This value represented a target LOCA frequency. Next, the geometric mean of the precursor failure frequency results of the respective system-level analyses were fit to lognormal distributions. Finally, the median conditional probability of LOCA was obtained by dividing the median target LOCA frequency by the median precursor rate. The resulting conditional probability of LOCA represents uncertainty in the 2004 state of knowledge when the NUREG-1829 expert elicitation was completed.

Lastly, in the fourth step, the uncertainty distributions developed in Steps 2 and 3 were convolved in a converged Monte Carlo uncertainty propagation to obtain the respective LOCA frequency uncertainty distributions.

The updated LOCA frequency results reflect the state of knowledge in 2024 and, relative to the NUREG-1829 results, indicate at least an order of magnitude reduction for LOCA Categories 4, 5, and 6. The significant reduction reflects the effectiveness of various material degradation mitigation processes that have been implemented for BWRs and PWRs, such as stress improvement processes, water chemistry changes, increased inspections, and more degradation resistant materials. The analysis methods included consideration of uncertainties in the state of knowledge regarding factors of improvement in reliability and integrity management and OpE.

A comparison was performed between the results for the base cases by the OpE and PFM approaches. For the LOCA categories considered, the results between the OpE and PFM approaches were generally similar for the PWR-1 and PWR-2 base cases. The differences in results observed for the BWR-1a and BWR-1b base cases align with the expected impact from the different assumptions used in the OpE and PFM approaches.,.

6 REFERENCES

[1] R. Tregoning, L. Abramson and P. Scott, "NUREG-1829 : Estimating Loss-of-Coolant Accident (LOCA) Frequencies Through the Elicitation Process," U.S. NRC, Washington D.C., 2008.

[2] C. Sallaberry and others, "TLR-RES/DE/CIB-2021-XX, "Probabilistic Leak-Before-Break Evaluation of Westinghouse Four-Loop Pressurized-Water Reactor Primary Coolant Loop Piping using the Extremely Low Probability of Rupture Code," NRC, ADAMS Accession Number ML21217A088, Washington, DC, 2021.

[3] C. J. Sallaberry, R. Kurth, E. Kurth-Twombly and F. W. Brust, "Probabilistic Leak-Before-Break Evaluations of Pressurized-Water Reactor Piping Systems using the Extremely Low Probability of Rupture Code," US NRC, TLR-RES/DE/REB-2021-14-R1, 2022.

[4] C. Sallenberry, "xLPR Software Requirements Description for Crack Optimization Module, Version 1.0," 2024.

[5] L. Hund, J. Lewis, N. Martin, M. Starr, D. Brooks, A. Zhang, R. Dingreville, A. Eckert, J. Mullins, P. Raynaud, D. Rudland, D. Dijamco and S. Cumblidge, "Technical Basis for the use of Probabilistic Fracture Mechanics in Regulatory Applications," NUREG/CR-7278, January 2022.

[6] Wikipedia, "Rule of three (statistics)," Wikipedia, 25 October 2023. [Online]. Available: https://en.wikipedia.org/wiki/Rule_of_three_(statistics). [Accessed 19 June 2024].

[7] M. Erickson, "xLPR Technical Report on Sources and Treatment of Uncertainties," ML19337C165, 2020.

[8] C. Casto and H. Christensen, "VC Summer Hot Leg Nozzle-to-pipe Weld Crack - Potential Generic Issues," United States Nuclear Regulatory Commission, Memorendum to Jack R. Strosnider, Director - Division of Engineering - Office of Nuclear Reactor Regulation, April 2001.

[9] xLPR WRS subgroup, "xLPR Version 2.0 Technical Basis Document : Welding Residual Stress Modelling Development," 2016.

[10] MPR Associates Inc., "Susquehanna Steam Electric Station - Leak Before Break Evaluation of Postulated Recirculation system pipe cracks," MPR-949 Rev. 1, Washington D.C., 1986.

[11] Nuclear Energy Agency, "Component Operational Experience, Degradation and Ageing Programme (CODAP)," Nuclear Energy Agency, January 2024. [Online]. Available: https://www.oecd-nea.org/jcms/pl_24823/component-operational-experience-degradation-and-ageing-programme-codap. [Accessed 27 August 2024].

[12] S. Kaplan, "On the method of discrete probability distributions in risk and reliability calculations - application to seismic risk assessment," *Risk Analysis,* vol. 1, no. 3, pp. 189-196, 1981.

[13] K. N. Fleming and B. O. Lydell, "Database Development and Uncertainty Treatment for Estimating Pipe Failure Rates and Rupture Frequencies," *Reliability Engineering adn System Safety,* vol. 86, pp. 227-246, 2004.

[14] B. Lydell and K. Fleming, "Use of Markov Piping Reliability Models to Evaluate Time Dependent Frequencies of Loss of Coolant Accidents," in *12th int. conference on nuclear Engineering (ICONE12)*, Arlington, CA, 2004.

[15] B. O. Y. Lydell, "The Probability of Pipe Failure on The Basis of Operating Experience," in *ASME Pressure Vessel and Piping Division Conference*, 2007.

[16] K. N. Fleming and B. O. Y. Lydell, "Insights Into Location Dependent Loss-of-Coolant-Accident (LOCA) Frequency for GSI-191 Risk-Informed Applications," *Nuclear Engineering and Design,* vol. 305, pp. 433-450, 2016.

[17] B. O. Y. Lydell, "A Review of the Progress with Statistical Models of Passive Component Reliability," *Nuclear Engineering and Technology,* vol. 49, pp. 345-359, 2017.

[18] IAEA, "Technical Insights from Benchmarking Different Methods for Predicting Pipe Failure Rates in Water Cooled Reactors, Final Report of a Coordinated Research Project," IAEA-TECDOC-1988, Vienna, Austria, 2021.

[19] B. Lydell, K. Chitose and J. Riznic, "Material Degradation Mitigation & New Degradation Scenarios: Lessons Learned from the Analysis of Operating Experience Data," in *FONTEVRAUD 10: International Symposium Contribution of Materials Investigations and Operating Experience to LWRs' Safety, Performand and Reliability*, Avignon, France, 2022.

[20] IAEA, "Methodologies for Assessing Pipe Failure Rates in Advanced Water Cooled Reactors," Nuclear Energy Series No. NR-T-2. 16, Vienna, Austria, 2023.

[21] xLPR Version 2.0 Technical Basis Document, "Input Group Report," xLPR-GR-IG, Version 1.0, [NRC Adams Accession No: ML19337B876], December 2017.

[22] ASME, "Nonmandatory Appendix Y - Crack Growth Rate Curves," in *ASME Boiler and Pressure Vessel Code - Section XI - Division 1*, New York, NY, ASME, 2023, pp. Y-2310.

[23] R. Carter and R. Pathania, "Technical Basis for BWRVIP Stainless Steel Crack Growth Correlations in BWRs," in *2007 ASME Pressure Vessels and Piping Division Conference*, San Antonio (TX), PVP2007-26618.

[24] D. Harris, D. Dedhia, E. Eason and S. Patterson, "Probability of Failure in BWR Reactor Coolant Piping," Lawrence Livermore National Laboratory, NUREG/CR-4792 Vol. 3, 1987.

[25] S. Rahman, N. Ghadiali, D. Paul and G. Wilkowski, " Probabilistic Pipe Fracture Evaluations for Leak-Rate-Detection Application," Battelle, NUREG/CR-6004, 1995.

[26] F. W. Brust, E. Punch, M. Benson and D. Rudland, "Three Dimensional Residual Stress in Dissimilar Metal Welds Including Part Repair and Start/Stop Effects," in *ASME PVP*, Anaheim, CA, 2014.

[27] F. W. Brust, M. R. Hill and Y. O. Yang, "Chapter 7: Residual Stress and Distortion," in *AWS Welding Handbook*, Miami, FL, American Welding Society, 2019.

[28] F. W. Brust, M. Benson, J. Broussard, A. Cox, R. Kurth and C. J. Sallaberry, "Welding Residual Stress Modeling Development - 2016 Technical Basis Document for xLPR Version 2 support," US NRC, Rockville, MD, 2016.

[29] D. L. Rudland, F. W. Brust, T. Zhang, D.-J. Shim and G. Wilkowski, "Evaluation of the Inlay Process as a Mitigation Strategy for Primary Water Stress Corrosion Cracking in Pressurized Water Reactors," NRC Adams Accession number ML101260554, ROckville, MD, 2010.

[30] M. Benson, D. Rudland and A. Csontos, "Weld Residual Stress Finite Element Analysis Validation: Part 1 - Data Development Effort," NRC Adams Accession number ML14087A118, Rockville, MD, 2014.

[31] M. Benson, P. Raynaud and J. Wallace, "Weld Residual Stress Finite Element Analysis Validation: Part 2 -Proposed Validation Procedure," NRC Adams accession number ML20212L592, Rockville, MD, 2020.

[32] M. Benson, "Phase 2b Finite Element Round Robin results Technical Letter Report," NRC Adams accession number ML16020A034, Rockville, MD, 2015.

[33] H. J. Rathburn, L. F. Fredette, P. M. Scott, A. A. Csontos and D. L. Rudland, "NRC Welding Residual Stress Validation Program International Round Robin PRogram and

Findings," in *ASME 2011 Presure Vessels and Piping Conference*, Baltimore, MD, PVP2011-57642.

[34] F. W. Brust, E. J. Punch, D. Rudland and H. Rathburn, "Weld Residual Stress Analysis and Axial PWSCC Predictions in a Double Vee Groove Large Diameter Nozzle," in *ASME 2013 Pressure Vessels and Piping Conference*, Paris, France, PVP2013-9806.

[35] F. Brust and R. Stonesifer, "Effect of Weld Parameters on Residual Stresses in BWR Piping Systems," NP-1743, Columbus, OH, 1981.

[36] T. E. Barber, F. W. Brust, H. W. Mishler and M. F. Kanniner, "Controlling Residual Stresses by Heat Sink Welding," WPRI NP-2159-LD, 1981.

[37] F. W. Brust and E. F. Rybicki, "A Computational Model of Backlay Welding for Controlling Residual Stresses in Welded Pipe," *Journal of Pressure Vessel Technology,* vol. 103, pp. 226-233, 1981.

[38] L. Fredette, P. M. Scott and F. W. Brust, "An Analytical Evaluation of the Effect of Weld Material Thickness on Residual Stresses Produced by Structural Weld Overlays on Pressurized Water Reactor Primary Coolant Piping," in *ASME 2009 Pressure Vessels and Piping Conference*, Prague, Czech Republic, PVP2009-77330.

[39] R. Hardies, D. Rudland, T. Lupold, D. Alley, A. Csontos, S. Dinsmore, R. Dyle and C. Harrington, "xLPR version 2.0 Technical Basis Document - Acceptance Criteria," U.S. Nuclear Regulatory Commission, October 2016.

[40] N. Glunt, M. Burkardt and G. Schmidt, "An Assessment of xLPR Estimation of Loss-of-Coolant Accident Frequencies," Electric Power Research Institute, 2021.

[41] N. Glunt, C. Harrington, M. Burkardt and G. Schmidt, "Use of the xLPR Code for Developing LOCA Frequency Estimates," in *4th ISPMNA*, Leicester, UK, November 1-3, 2022.

[42] WCAP-16925-NP Rev 1, "Flaw Evaluation of CE Design RCP Suction and Discharge, and Safety Injection Nozzle Dissimilar-Metal Welds," Westinghouse, [Accession No: ML092740086], July 2009.

[43] Technical Report 1022852 (MRP 307), "Materials Reliability Program: Probabilistic Assessment of Chemical Mitigation of Primary Water Stress Corrosion Cracking in Nickel-Base Alloys," EPRI, Palo Alto, CA, June 2011.

[44] F. Brust and R. Stonesifer, "Effect of Weld Parameters on Residual Stresses in BWR Piping Systems," NP-1743, Columbus (OH), 1981.

[45] S. Kaplan and B. J. Garrick, "On The Quantitative Definition of Risk," *Risk Analysis,* vol. 1, pp. 11-27, 1981.

7 APPENDICES

7.1 xLPR Inputs

7.1.1 Case PWR-1: PWR RVON

The inputs values used for PWR-1 are based on Section 3.2.1 of TLR-RES/DE/REB-2021-14-R1 [3]. The following input changes have been implemented.

The crack orientation (Global ID 0003) was set to 1 to only include circumferential cracks. While axial cracks are more likely to occur, sensitivity studies in [2, 3] have shown that leakage from axial cracks was low enough (i.e., a maximum of around 0.2 gpm per crack) to not have an impact on LOCA size or leak rate detection.

A sample of size 5,000 was used for PWR-1, with optimization applied to the xLPR initiation model “Direct model 1”. This gives an equivalent sample size of more than 200,000, which is twice the size used for the reference case (Case 1.1.0) in [2].

7.1.2 Case PWR-2: PWR Surge Line

The input values used for PWR-2 base case were listed in Section 2.4.2 of [3].

A sample of size 5,000 was used for this case, with optimization applied to the xLPR initiation model “Direct model 1”. Since the likelihood of having a crack is lower than for PWR-1, the equivalent sample size is more than 2,000,000, which is 20 times the size used for the reference case (Case 2.1.0) in [3].

7.1.3 Case BWR-1a: BWR Recirculation Line for the 28” Pipe

Available xLPR inputs [21] currently include PWSCC and fatigue for PWR environments. The active degradation mechanism in BWR recirculation lines is IGSCC.

To model IGSCC, the xLPR model for PWSCC growth rates was used. The model takes the following form:

$$\dot{a}_{PWSCC} = \begin{cases} \alpha f_{comp} f_{flaw} e^{-\frac{Q_g}{R_{gas}\left(\frac{1}{T}-\frac{1}{T_{Ref}}\right)}} (K_I - K_{th})^{\beta} & K_I > K_{th} \\ 0 & K_I \leq K_{th} \end{cases} \qquad \text{Eq. (3)}$$

Where:

Q_g is the activation energy (kJ/(mol.K))

R_{gas} is the universal gas constant (kJ/mol)

T is the temperature (K)

T_{Ref} is a reference temperature (K)

K_I is the stress intensity factor (MPa.sqrt(m))

K_{th} is a threshold stress intensity factor (MPa.sqrt(m))

$\alpha, \beta, f_{comp}, f_{flaw}$ are fitting parameters

In its 2023 edition ASME Boiler and Pressure Code, Division 1, Section XI article Y-2310 [22] uses the IGSCC model described in [23], which has the following form:

$$\ln\left(\frac{da}{dt}\right) = 2.181\ln(K) - 0.787\, Cond^{-0.586} + 0.00362\, ECP + \frac{6730}{T_{abs}} - 33.235 \qquad \text{Eq. (4)}$$

Where:

K is the stress intensity factor (MPa.sqrt(m))

$Cond$ is the average conductivity (determined at room temperature) (μS/cm)

ECP is the electrochemical corrosion potential (mV(Standard Hydrogen Electrode))

T_{abs} is the temperature (K)

With recommended parameters given for different water chemistries and locations. Both BWR base cases were modeled using parameter values for nominal water chemistry.

A noticeable change in the conversion is to use a negative number for the activation energy. The cause of the change of sign is due to having a IGSCC growth rate decreasing with an increase in temperature, while PWSCC growth rate increases when the temperature increases.

Since the purpose of this study was to reproduce the base case from NUREG-1829 [1], the resulting IGSCC growth rates from [23] and ASME BPVC Code case 2023 edition [22] at the selected temperature (288°C) were compared to the model used by Dave Harris in NUREG-1829 and which is described in NUREG/CR-4792 Vol. 3 [24].

Figure 25 shows a comparison between the different models and the comparison was deemed satisfactory enough so that the ASME model could be used. Note that while the older model used by Dave Harris (from NUREG/CR-4792) had lower growth rates at lower K, the ASME model was using newer data and is considered more realistic.

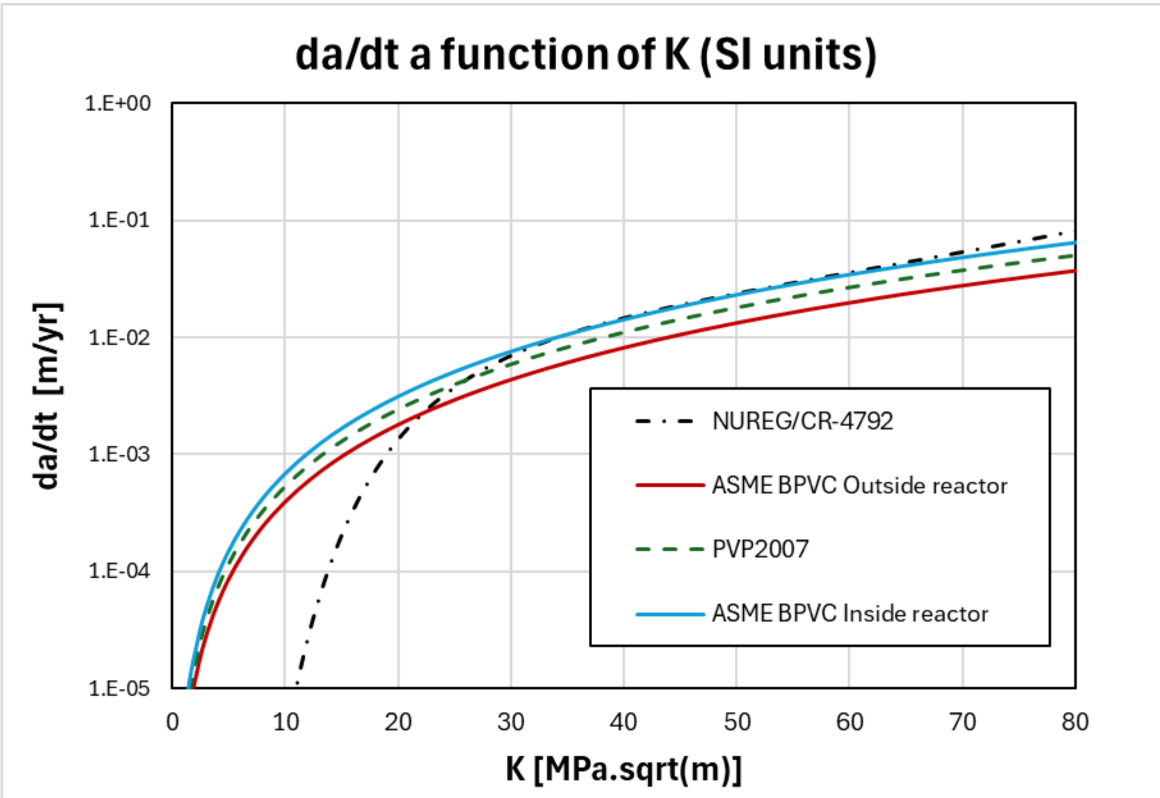

Figure 25: Comparison of IGSCC Models at a temperature of 288°C

The selected sample size was again 5,000, each realization having a crack starting at the top dead center at the beginning of the simulation. The following lists present the inputs used in the xLPR code to run the 28 inches recirculation line. Each of the headings correspond to a specific sheet with the same name on the Excel input file.

User options

- Operation time: *80 years* (to be consistent with the other runs).
- Crack orientation: *circumferential only*.
- Sample size: *5000*.
- DM Weld Mixture Ratio: *0.5* (kept at 0.5, since the left pipe and right pipe are same material).
- Mitigation choice: *Stress-based – MSIP.*
- Mitigation time: *240 Months* (= 20 years expressed in months).
- Crack initiation type: *Initial flaw density.*

- Growth type: *SCC only*.
- Detectable leak rate: *5 gpm* (covered in post-processing).
- Inspection schedule: *by frequency*.
- Inspection frequency: *0.05/yr* (one every 20 years – applied both before and after mitigation).
- Global roughness: *80.01* μm (from NUREG/CR-6004 [25]).
- Local Roughness: *4.699* μm (from NUREG/CR-6004).
- Number of turns: *28230* $/m$ (from NUREG/CR-6004).
- Global path deviation factor: *1.07* (from NUREG/CR-6004).
- Local path deviation factor: *1.33* (from NUREG/CR-6004).
- Pmax: *8.2 MPa*.
- Pmin: *7.24 MPa* (reference value in most documentation. Cannot be lower as it affects Tmax).
- Tmax: *288 °C* (reference value in most documentation. Cannot be higher as it affects Pmin).
- Tmin: *280 °C* (low value, not expected to be used in BWR).

Properties:

- EFPY: *80 years* (to be consistent with the other runs).
- Pipe Outer diameter: *0.7112 m* (~28" from Table F.17 of NUREG 1829 Vol. 2). (1)
- Pipe Wall Thickness: *0.03051 m* (~1.201" from Table F.17 of NUREG 1829 Vol. 2).
- Weld Material Thickness: *0.03051 m* (= pipe thickness).
- Number of initial circumferential flaws: *1*
- Initial flaw full-length: *LN*[4]*(4.8e-3,2.226) m* (regular xLPR initial crack size distribution)
- Initial full-length multiplier: *1.*
- Initial flaw depth *LN(1.5e-3,1.419,min=5e-4,max=0.03051) m.*
- Initial depth multiplier: *1.*
- Operating Pressure: *7.24 MPa* (LBB Database). (2)
- Operating Temperature: *288°C* (LBB Database).
- Membrane Stress (DW): *0 MPa* (from Table F.17 of NUREG 1829 Vol. 2). (3)
- Maximum Bending Stress (DW): *13.8 MPa* (from Table F.17 of NUREG 1829 Vol. 2). (3)
- Membrane Stress (Thermal): *0 MPa* (from Table F.17 of NUREG 1829 Vol. 2). (3)
- Bending Stress (Thermal): *44.36 MPa* (from Table F.17 of NUREG 1829 Vol. 2). (3)
- β_0 parameter for the xLPR POD curve: *-3.94* (xLPR curve fit to Dave Harris Good IGSCC detection curve – same values used before and after mitigation).
- β_1 parameter for the xLPR POD curve: *7.75* (xLPR curve fit to Dave Harris Good IGSCC detection curve – same values used before and after mitigation).

[4] LN(μ,σ) = lognormal distribution with mean μ and standard deviation σ

(1) Note that the pipe outer diameter is highlighted red in the xLPR input file as it is not compatible with the axial COD module. Since we do not consider axial cracks, it should not be an issue.
(2) Dave Harris has used a slightly higher pressure value of 1.25 ksi (~8.62 MPa). See Table F.2 in NUREG-1829 Vol. 2. This is not necessarily less conservative as the thermal stresses are scaled to the pressure (see (3)).
(3) Stresses come from Table F.17 of NUREG 1829 [1] Vol. 2 –
The nominal stresses recorded include DW, pressure and thermal. Pressure is equal to 7.24 MPa according to the LBB database, and Appendix F in NUREG 1829 assumed dead weight stresses to be 2 ksi (~13.8 MPa). Assuming these stresses include thermal expansion stresses, the thermal stress portion of these stresses can be deduced. The thermal stresses are applied as bending instead of membrane stresses because bending stresses are expected to be the biggest contributors to crack growth. It should not affect the results either way considering only one crack at top dead center is modeled. The stresses used are summarized in Table 44.
The stresses from [10] were also considered but were lower than the ones in NUREG-1829. Since [10] was representing a single plant, the NUREG-1829 data was selected as a conservative approach.

Table 44: Distribution of loads for BWR-1a and BWR-1b

Line size (Case)	28" pipe (BWR-1a)	12"pipe (BWR-1b)
Pressure	7.24 MPa	7.24 MPa
Deadweight	13.8 MPa	13.8 MPa
Thermal expansion	44.36 MPa	120.66 MPa
Total Stresses	**65.4 MPa**	**141.7 MPa**

Left and Right Pipe properties:

- Material: Stainless Steel 304
- Yield Strength: *LN (mean=153.6, stdev=14.38, min=123, max=190) MPa* (from xLPR Material Properties Uncertainty Report – July 2016)
- Ultimate Strength: *LN (mean=443, stdev=25.86, min=386, max=507) MPa* (from xLPR Material Properties Uncertainty Report – July 2016)
- Elastic Modulus: *N(mean=176 720, stdev=25 508,min=150 212, max= 203 228) MPa* (from xLPR Material Properties Uncertainty Report – July 2016)
- J_{IC} : *N(mean=1182, stdev=611.9,min=175, max= 2605) N/mm* (from xLPR Material Properties Uncertainty Report – July 2016)
- C: *N(mean=335.1, stdev=112.8,min=117, max= 615.9)* (from xLPR Material Properties Uncertainty Report – July 2016)

- m: *N(mean=0.728, stdev=0.155,min=0.2, max= 1.0)* (from xLPR Material Properties Uncertainty Report – July 2016)
- Correlation Yield Strength – Ultimate Strength: *0.607*

Weld Pipe properties:

- Material: Stainless Steel 308L (similar to 304L)
- Yield Strength: *LN (mean=128.8, stdev=14.38, min=99, max=166) MPa* (from xLPR Material Properties Uncertainty Report – July 2016)
- Ultimate Strength: *LN (mean=399.4, stdev=25.86, min=343, max=463) MPa* (from xLPR Material Properties Uncertainty Report – July 2016)
- Elastic Modulus: *N(mean=176 720, stdev=25 508,min=150 212, max= 203 228) MPa* (from xLPR Material Properties Uncertainty Report – July 2016)
- J_{IC} : *N(mean=1182, stdev=611.9,min=175, max= 2605) N/mm* (from xLPR Material Properties Uncertainty Report – July 2016)
- C: *N(mean=335.1, stdev=112.8,min=117, max= 615.9)* (from xLPR Material Properties Uncertainty Report – July 2016)
- m: *N(mean=0.728, stdev=0.155,min=0.2, max= 1.0)* (from xLPR Material Properties Uncertainty Report – July 2016)
- Correlation Yield Strength – Ultimate Strength: *0.607*
- **Growth**
- Growth factor α: *8.38E-14* (m/s)(MPa-m$^{1/2}$)^(beta) (fitting ASME IGSCC Model in [22])
- Growth exponent β: *2.181* (fitting ASME Code IGSCC Model in [22])
- Comp. to comp. variability: *1* (fitting ASME Code IGSCC Model in [22])
- Within comp. variability: *1* (fitting ASME Code IGSCC Model in [22])
- Reference Temperature: *288°C* (fitting ASME Code IGSCC Model in [22])
- Crack Growth Material Flag: *10* (using custom model to fit IGSCC model)

7.1.4 Case BWR-1b: BWR Recirculation Line Inputs for the 12” Pipe

The selected sample size was again 5,000, each realization having a crack starting at the top dead center at the beginning of the simulation. Most of the input parameters for the 12-inch recirculation line are the same than the ones used for the 28-inch recirculation line. The values that were updated as compared to the 28” pipe are listed below.

Properties:

- Pipe Outer diameter: *0.32385 m* (~12.75” from Table F.17 of NUREG 1829 Vol. 2)
- Pipe Wall Thickness: *0.01745 m* (~0.687” from Table F.17 of NUREG 1829 Vol. 2)
- Weld Material Thickness: *0.01745 m* (= pipe thickness)
- Bending Stress (Thermal): *120.66 MPa* (from Table F.17 of NUREG 1829 Vol. 2) (from Table 44)

7.2 WRS Profile Development

The LOCA study detailed in this report considered both PWRs and BWRs. The WRS have been compiled in previous NRC work for PWRs, however WRS fields are needed for BWRs for the LOCA assessments performed in this report. This section provides the WRS fields for two BWR lines considered here: 12-inch diameter and 28-inch diameter recirculation lines.

7.2.1 PWR-1

The inside-outside axial WRS profile representing the Virgil C. Summer (VCIO) Nuclear Generating Station RVON was used instead of the generic RVON WRS [18]. For the VCIO WRS field repair sequence, it is not certain whether the inside repair or outside repair was performed last. This is discussed in detail in [18]. The VCIO WRS profile, which is shown in red in Figure 26, is higher at the ID and has a larger standard deviation than the generic WRS profile (in blue), leading to a higher probability of crack initiation.

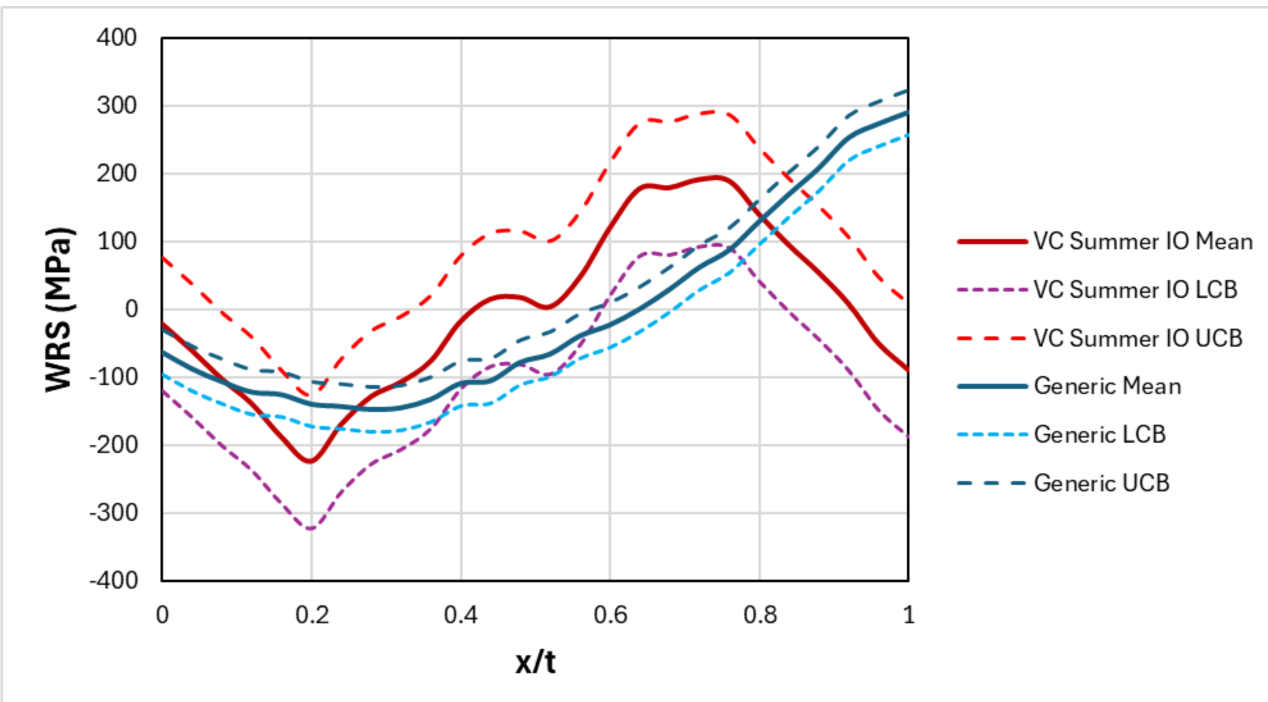

Figure 26: WRS mean profile and 90% probability interval for the VC Summer IO RVON Weld and the Generic RVON Weld.

7.2.2 General Procedure for WRS Development for BWR

Welding is the preferred method for connecting many components in nuclear power plants. Welds are used for vessel fabrication, piping and nozzle connections, reactor and piping supports, head and vessel bottom penetration connections, along with many other component fabrications. The welding process consists of applying a heat source and often weld filler metal along the weld path. Shrinkage of the weld beads during cooling leads to the development of WRS in components. The WRS profiles may have stress components greater than the yield stress because the stress state is multiaxial and, at locations where the mean stress is high, the component stresses can be quite high. Material hardening also plays a role. Moreover, in many applications, especially nuclear components, weld repairs are often necessary to remove defects. The WRS profiles caused by the repair welds are often more severe (i.e., produce higher tensile WRS that can enhance crack growth) compared with the original WRS state. Axial WRS profiles are self-equilibrating for axisymmetric analysis within the piping cross section, while hoop stresses are not self-equilibrating. For instance, the axial WRS profiles produced from the nozzle-to-piping dissimilar metal butt welds are typically close to self-equilibrating while the hoop WRS are not. However, it is noted that repair welds have repair lengths only partway around the circumference of the weld. Therefore, the WRS profile near the start and stop locations of the repair are often quite different from those at the midpoint of the repair through the center of the weld [26].

A physical perspective for the development of WRS profiles is provided in [27] along with general guidance on development of WRS fields for various geometries including pipes. This reference describes the weld bead shrinkage and geometry effects of residual stress development, among other factors. For complex geometries, the development of the WRS profile can be more involved and requires a nonlinear finite element solution of the welding process where the deposition of each pass is modeled. The history behind the development of computational weld models is summarized in many of the references cited in the American Welding Society Welding Handbook chapter 7 [27].

Detailed discussion of WRS modeling procedures performed for the US NRC are summarized in [28] and the many references cited therein. In particular, [28] summarizes the development of the WRS field libraries that are in the xLPR probabilistic computer code for PWR dissimilar welds. Other works that discuss the development of WRS fields for nuclear systems are provided in [29] [30], [31], [32], [33], [34] and the many publications therein. This includes discussion of the accuracy or WRS predictions in [30], [31], and [32].

7.2.3 Background on WRS Development in BWRs

IGSCC became a problem in BWRs in the 1980s. At that time the NRC and EPRI performed a number of studies to determine the WRS fields in stainless steel BWR piping. This work included residual stress measurement work and WRS model development work. The WRS fields that were developed in the 1980s were rather crude models that represented the state of the art at the time. In addition, the WRS measurements performed at the time were developed using older cutting methods. This prior work is summarized in the ERPI report (EPRI NP-1743) and the many references cited therein [35]. Methods to reduce tensile WRS fields in the heat affected zones (HAZ) of welds, where IGSCC was occurring, were developed and implemented as mitigation measures for BWRs partially based on that work (MSIP, heat sink welding, IHSI).

Modern methods were used to develop the WRS fields for the LOCA assessments performed in this study. The methods are detailed in [27] which is the technical basis document for the WRS fields that reside in the xLPR library of solutions. These procedures consist of performing analyses using isotropic and kinematic hardening and then using the average of these results. Reference [27] shows that using this average of isotropic and kinematic hardening produces results that are close to the mixed hardening results that were found to be most accurate compared to measurements. Here we use only isotropic hardening since it produces upper bound tensile WRS fields and results in faster crack growth of IGSCC.

7.2.4 BWR-1a: WRS Fields for 28-Inch Recirculation Line

The weld groove geometry considered for the 28-inch line were obtained from Table 8-1 of EPRI NP-1743 ([34]) which are typical for BWR large diameter recirculation piping with thicknesses greater than 1-inch. The groove geometry type and dimensions of the 28-inch case is shown in Figure 27 where the dimensions are shown in metric units. The number of weld deposition layers, total number of weld passes, and weld heat inputs were estimated from Table 8-2 of EPRI NP-1743. Nine layers of weld and 37 total passes were used as shown in Figure 28. It is seen that a length of the recirculation line chosen for this analysis was about eight times the diameter of the pipe. The material properties used for the base metal pipe are 304 stainless steel properties and those for the weld metal are 308 stainless steel properties. The physical properties used for the thermal analysis consist of conductivity, heat capacity, density, and convective constants which are temperature dependent. The material properties for the structural analysis, which uses the temperature versus time history produced from the thermal analysis, consist of elastic modulus, Poisson ratio, and thermal expansion which are also temperature dependent. The stress strain curves used are shown in Figure 29. Isotropic hardening was used for the axisymmetric analyses to ensure upper bound WRS fields are produced for the crack growth assessments discussed in the main body of the report. The detailed analysis procedures used are discussed in [27].

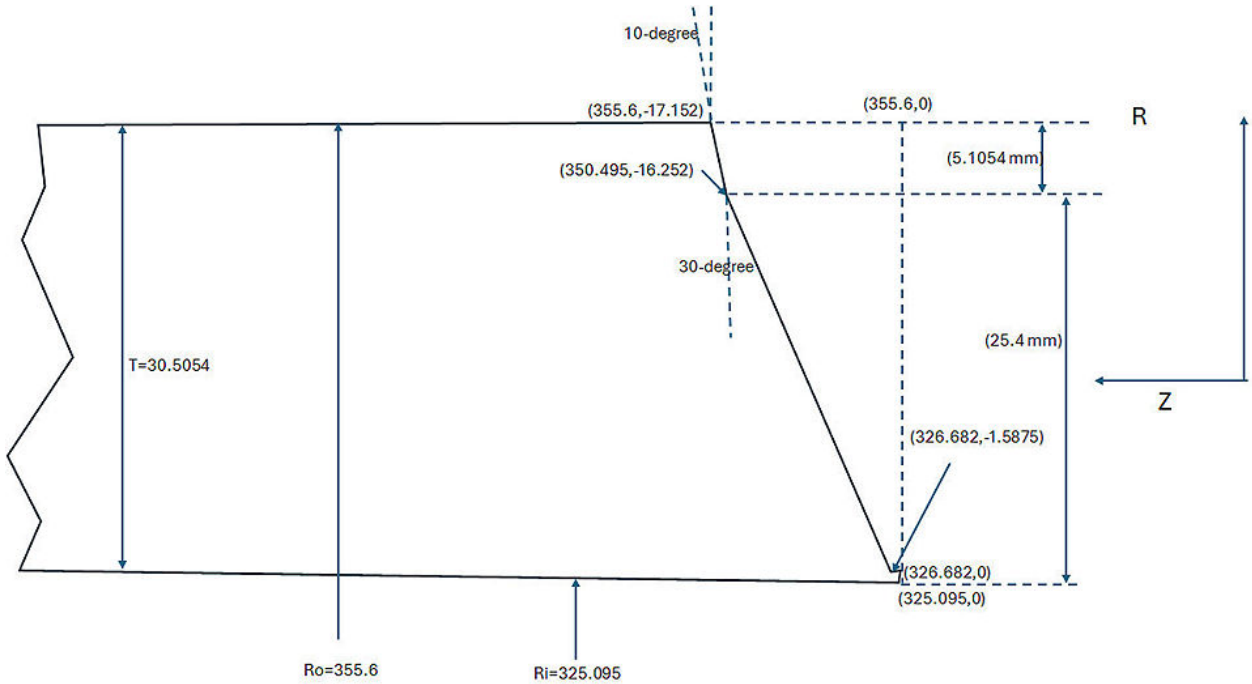

Figure 27 Weld groove geometry (in mm) for 28-inch recirculation line.

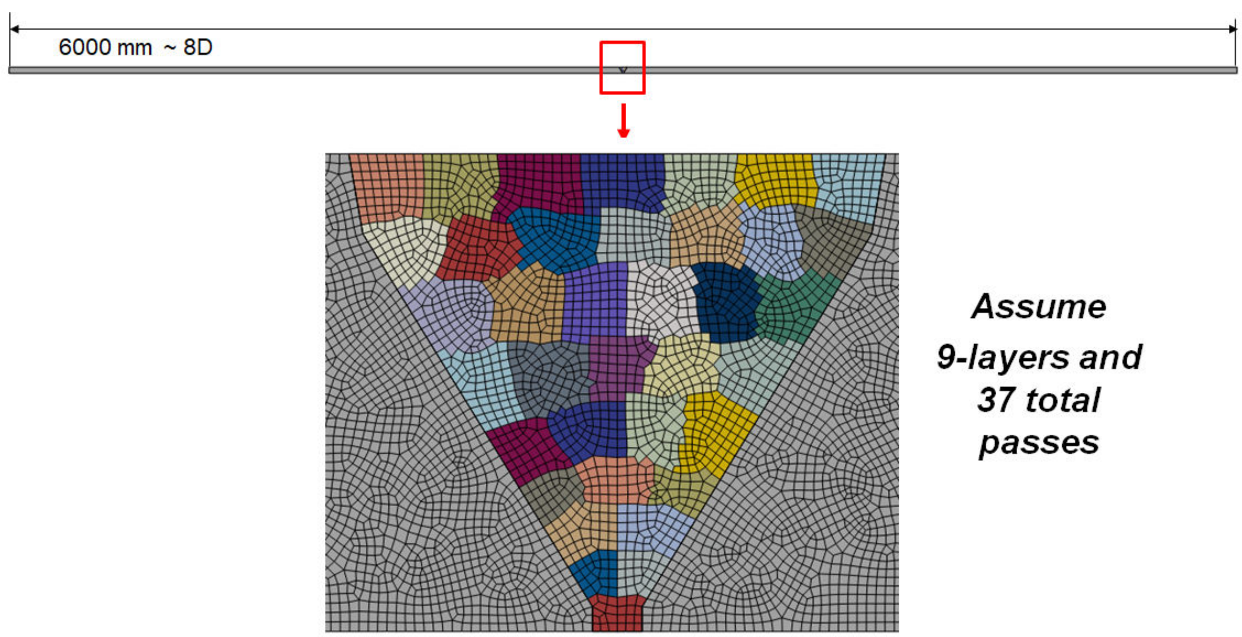

Figure 28*:* Weld model for 28-inch recirculation line with weld passes shown.

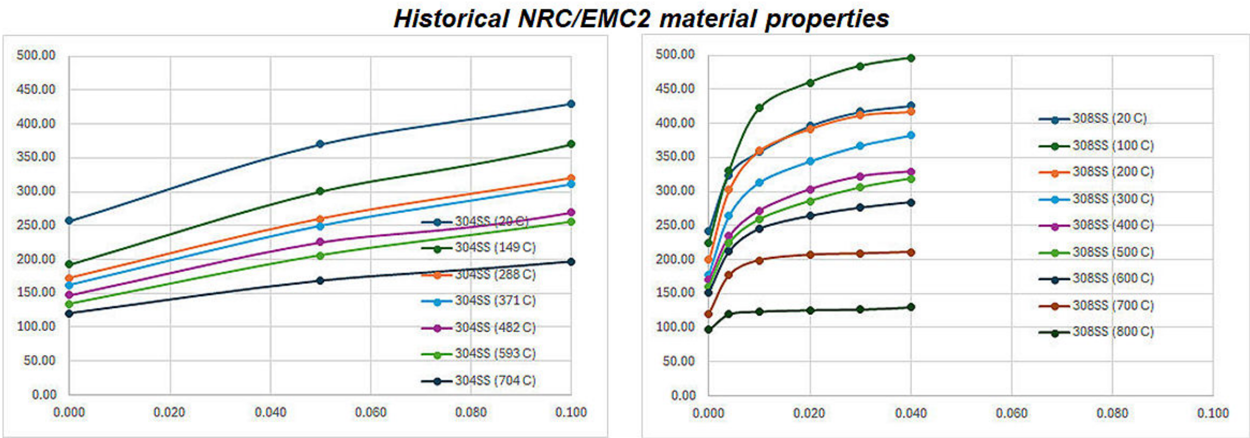

Figure 29*:* **Stress versus plastic strain curves used for weld analysis.**

7.2.4.1 Baseline results

The thermal solution consists of matching the fusion zone for the weld for each pass deposition as shown in Figure 30.

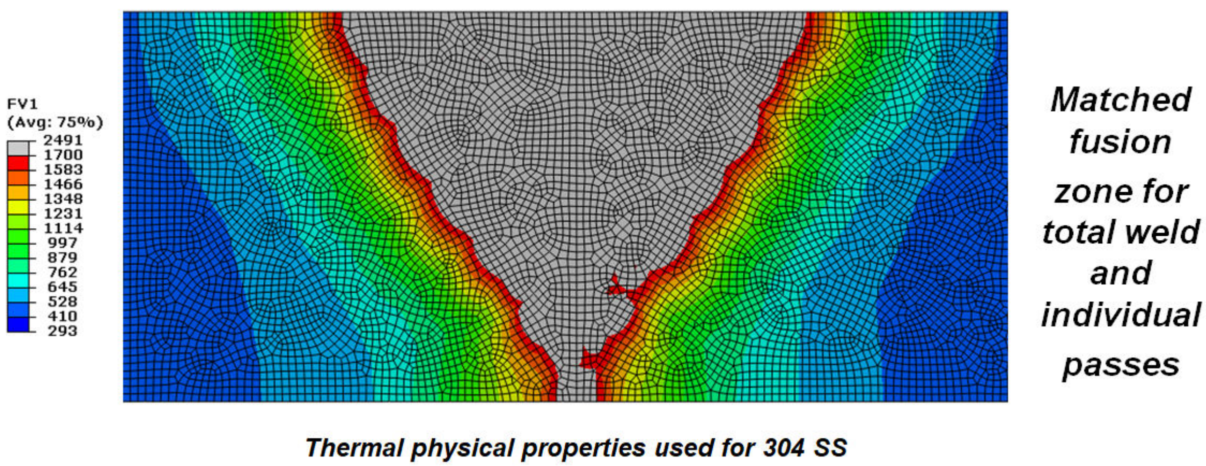

Figure 30*:* **Matched fusion zone for 28-inch recirculation line (1700 Kelvin is melting).**

Contour plots of the axial WRS field after welding, after hydrotest and removal, and at operation temperature are shown in Figure 31. The hydrotest modeling consists of applying a pressure of 1.25 times the operation pressure of 7.24 MPa (9.05 MPa) at room temperature. In this case the hydrotest does not alter the WRS field appreciatively. The operation temperature (288C) WRS field is shown on the bottom of Figure 31. This is the WRS field at operating temperature and the other service loads are applied separately within the xLPR code. The scale in Figure 31 of 242 MPa represents the room temperature yield stress of the 308SS weld metal. The axial WRS fields are used in the circumferential crack growth assessments.

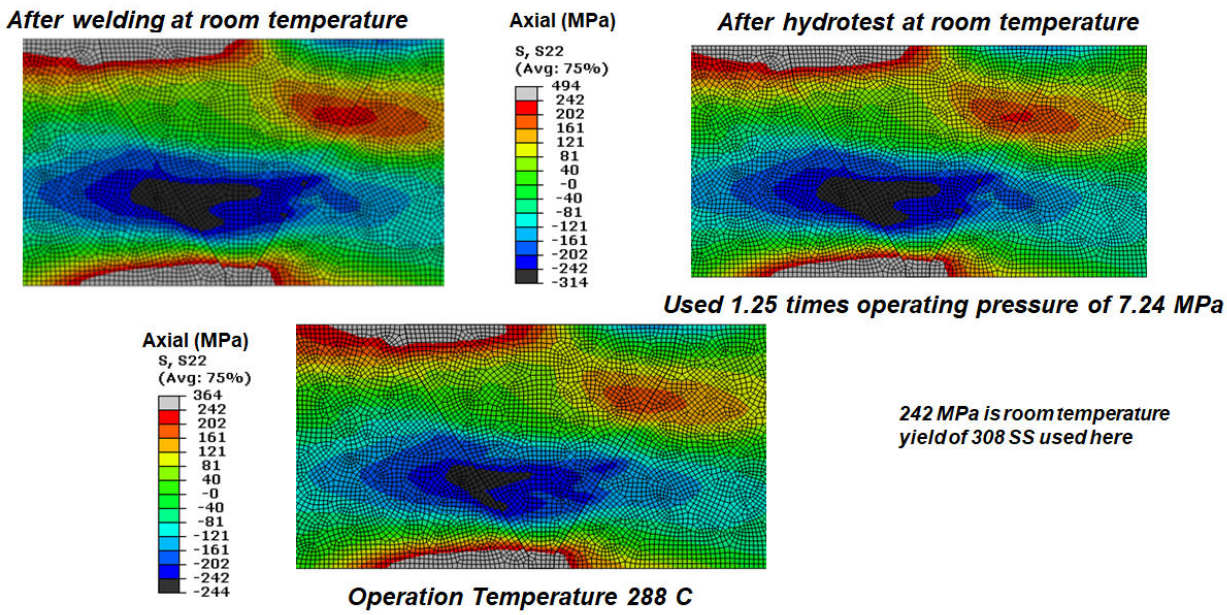

Figure 31: Predicted axial WRS field after welding at room temperature (upper left), after hydrotest and removal (upper right), and at operation temperature of 288C.

Contour plots of the hoop WRS field after welding, after hydrotest and removal, and at operation temperature are shown in Figure 32. The hydrotest does reduce the hoop WRS field somewhat. The operation temperature (288C) WRS field is shown on the bottom of Figure 32. This field, used for the axial crack growth assessments, is added for completeness.

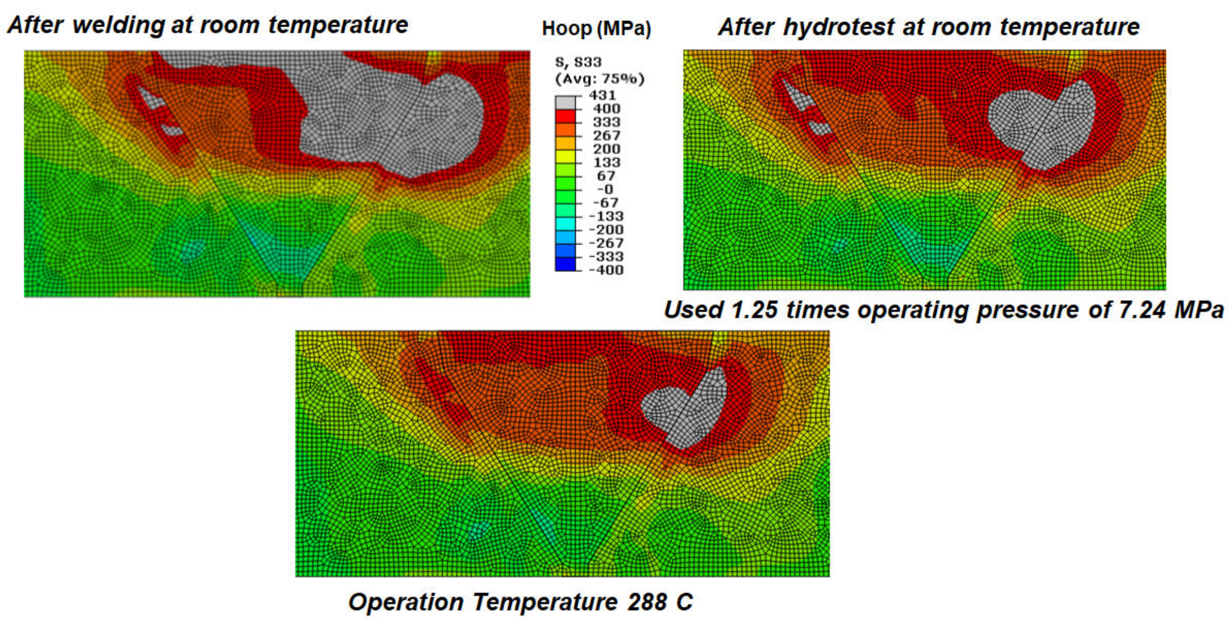

Figure 32 Predicted hoop WRS field after welding at room temperature (upper left), after hydrotest and removal (upper right), and at operation temperature of 288C.

The effect of the hydrotest on the WRS fields at room temperature can be seen in the line plots shown in Figure 33 plotted through the center of the weld. The effect of the hydrotest on the axial stresses is minimal and the hydrotest reduces the hoop stresses near the OD somewhat. A hydrotest of 1.4 times operation pressure was also applied and results were also minimal. The operation stresses at 288C plotted through the center of the weld are shown in Figure 34 and plotted through the HAZ are shown in Figure 35. These are used in the IGSCC LOCA assessment in the xLPR code.

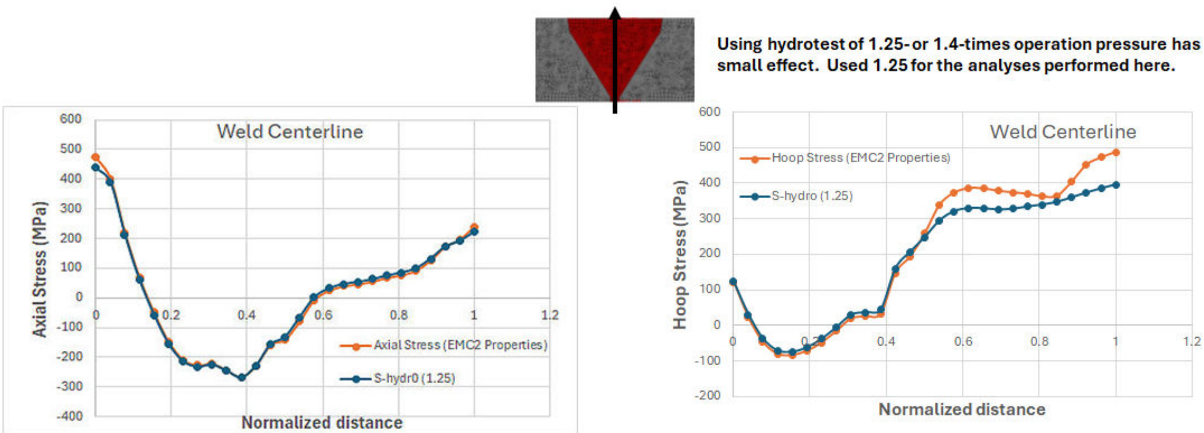

Figure 33 Line plots of axial and hoop WRS fields and effect of hydrotest (room temperature).

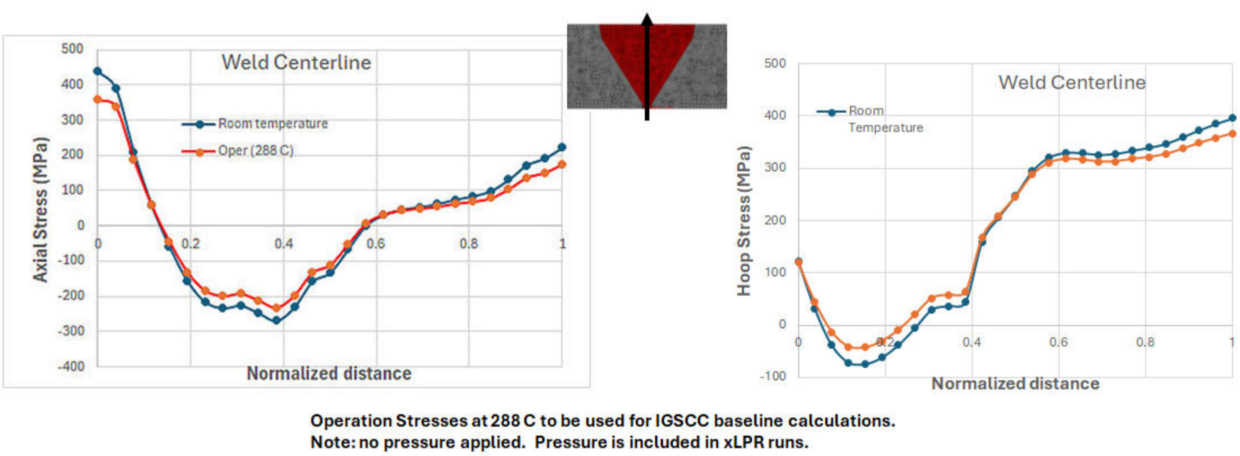

Figure 34 Line plots of axial and hoop WRS fields at operation temperature of 288C along weld centerline.

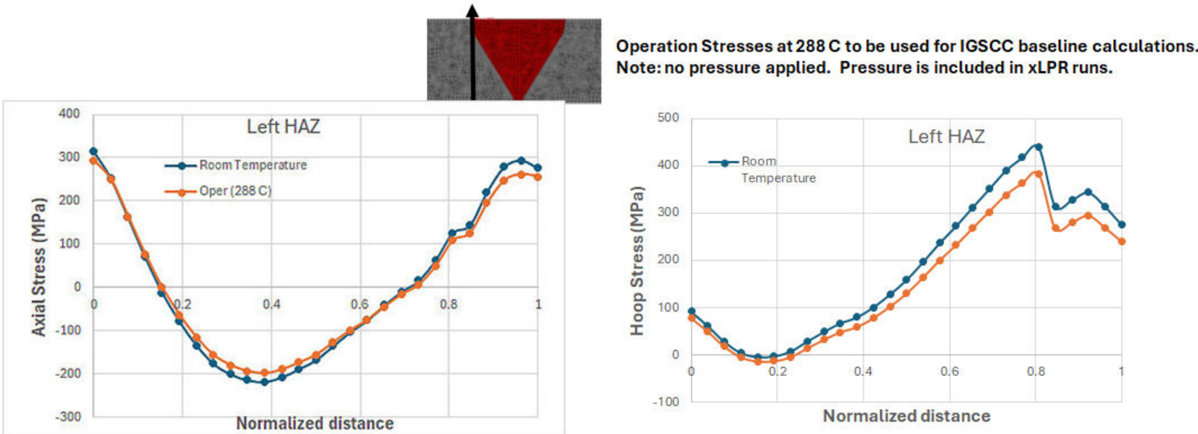

Figure 35 Line plots of axial and hoop WRS fields at operation temperature of 288C in HAZ.

MISP For Baseline Case

Mitigation of WRS fields, to reduce the tension stress and even reverse it to compression was introduced in BWR systems in the 1980s. This was done to help mitigate IGSCC that was occurring in the HAZs of BWR piping systems. There are several methods that were developed to accomplish this goal. These include heat sink welding (HSW), backlay welding, and mechanical stress improvement (MSIP). HSW consists of making some or all of the welds after the root pass with water flowing through the pipe so that the inner surface is kept cool while the latter passes shrink [36]. If done properly, compressive WRS fields can result. Backlay welding consists of depositing additional weld metal over the weld on the OD of the pipe [37]. This is similar to the current overlay welding that is often performed on PWR piping to reduce WRS fields. MSIP consists of applying a ring load on the pipe near the weld and then releasing [38]. The plastic deformation caused by the mechanical ‘squeeze’ can result in compressive WRS fields in the weld and HAZ. The MSIP method has been applied to a number of both BWR and PWR piping systems to reduce the WRS fields in welds and is chosen here to examine the mitigation of WRS fields for the LOCA assessments in this report.

The MSIP process is illustrated in Figure 36. This shows the MSIP process applied to an axisymmetric pipe. A ring load is applied to the pipe at a distance from the weld centerline. In Figure 36 the ring is 2.25-inch long and is applied 2 inches from the weld centerline. Both the width of the squeeze ring and the distance from the weld are design parameters determined from analysis. The ring is then squeezed a certain amount and then released. Here squeeze amounts of 1.22, 1.35, and 1.48 % were applied and released. Percent squeeze is defined as the amount of deformation that remains after release of the tool and load release divided by the outer diameter of the pipe multiplied by 100. During the squeeze process plastic deformation is produced under the tool resulting in a ‘ring’ shrinkage type load. This ring load then results in compression in the region of the weld and HAZ.

The effect of the MSIP application on the axial and hoop stress distribution both before and after application is illustrated in Figure 37 and Figure 38, respectively. It is seen that MSIP produces compressive stresses in the weld and HAZs.

- Applied MSIP treatment following process used by NuVision (displacement control).
- Looked at two tools. Both 2.25 inch long rings but one at a distance of 1.5 inch and one at 2 inch from the weld centerline. This is a typical tool.
- The tool to the right was assumed as it improved the compressive WRS field compared to the 1.5 inch case.
- Examined squeeze cases of 1.22%, 1.35% and 1.48 %. Squeeze is defined (by NuVision) as the amount of deformation after tool removal springback divided by the OD of the pipe (times 100). The values above are typical values based on recent EMC2 assessment of NuVision plans for Swiss regulator.
- The amount of squeeze applied here did not have a large effect on changing the WRS field.

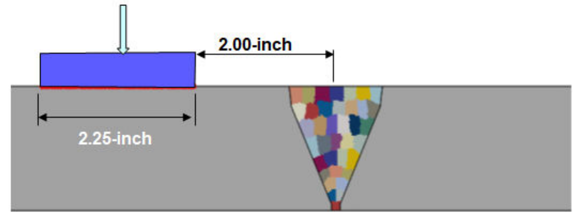

Figure 36*:* **Illustration of the MSIP process.**

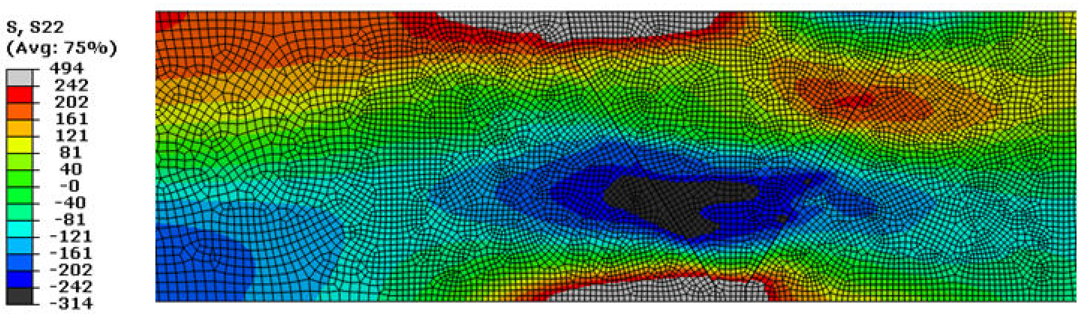

Axial Stress Before MSIP (1.22% Squeeze)

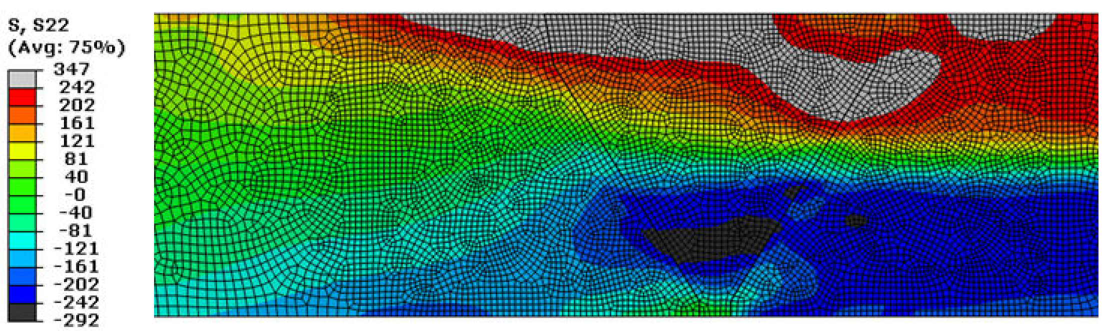

Axial Stress After MSIP (1.22% Squeeze)

Figure 37*:* **Effect of MSIP on axial stresses before and after application.**

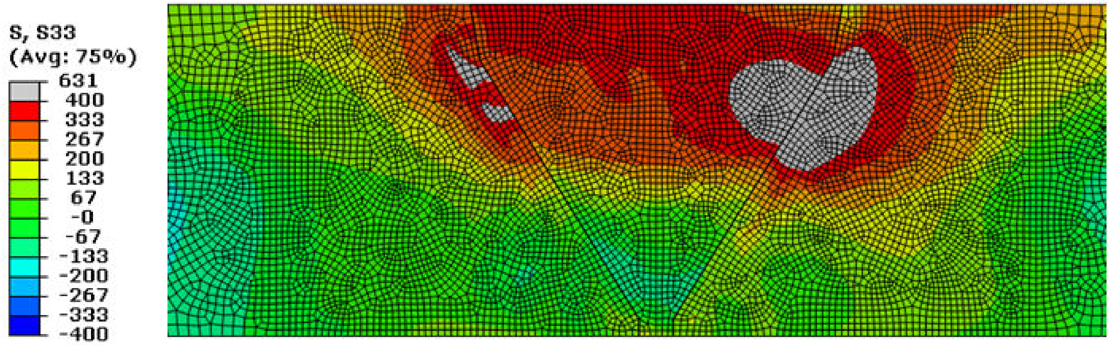

Hoop Stress Before MSIP (1.15% Squeeze)

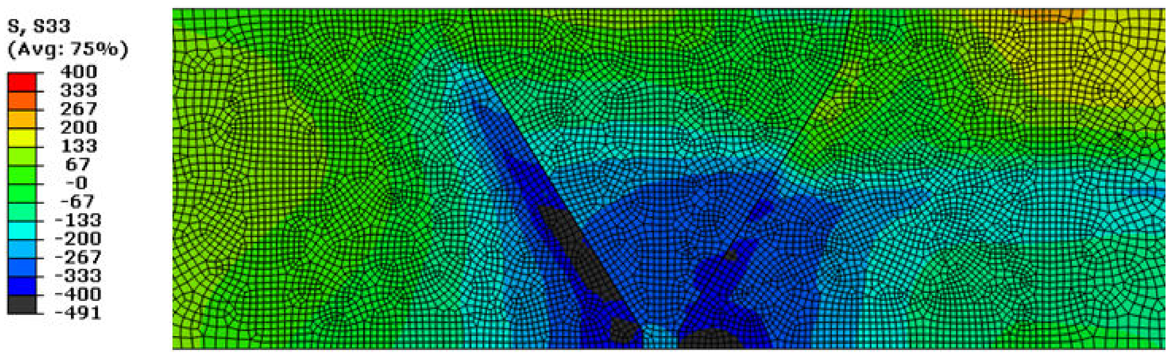

Hoop Stress After MSIP (1.15% Squeeze)

Figure 38: Effect of MSIP on hoop stresses before and after application.

Line plots of the WRS fields both before and after different MSIP squeeze amounts is shown in Figure 39 at room temperature. It is seen that for this diameter and thickness (28-inch recirculation line) that the amount of squeeze has a small effect on the WRS field. Line plots of the WRS fields both before and after different MSIP squeeze amounts is shown in Figure 40 at operation temperature. The WRS fields of Figure 40 are used in the xLPR code for the assessment of the effect of MSIP after 20 years of operation as discussed in the main body of the report.

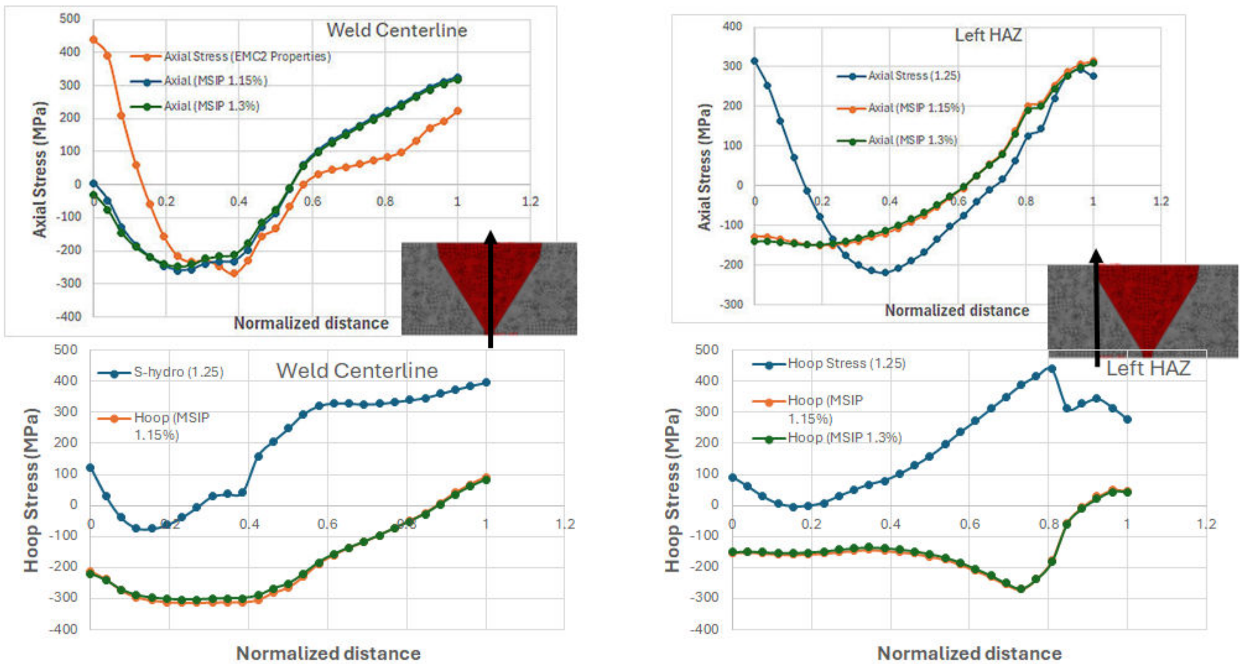

Figure 39: Line plots of WRS fields along the centerline and in the HAZ at RT.

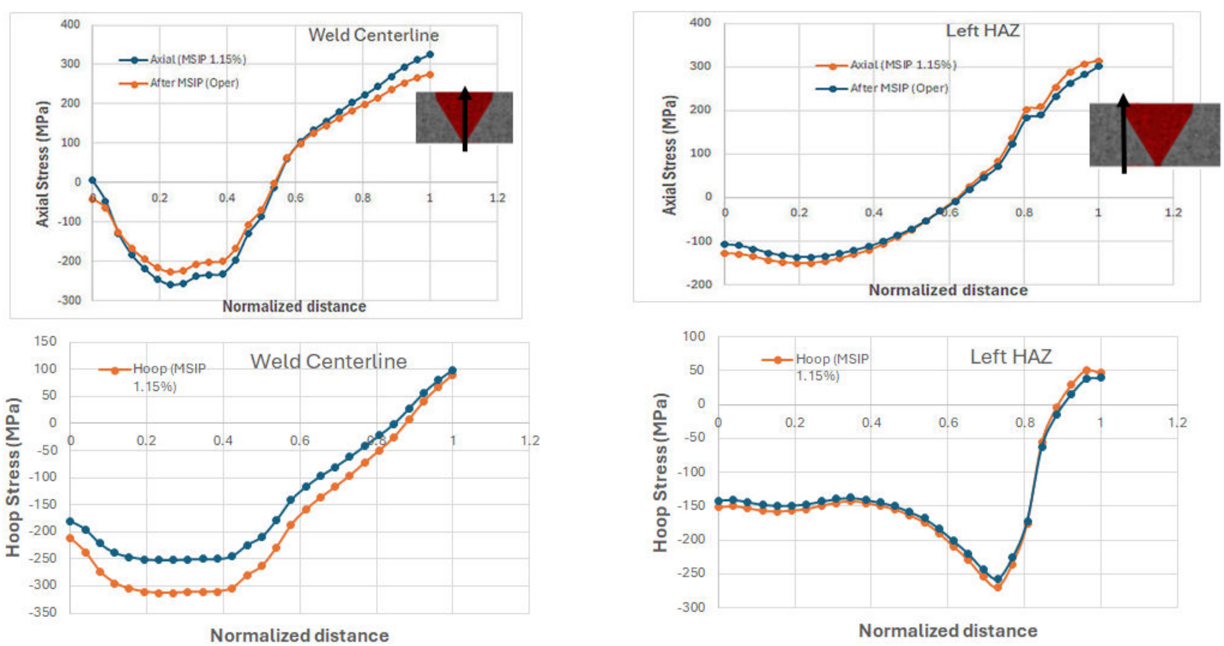

Figure 40*:* Line plots of WRS fields along the centerline and in the HAZ at operation.

7.2.4.2 Repair weld effects and MSIP after repair

It is known that repair welds can affect the WRS field in pipe welds and often increases the magnitudes of the stresses especially at the repair region. Figure 41 illustrates the repair weld modeling process performed here for the 28-inch recirculation line. A 10% of the thickness repair is assumed. First material is removed from the model after the original weld is made. This is illustrated with the red color in the top illustration of Figure 41. Then four passes were assumed to complete the 10% repair as seen in the bottom illustration of Figure 41. Next the hydrotest is applied to the pipe after the repair. Then the WRS field at operation after the repair is extracted for the xLPR LOCA analyses. In addition, MSIP is also applied and the operation WRS after MSIP is also extracted for the LOCA analyses.

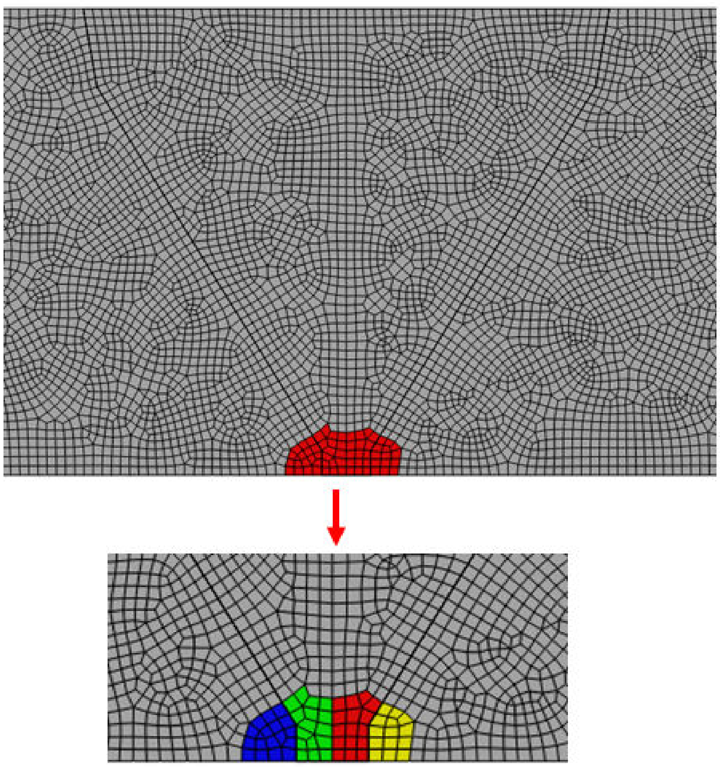

- **Assumed 10% deep repair**
- **Remove passes after original weld assuming fabrication defect**
- **Deposit repair passes with 4 passes (from left to right here)**
- **Apply hydrotest after repair**
- **Operation stresses after repair**
- **Apply MSIP over repair**
- **Operation stresses after MSIP**

Figure 41: Illustration of the repair weld process modeled for 28-inch line.

The axial and hoop WRS fields after the 10% repair weld is made (and after hydrotest) is shown in Figure 42. By comparing the axial stresses to those in Figure 31 (axial stress) and Figure 32 (hoop stress) after hydrotest it is clear that a 10% repair increases both the magnitude and volume of WRS near the ID.

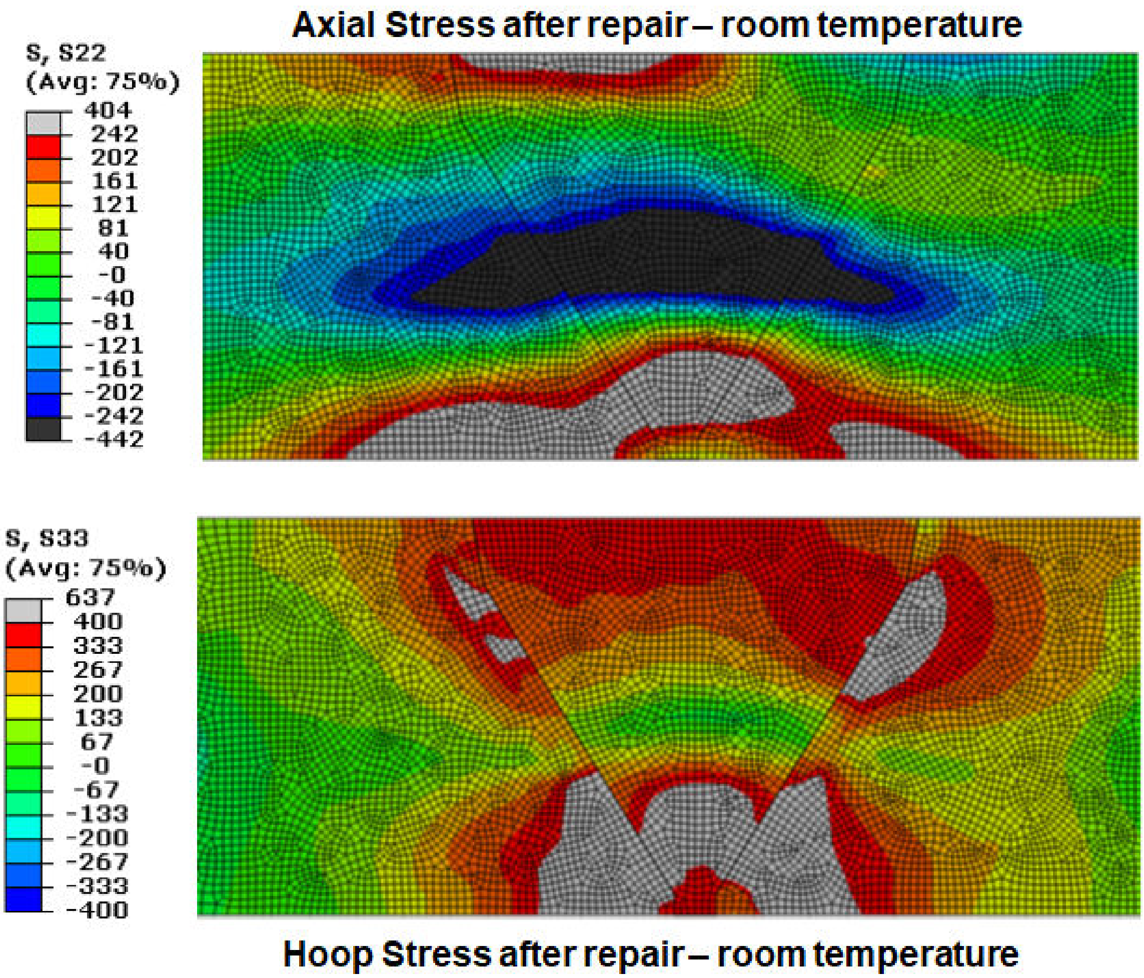

Figure 42: Axial and Hoop WRS after 10 % repair.

The WRS field after repair and application of the MSIP process are illustrated in Figure 43 for axial stresses and Figure 44 for hoop stresses. It is clear that the MSIP reduces the WRS fields for both axial and hoop stresses.

The axial and hoop stresses after the repair at operation are shown in Figure 45 (blue curves) at the weld centerline and in the HAZ. These are used in the LOCA assessments when considering the repair cases. The axial and hoop WRS fields after repair and MSIP at operation temperature of 288 C at the weld centerline and HAZ are shown in Figure 46 (blue curves) and these are used for the xLPR LOCA analyses shown in the above sections for the 28-inch recirculation line.

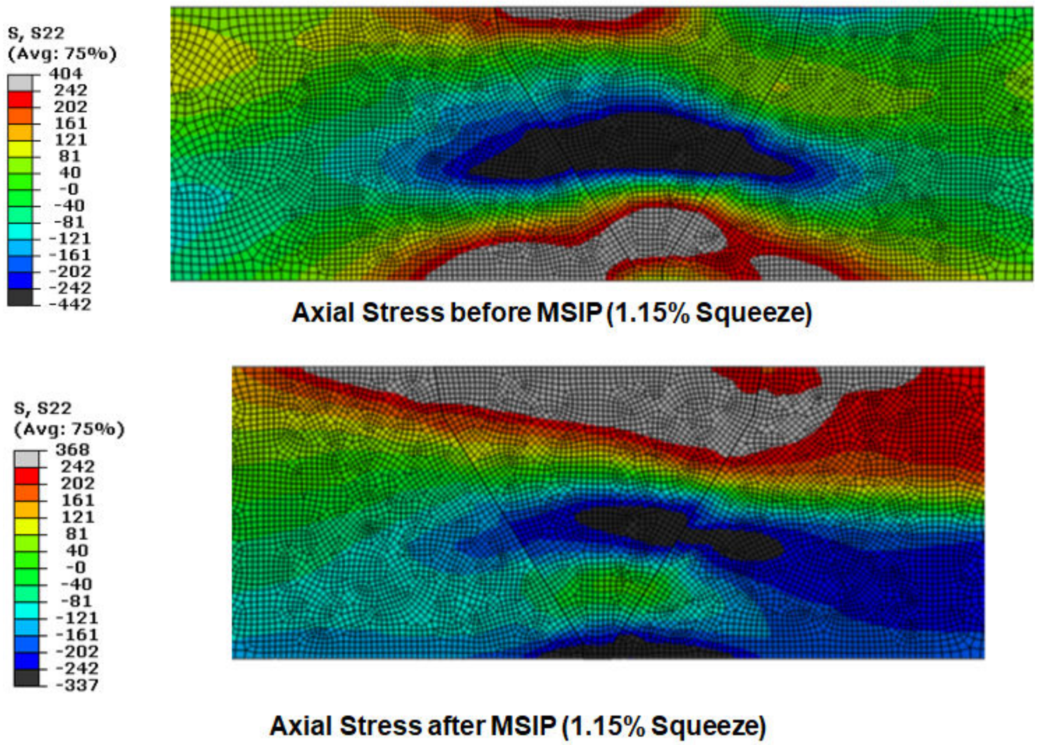

Figure 43: Axial WRS before and after 10 % repair and MSIP.

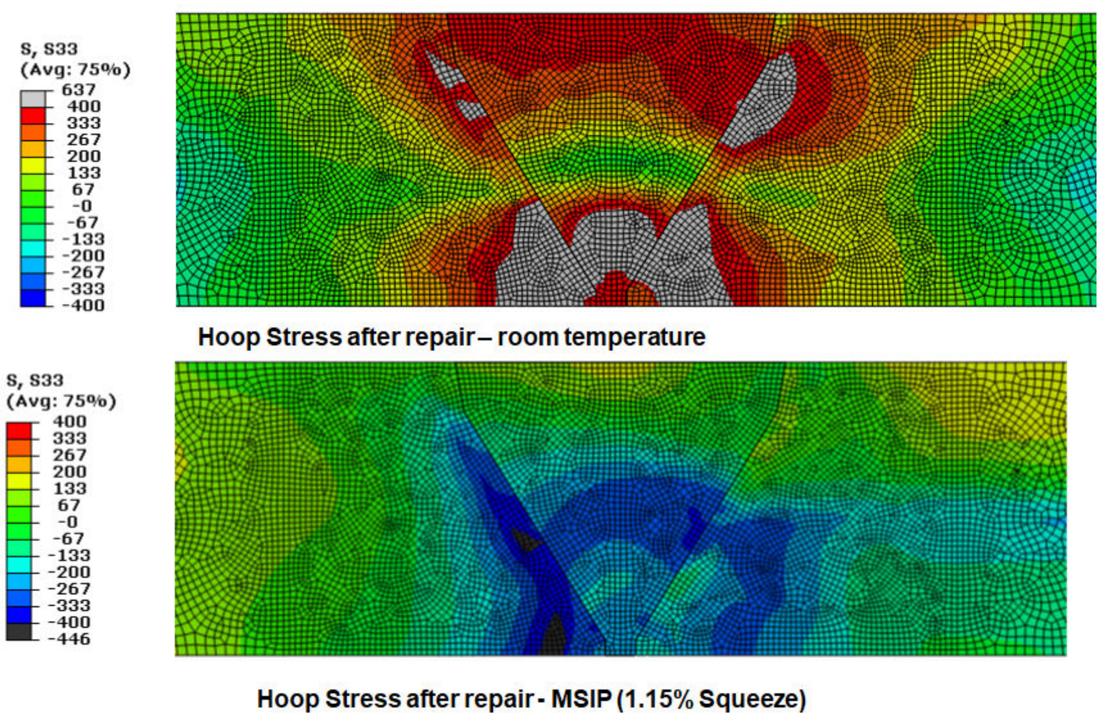

Figure 44: Hoop WRS before and after 10 % repair and MSIP.

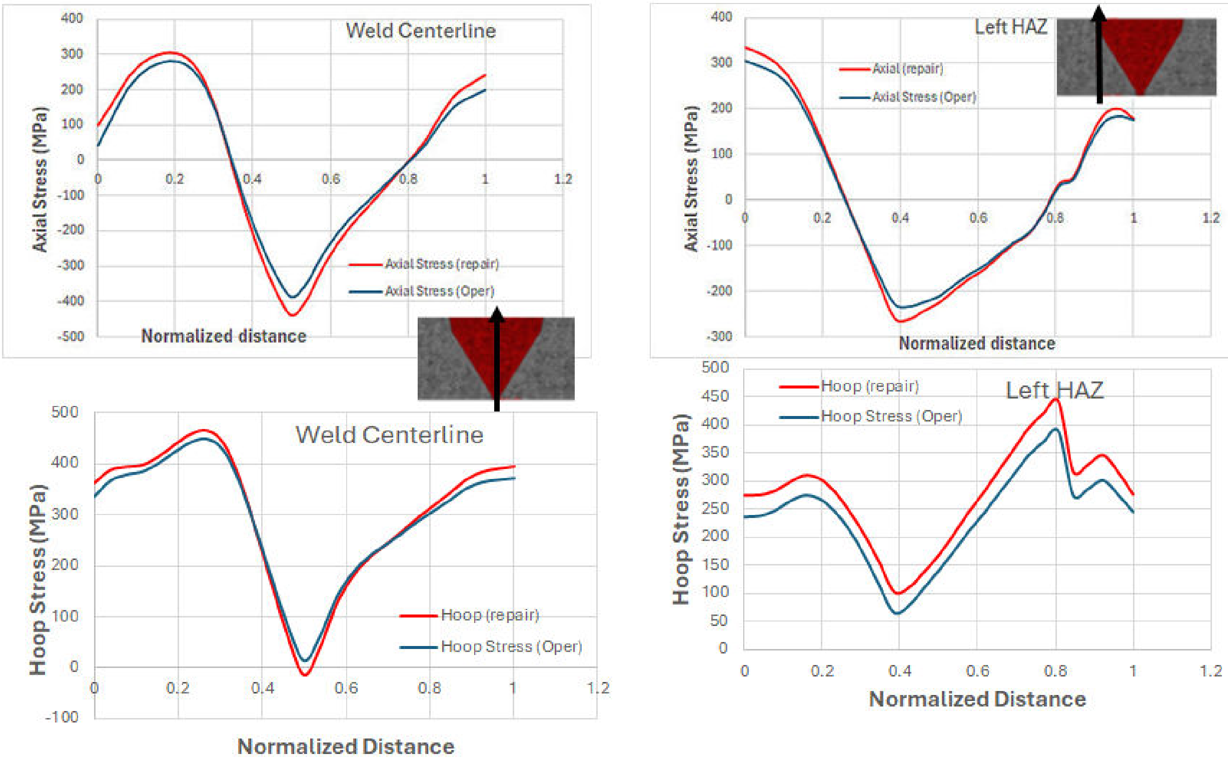

Figure 45: Operation WRS fields at weld centerline and HAZ after repair.

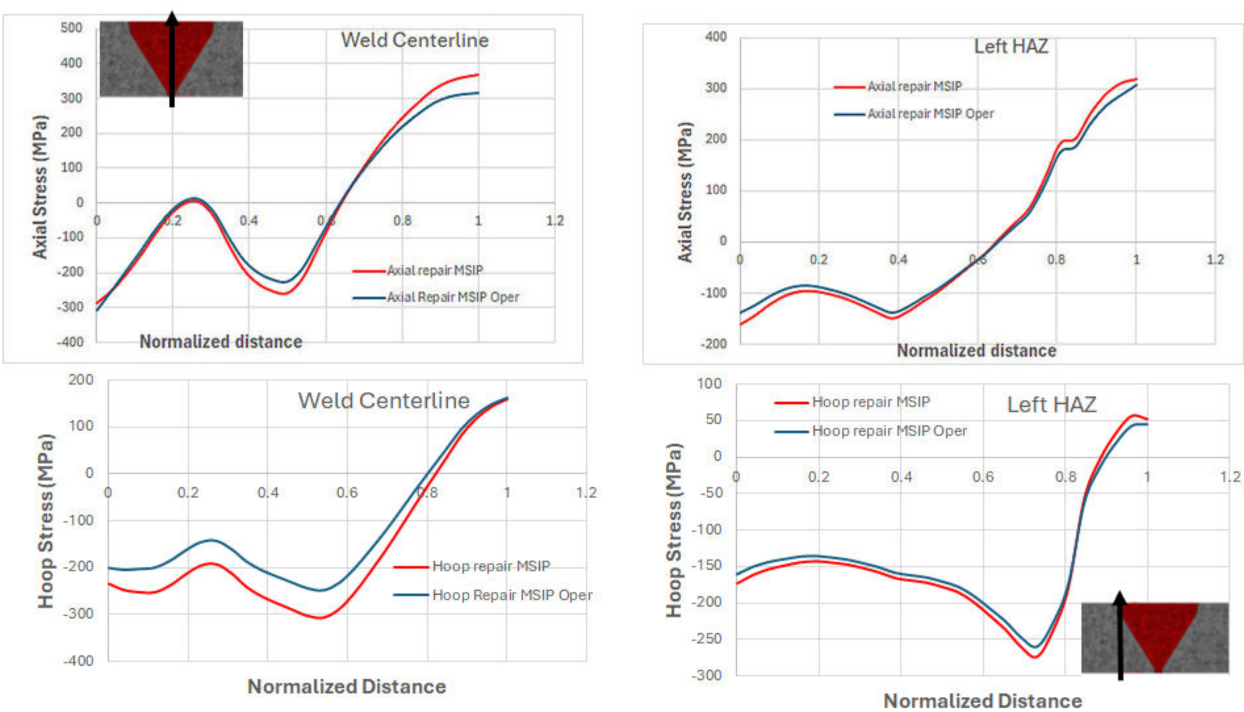

Figure 46: Operation WRS fields at weld centerline and HAZ after repair and MSIP.

7.2.4.3 *Mean WRS profiles and tabulated value for the 28-inch Recirculation line (BWR-1a)*

The mean WRS profiles for each of these cases are shown below (Figure 47), with the values recorded in Table 45. Each profile had a standard deviation of 50 MPa to represent the uncertainty.

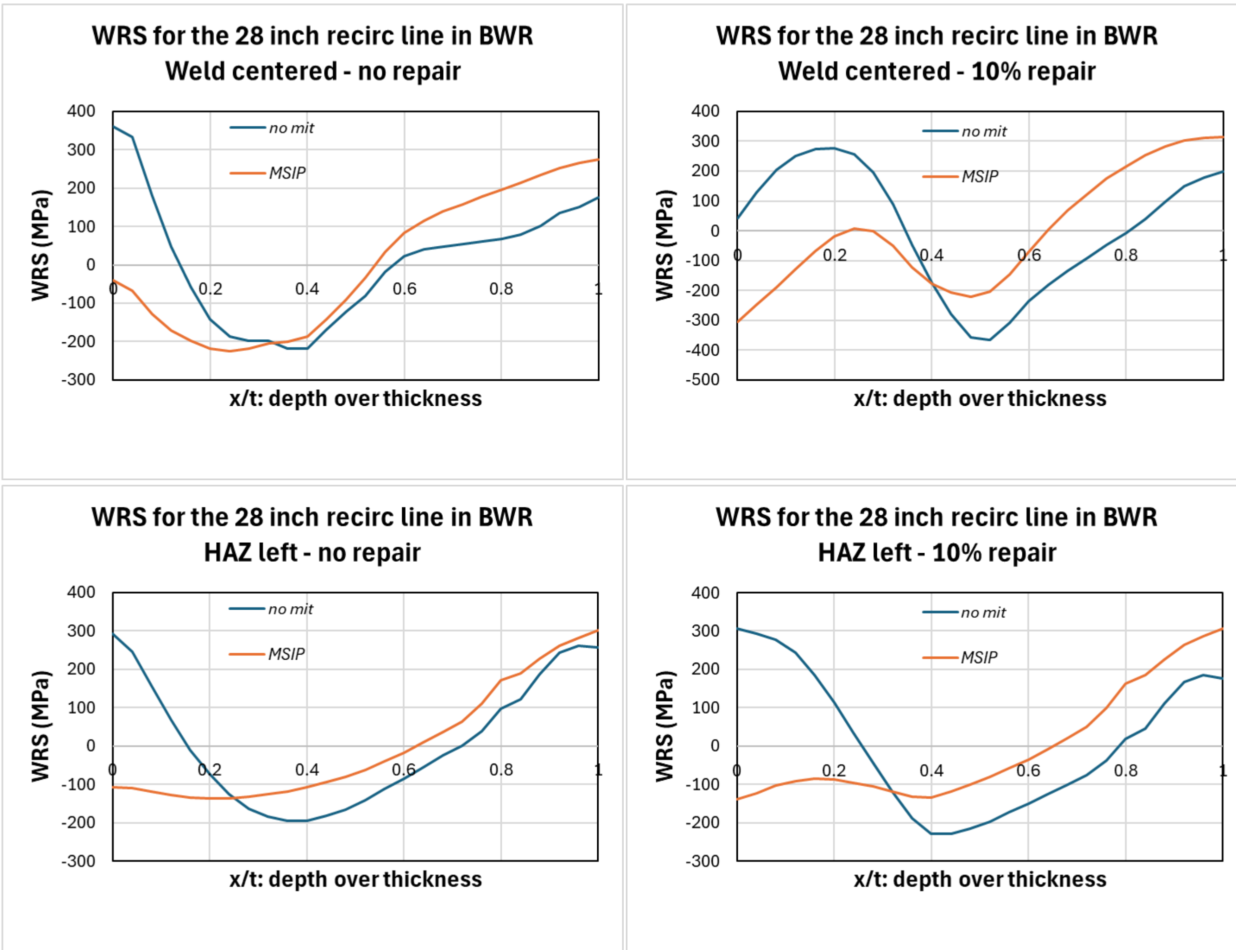

Figure 47: Resulting mean WRS with and without MSIP for the four considered cases for the 28" recirculation line

A standard deviation of 50 MPa is applied at all locations through the thickness. The large standard deviation represents the uncertainty associated with using a single analysis and the consideration that WRS is an impactful parameter in the xLPR analyses, such that a misrepresentation could have a potential impact on the conclusions.

Table 45: Mean WRS values as function of x/t for BWR-1a.

	Weld baseline		Weld repair		HAZ baseline		HAZ repair	
x/t	no mit	MSIP	no mit	MSIP	no mit	MSIP	no mit	MSIP
0	359.563	-41.2381	42.146	-305.936	293.257	-106.895	306.191	-138.025
0.04	332.9812	-67.5313	128.098	-247.837	245.2139	-110.498	293.7439	-122.299
0.08	179.535	-128.477	205.196	-188.032	157.2103	-118.506	276.9597	-103.552
0.12	46.78782	-170.178	251.1831	-127.993	67.85049	-127.392	243.5287	-90.4037
0.16	-57.6895	-198.391	273.7634	-66.8486	-9.96309	-133.427	186.1331	-85.2759
0.2	-140.733	-218.95	277.6943	-18.2388	-73.2775	-135.958	114.0789	-87.9481
0.24	-186.906	-225.981	256.464	8.226443	-125.031	-135.738	35.2776	-95.4032
0.28	-196.974	-218.27	195.1771	0.158056	-162.551	-132.339	-43.2585	-105.358
0.32	-198.568	-205.364	87.11858	-50.1112	-183.921	-125.81	-118.788	-118.246
0.36	-218.783	-200.883	-48.5398	-121.657	-195.011	-117.586	-188.319	-131.049
0.4	-217.438	-186.636	-175.074	-176.718	-194.611	-107.596	-229.134	-133.227
0.44	-168.36	-141.143	-278.732	-207.703	-182.416	-94.3483	-228.011	-118.402
0.48	-121.931	-88.8965	-355.969	-221.156	-164.777	-79.3222	-216.214	-99.8497
0.52	-80.1034	-34.4446	-366.73	-204.912	-140.548	-61.6961	-196.776	-79.6993
0.56	-18.9497	33.4987	-306.402	-146.658	-111.048	-40.5149	-172.006	-56.9691
0.6	22.68784	84.29018	-236.264	-69.674	-84.3236	-18.0949	-150.579	-34.1601
0.64	40.55658	115.8858	-179.551	3.845264	-55.0833	8.764544	-125.984	-7.38756
0.68	47.99068	138.439	-133.841	67.54633	-25.1949	37.18451	-99.5453	21.35363
0.72	53.43508	158.5188	-91.8228	124.0876	-0.05363	64.48509	-76.2899	50.69989
0.76	61.64268	178.5807	-48.882	174.7085	39.38762	110.6247	-37.6355	99.72923
0.8	68.3223	195.9639	-7.47921	217.0031	96.50525	170.566	19.30415	163.0361
0.84	77.92686	212.7334	38.07686	252.6471	122.7948	189.2818	45.23614	184.8066
0.88	101.9788	232.9446	98.02971	283.3208	186.3348	227.4065	110.2024	226.8271
0.92	135.1974	252.2875	150.4443	302.2216	242.4934	260.5652	166.7576	263.4894
0.96	150.8525	265.2182	177.2915	310.9184	260.8453	281.383	184.4207	286.5658
1	175.759	275.375	198.554	314.481	256.296	301.232	176.919	306.812

7.2.5 BWR-1b: WRS Fields for 12-Inch Recirculation Line

The analysis for the 12-inch recirculation line is quite similar to that for the 28-inch line discussed above. Therefore, not all the detailed comparison results will be shown and we focus on the WRS fields necessary to perform the xLPR based LOCA analyses in this section.

The weld groove geometry considered for the 12-inch line was obtained from Table 8-1 of EPRI NP-1743 ([34]) which are typical for BWR large diameter recirculation piping with intermediate thicknesses of between 0.5 and 0.75 inches. The groove geometry type and dimensions of the 12-inch case is shown in Figure 48 where the dimensions are shown in metric units. The number of weld deposition layers, total number of weld passes, and weld heat inputs were estimated from Table 8-2 of EPRI NP-1743. Six layers and 17 total passes were assumed as illustrated in Figure 49. It is seen that a length of the recirculation line chosen for this analysis was about five times the diameter of the pipe. The material properties used for the base metal pipe are 304 stainless steel and those for the weld metal are 308 stainless steel. The physical properties used for the thermal analysis consist of conductivity, heat capacity, density, and convective constants which are temperature dependent. The material properties for the structural analysis, which uses the temperature versus time history produced from the thermal analysis, consist of elastic modulus, Poisson ratio, and thermal expansion which are temperature dependent also. The stress strain curves used are shown in Figure 29. Isotropic hardening was used for the axisymmetric analyses to ensure upper bound WRS fields are produced for the crack growth assessments discussed in the main body of the report. The detailed analysis procedures are discussed in [27].

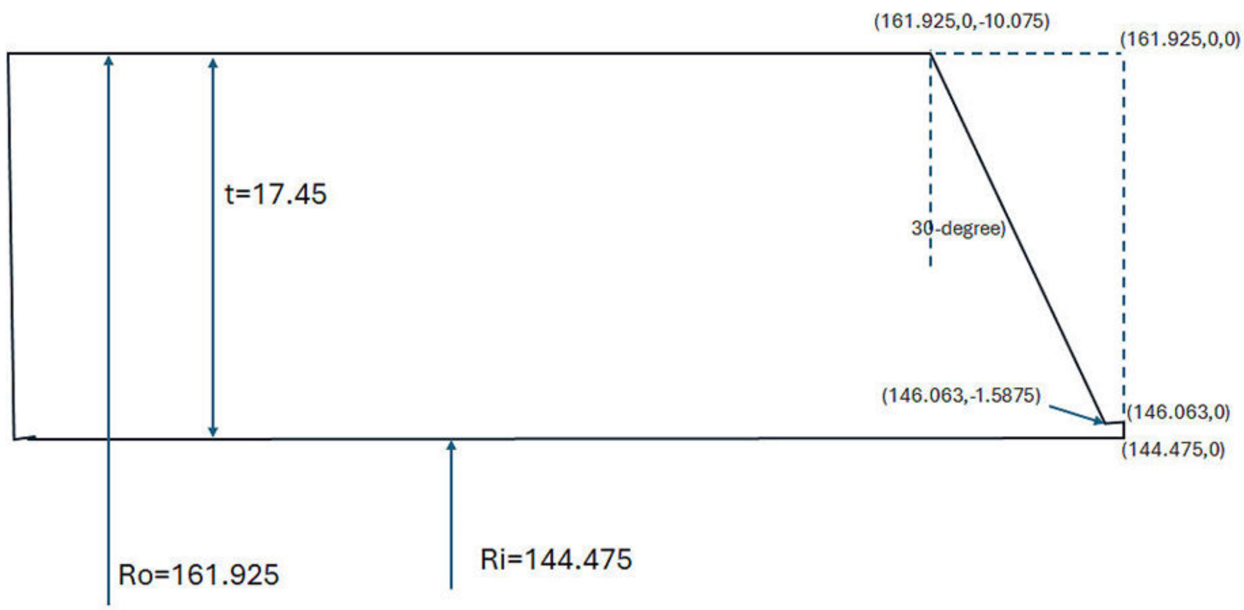

Figure 48: Geometry (in mm) and groove type for the 12-inch recirculation line WRS analysis.

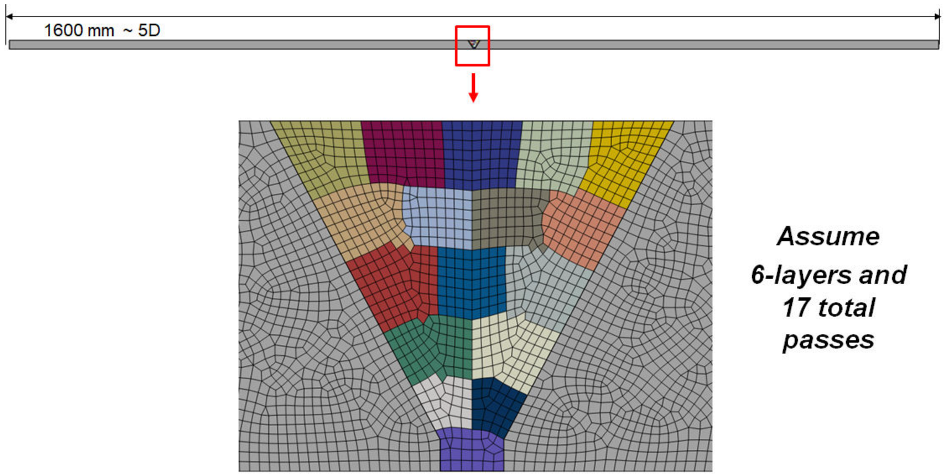

Figure 49: Weld model and weld passes for the 12-inch line.

7.2.5.1 Baseline results 12 inch line

Contour plots of the axial WRS field after welding, after hydrotest and removal, and at operation temperature are shown in Figure 50. The hydrotest modeling consists of applying a pressure of 1.25 times the operation pressure of 7.24 MPa (9.05 MPa). The operation temperature (288C) WRS field is shown on the bottom of Figure 50. The axial WRS fields are used in the circumferential crack growth assessments for the 12-inch line.

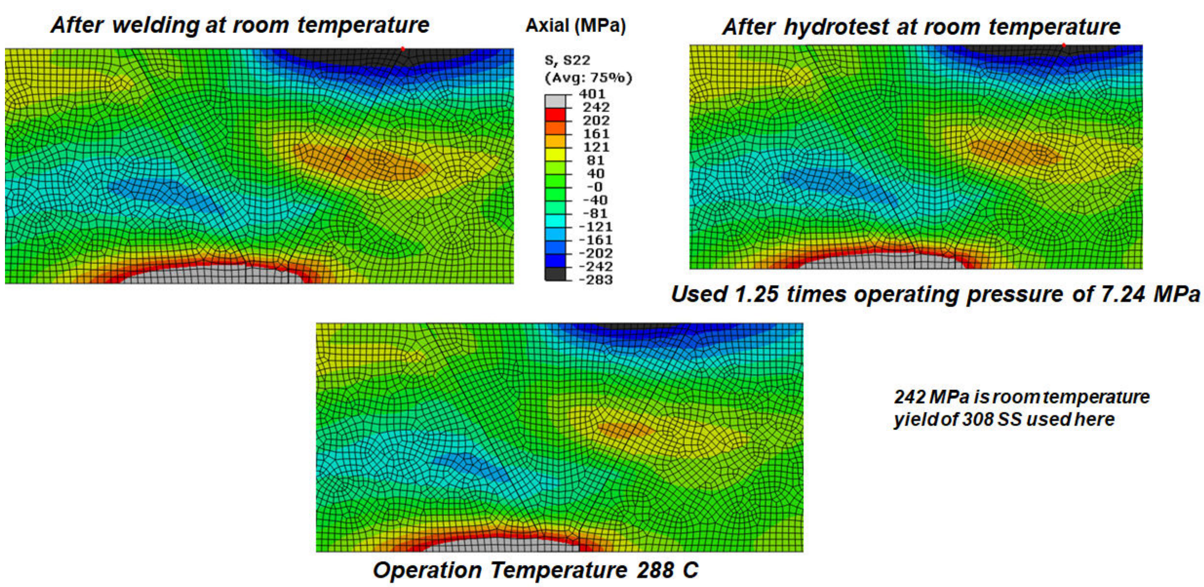

Figure 50: Predicted axial WRS field after welding at room temperature (upper left), after hydrotest and removal (upper right), and at operation temperature of 288C 12-inch line.

Contour plots of the hoop WRS field after welding, after hydrotest and removal, and at operation temperature are shown in Figure 51 for the 12-inch line. The hydrotest does reduce the hoop

WRS field somewhat for the 12-inch line. The operation temperature (288C) WRS field is shown on the bottom of Figure 51. This field, used for axial crack growth assessments, is included for completeness. Interestingly the hoop stresses are rather large in the HAZ. Figure 52 illustrates the effect of the hydrotest on reducing the WRS field for the 12-inch baseline analysis. As can be seen the hoop stresses are reduced over the last half of the thickness due to hydrotest application and removal.

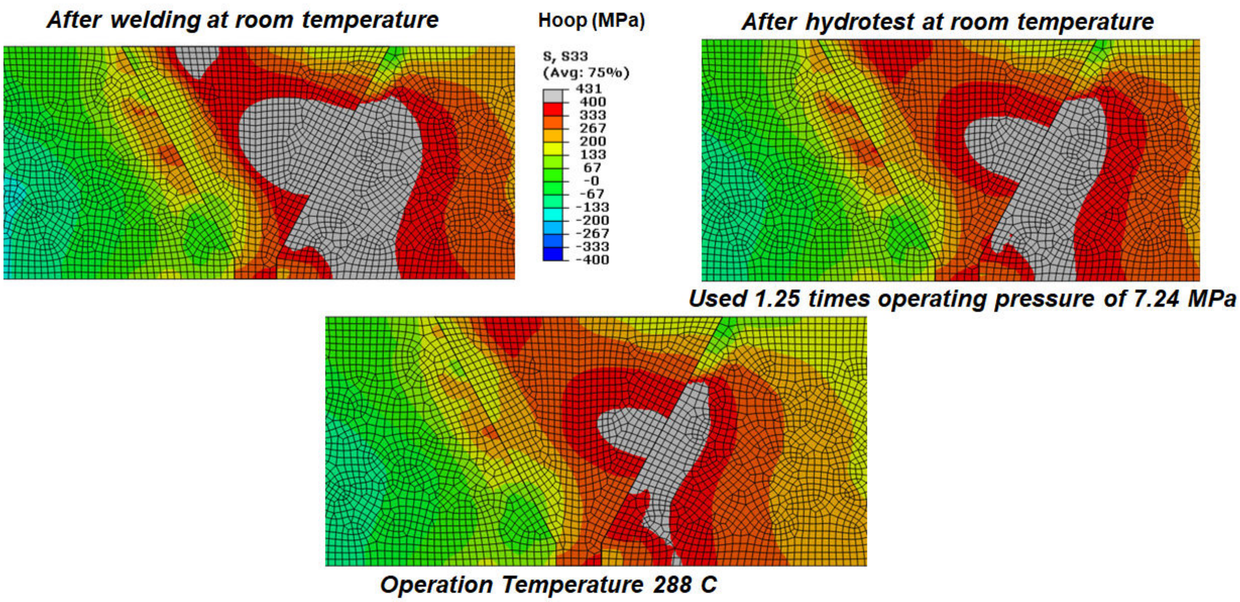

Figure 51: Predicted hoop WRS field after welding at room temperature (upper left), after hydrotest and removal (upper right), and at operation temperature of 288C 12-inch line.

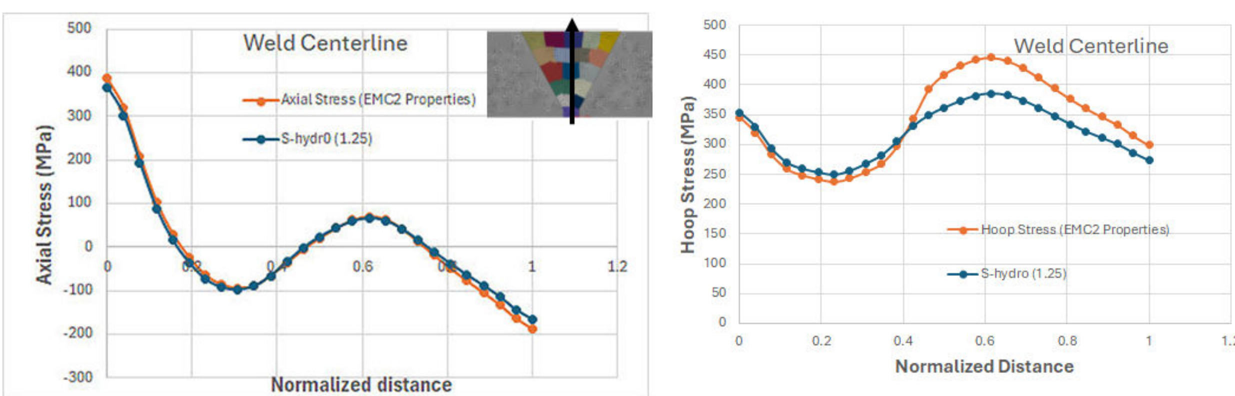

Figure 52*:* Effect of hydrotest on WRS fields plotted through center of weld.

The operation stresses at 288C (without service loads applied) are shown in Figure 53 through the center of the weld and Figure 54 in the HAZ region. The operation axial stresses are used for the xLPR LOCA analyses of these lines for circumferential crack growth calculations while the hoop streses are used for axial crack growth calculations.

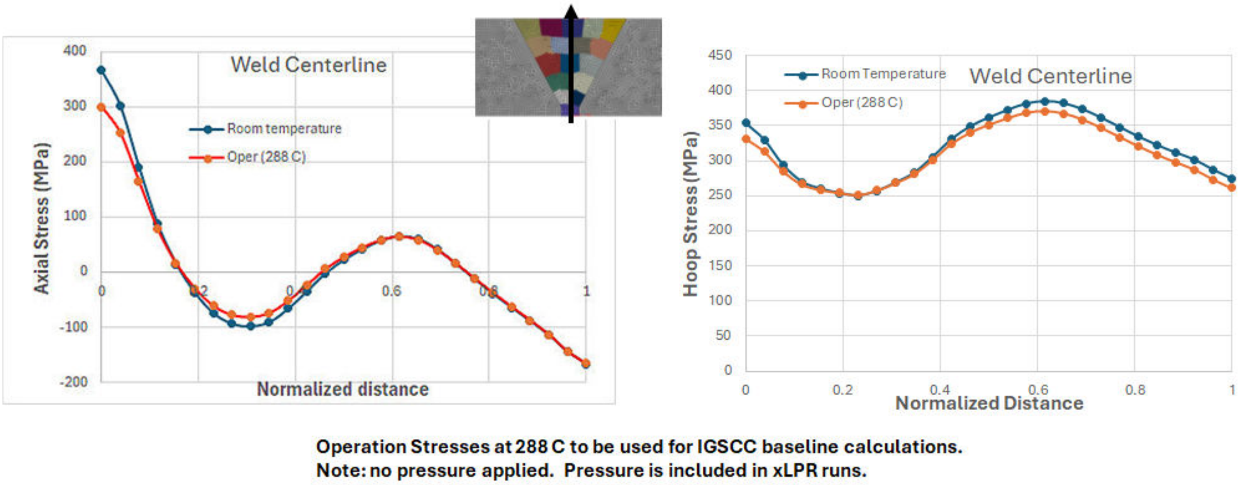

Figure 53: Operation temperature (288C) axial WRS field for 12-inch line (centerline).

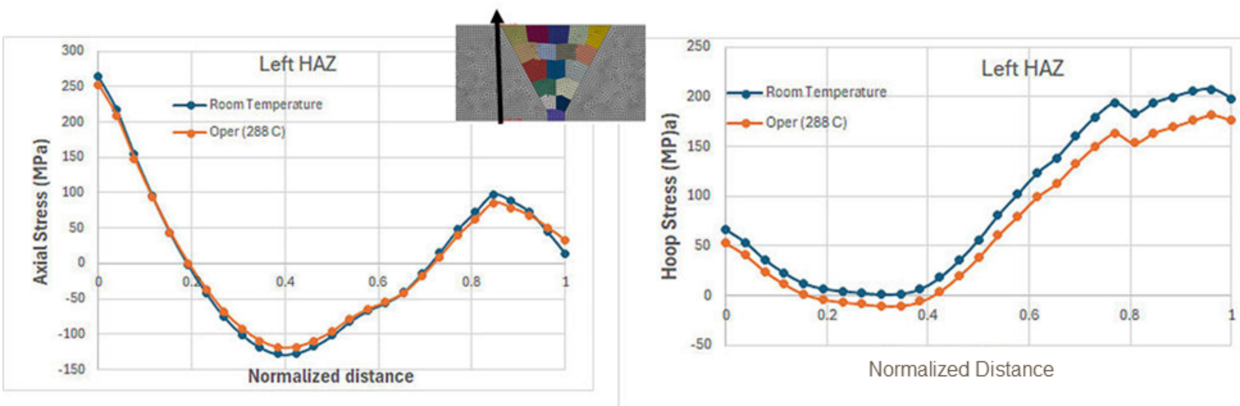

Figure 54: Operation temperature (288C) hoop WRS field for 12-inch line (HAZ).

7.2.5.2 MISP for baseline case 12-Inch line

The MSIP process for the 12-inch line is a little different to that used for the 28-inch line as is illustrated in Figure 55. In Figure 36 (for the 28-inch line) the ring is 2.25-inch long and is applied 2 inches from the weld centerline for the 28-inch line while, as seen in Figure 55, this distance is 1.5-inch for the 12-inch line. Both the width of the squeeze ring and the distance from the weld are design parameters determined from analysis. The ring is then squeezed and released resulting in 1.31% squeeze for the 12-inch line as this reduced the WRS field optimally. Percent squeeze is defined the amount of deformation that remains after release of the tool divided by the outer diameter of the pipe multiplied by 100. During the squeeze process plastic deformation is produced under the tool resulting in a ‘ring’ load. This ring load then results in compression in the region of the weld and HAZ.

The effect of the MSIP application on the axial and hoop stress distribution both before and after application is illustrated in Figure 56 and Figure 57, respectively. It is seen that MSIP produces compressive stresses in the weld and HAZs. The improvement in axial WRS is a little better in the HAZ to the right of the weld while the improvement in hoop WRS fields is a little better to the left HAZ of the weld.

- **Applied MSIP treatment following process used by NuVision (displacement control).**
- **Used 2.25 inch long rings and at 2 inch from the weld centerline. This did not perform optimally and WRS to the right of the weld in the HAZ were not reduced enough.**
- **Used 2.25 inch long tool at 1.5 inch from the weld centerline. This resulted in better compression residual stresses, especially on the right side of the weld for the hoop stresses and was therefore used here.The tool to the right was assumed.**
- **Provided squeeze of 1.31% (examined other squeeze amounts also). Squeeze is defined (by NuVision) as the amount of deformation after tool removal springback divided by the OD of the pipe (times 100). The value used is typical values based on recent EMC2 assessment of NuVision plans for Swiss regulator.**

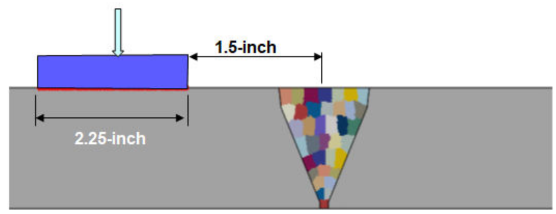

Figure 55: Illustration of the MSIP process for 12-inch recirculation line.

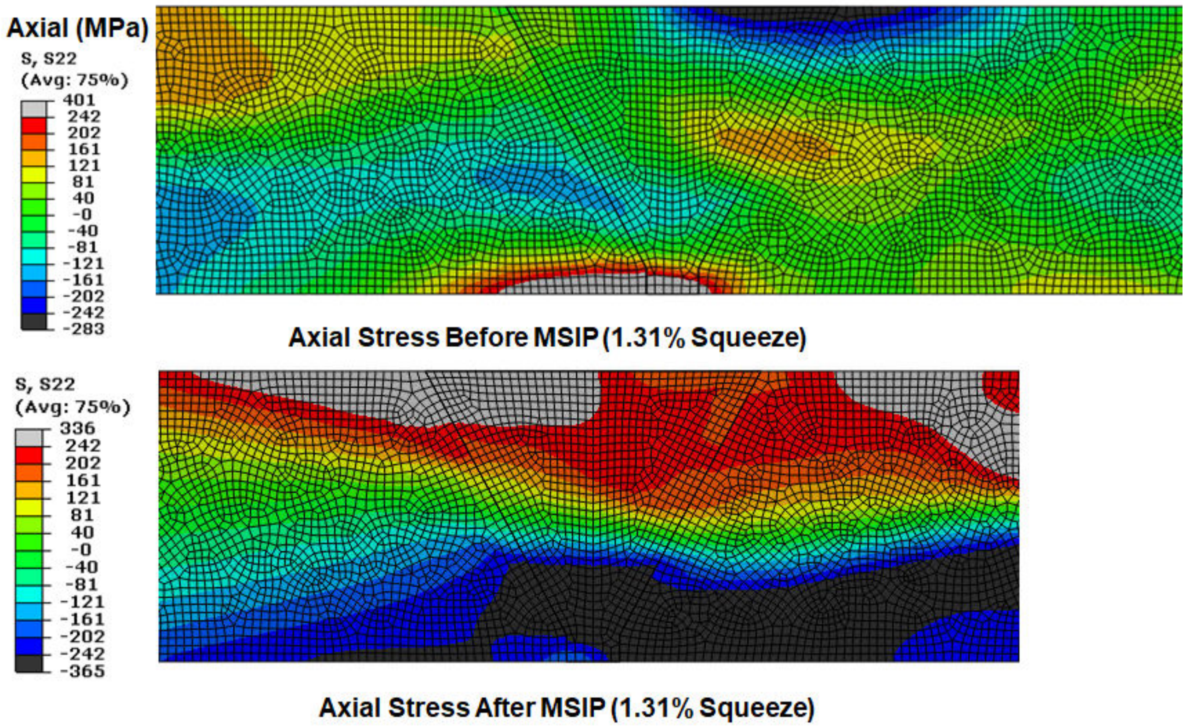

Figure 56: Effect of MSIP on axial stresses before and after application.

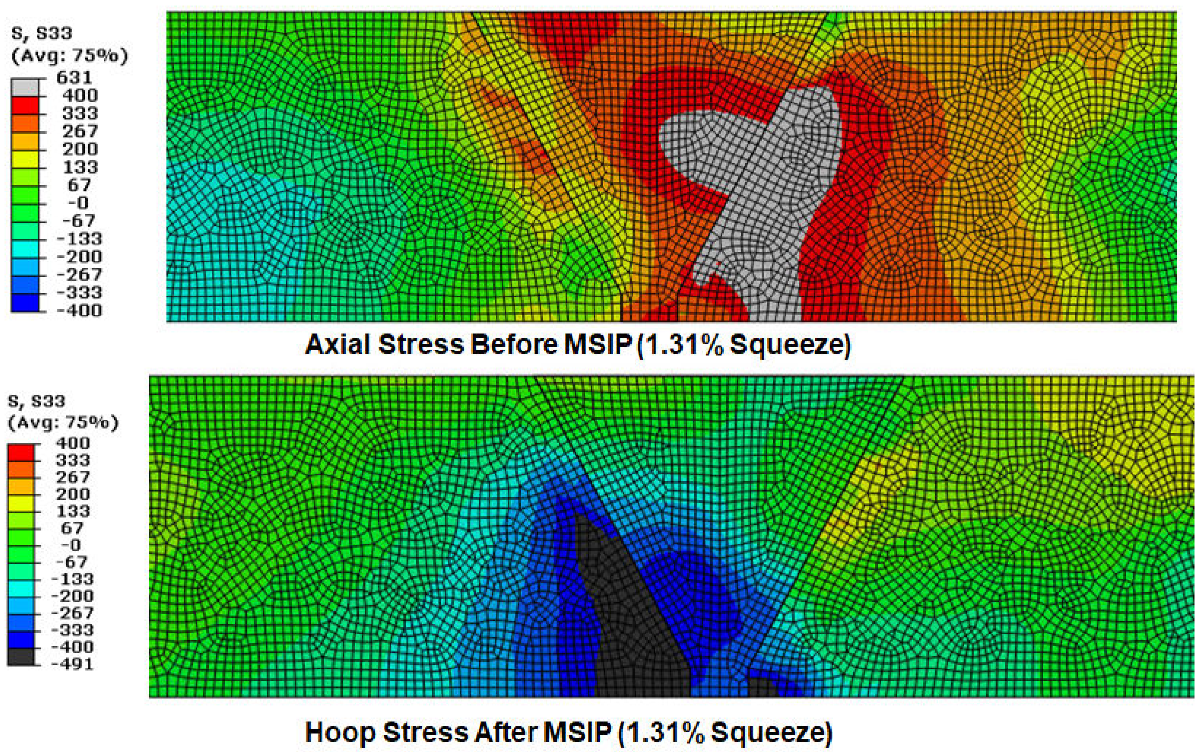

Figure 57: Effect of MSIP on hoop stresses before and after application.

Line plots of the WRS fields both before and after MSIP squeeze of 1.31% is shown in Figure 58 at room temperature for the 12-inch line. The MSIP process reduces the WRS field in the weld and HAZ significantly. Line plots of the WRS fields after MISP and operation temperature are shown in Figure 59 at for the 12-inch line. The WRS fields of Figure 59 are used in the xLPR code for the assessment of the effect of MSIP after 20 years of operation as discussed in the main body of the report.

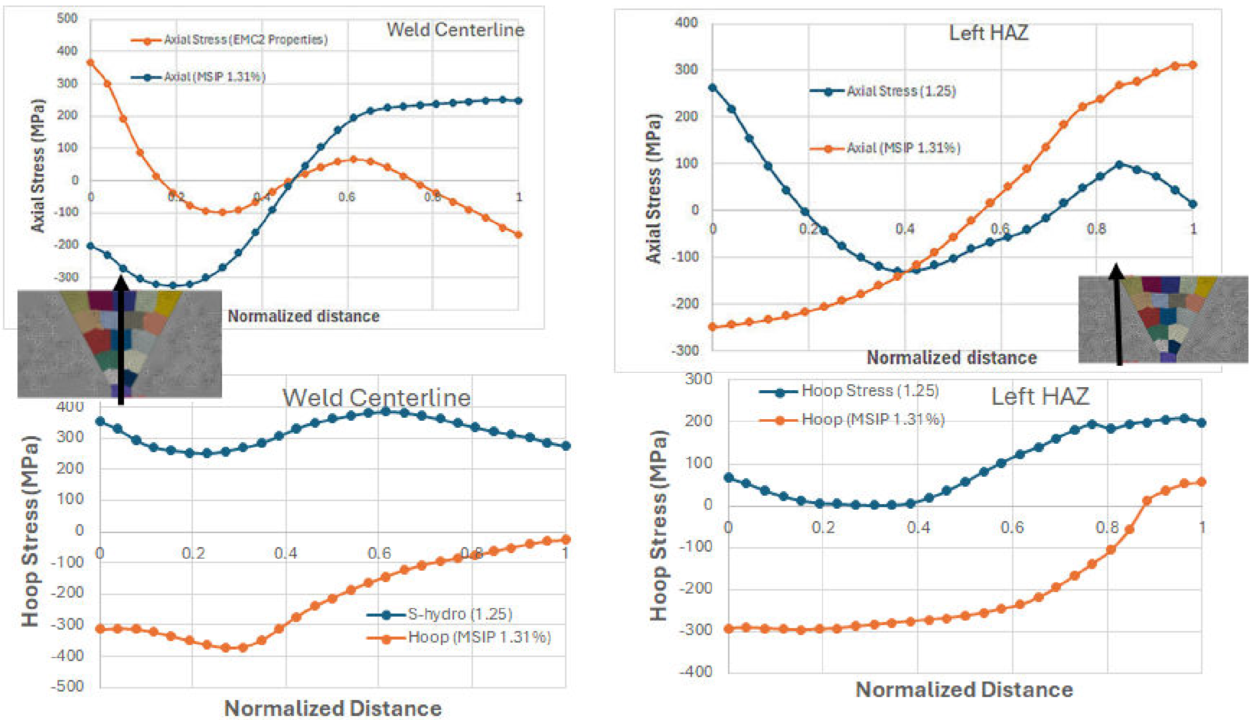

Figure 58: Line plots of WRS fields along the centerline and in the HAZ at RT after MSIP.

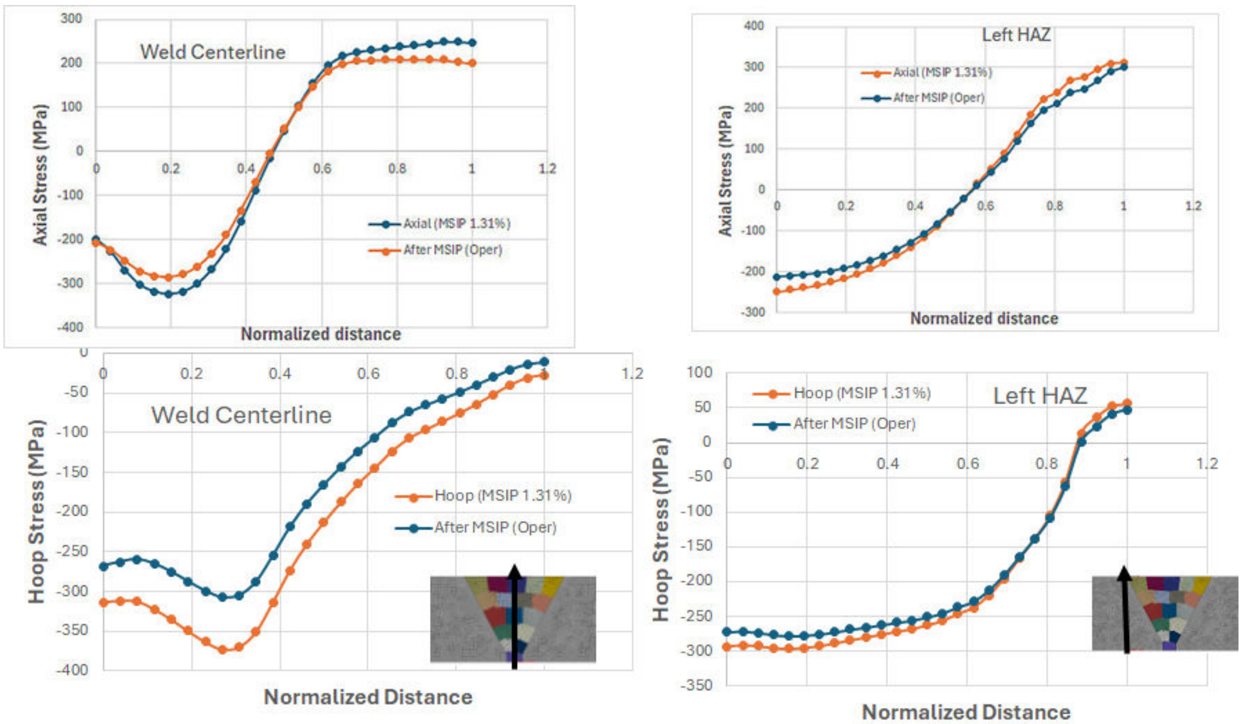

Figure 59: Line plots of WRS fields along the centerline and in the HAZ at operation.

7.2.5.3 Repair Weld Effects and MSIP After Repair for 12-inch line

The repair for the 12-inch line is similar to that described for the 28-inch line above. A 10% of the thickness weld repair is assumed. The material is removed after the baseline WRS analysis and four passes were assumed for the repair weld with deposition from left to right HAZ in the weld. Next the hydrotest is applied to the pipe after the repair. Then the WRS field at operation after the repair is extracted for the xLPR LOCA analyses. In addition, MSIP is also applied and the operation WRS after MSIP is also extracted for the LOCA analyses.

The axial and hoop WRS fields after the 10% repair weld is made (and after hydrotest) is shown in Figure 60. By comparing the axial stresses to those in Figure 50 (axial stress) and Figure 51 (hoop stress) after hydrotest it is clear that a 10% repair increases both the magnitude and volume of WRS near the ID.

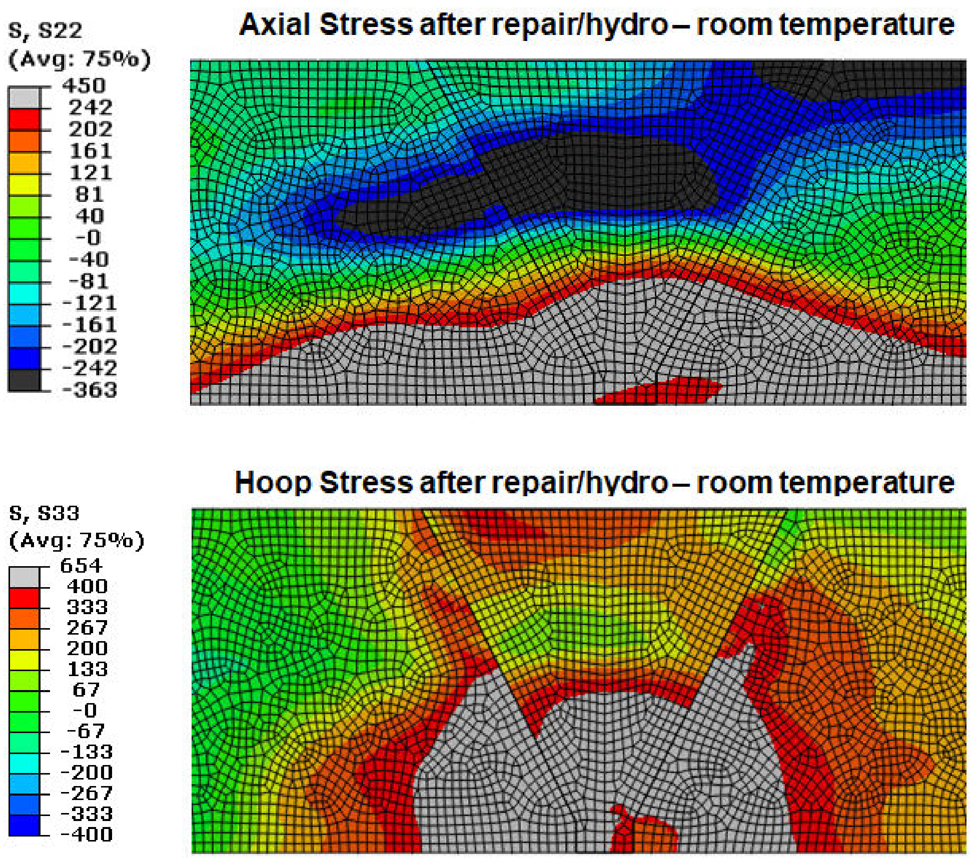

Figure 60: Axial and Hoop WRS after 10 % repair for 12-inch line.

The WRS field after repair and application of the MSIP process are illustrated in Figure 61 for axial stresses and Figure 62 for hoop stresses for the 12-inch line. It is clear that the MSIP reduces the WRS fields for both axial and hoop stresses.

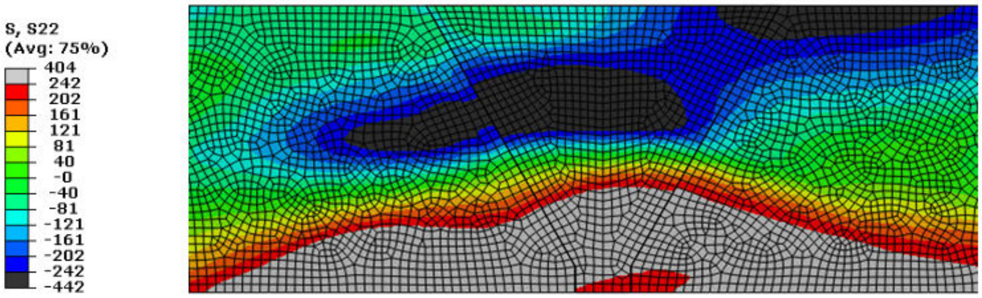

Axial Stress before MSIP (1.15% Squeeze)

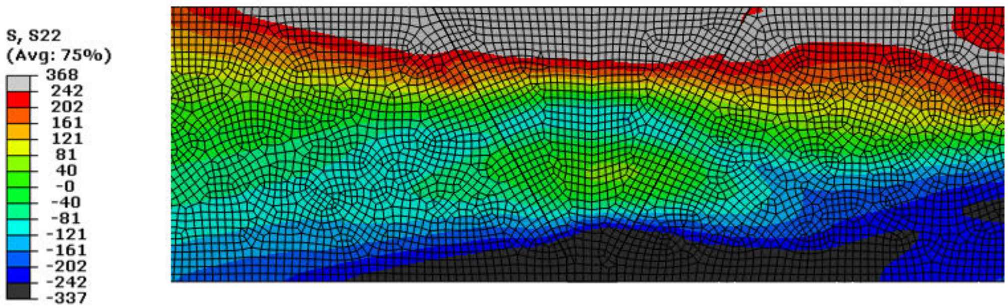

Axial Stress after MSIP (1.15% Squeeze)

Figure 61: Axial WRS before and after 10 % repair and MSIP for 12-inch line.

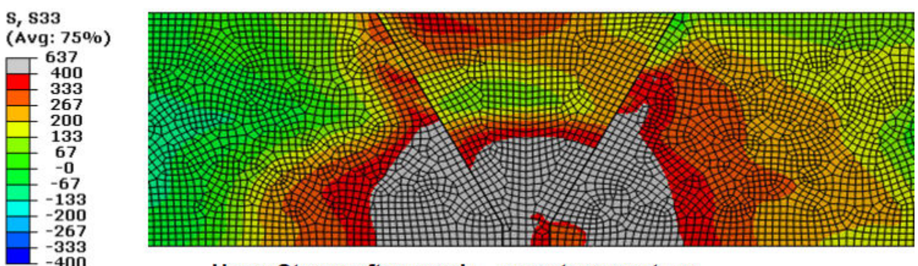

Hoop Stress after repair – room temperature

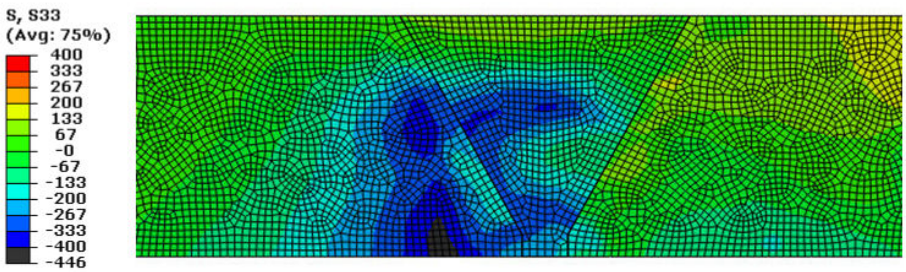

Hoop Stress after repair - MSIP (1.15% Squeeze)

Figure 62: Hoop WRS before and after 10 % repair and MSIP for 12-inch line.

The axial and hoop stresses after the repair at operation are shown in Figure 63 (blue curves) at the weld centerline and in the HAZ for the 12-inch line. These are used in the LOCA assessments when considering the repair cases. The axial and hoop WRS fields after repair and MSIP at operation temperature of 288 C at the weld centerline and HAZ are shown in Figure 64 (blue curves) and these are used for the xLPR LOCA analyses shown in the above sections for the 12-inch recirculation line with repairs considered.

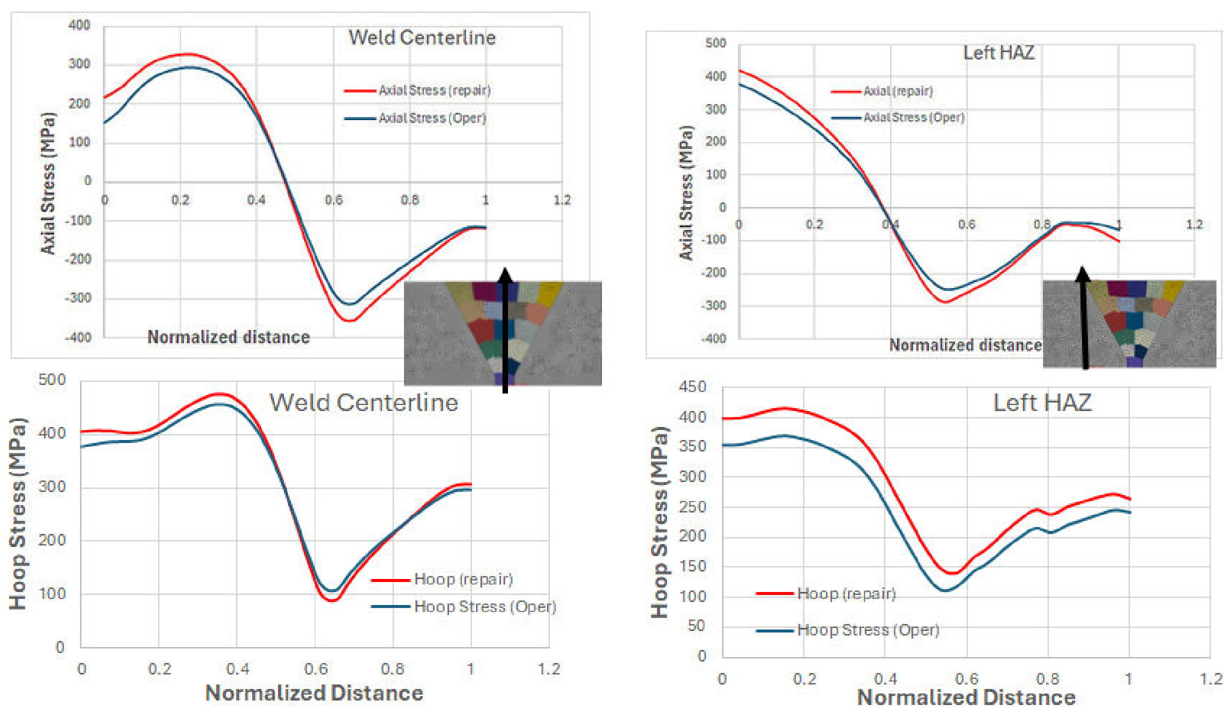

Figure 63: Operation WRS fields at weld centerline and HAZ after repair (12-inch).

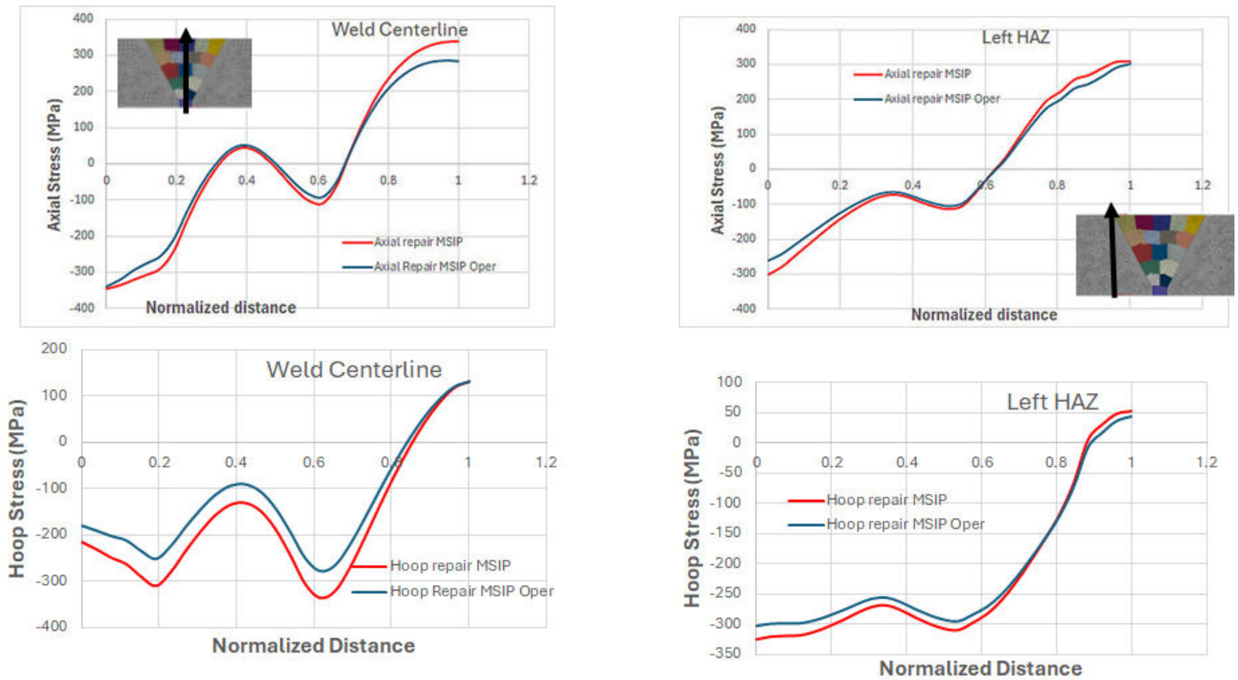

Figure 64: Operation WRS fields at weld centerline and HAZ after repair and MSIP.

7.2.5.4 Mean WRS profiles and tabulated values for the 12-inch Recirculation Lines (BWR-1b)

The same reference case and three sensitivity cases defined for the 28" recirculation line were generated for the WRS profiles on the 12" recirculation line. The mean WRS profiles for each of these cases are shown below (Figure 65).

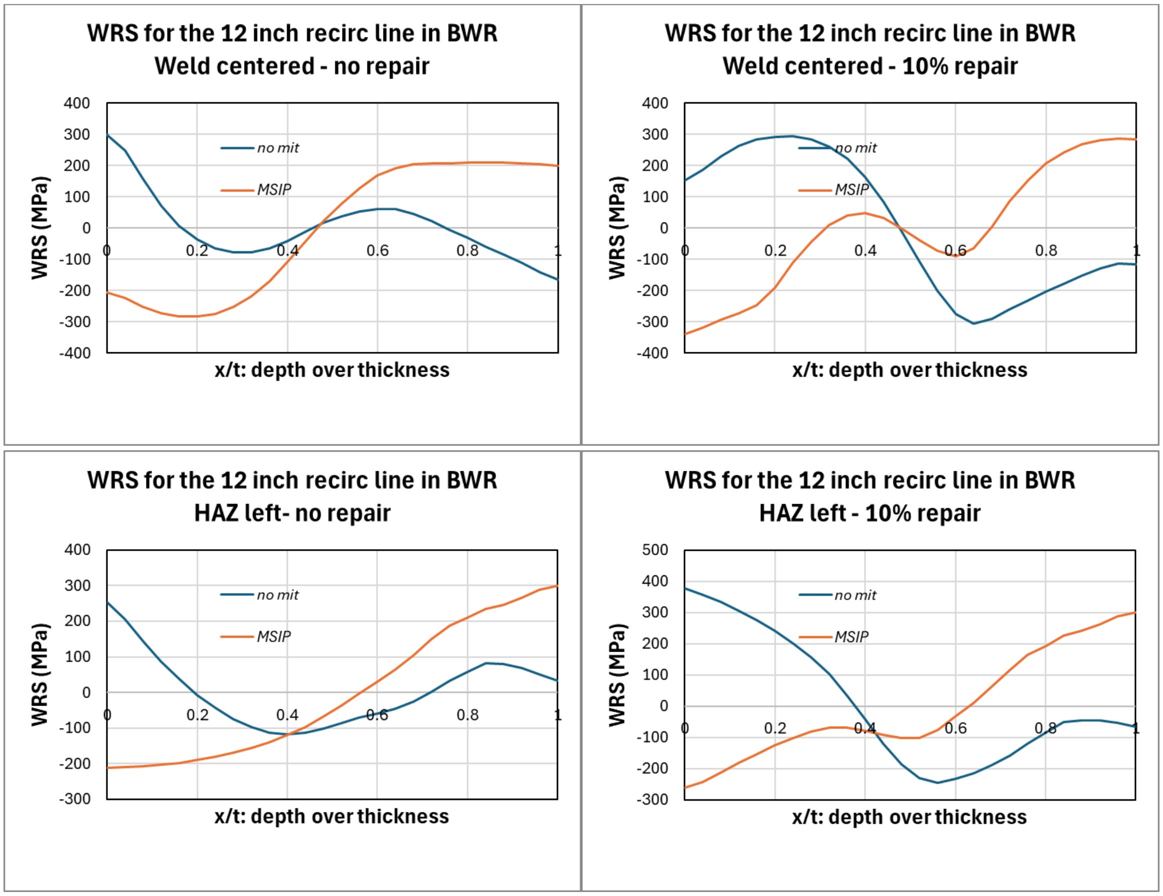

Figure 65: Resulting mean WRS with and without MSIP for the four considered cases for the 12" recirculation line

In addition, a standard deviation of 50 MPa is applied at all locations through the thickness. The large standard deviation represents the uncertainty associated with using a single analysis and the consideration that WRS is an impactful parameter in the xLPR analyses, such that a misrepresentation could have potential impact in the conclusions.

Table 46: Mean WRS values as function of x/t for BWR-1b.

	Weld baseline		Weld repair		HAZ baseline		HAZ repair	
x/t	no mit	MSIP	no mit	MSIP	no mit	MSIP	no mit	MSIP
0	299.831	-207.098	154.114	-340.047	252.194	-212.862	378.394	-262.481
0.04	248.3417	-223.711	185.9618	-320.152	206.2942	-210.315	358.4992	-242.147
0.08	157.7244	-250.959	230.3939	-293.429	143.8282	-207.205	333.1462	-212.594
0.12	70.70278	-272.477	264.336	-272.73	87.43154	-203.569	306.0618	-182.715
0.16	8.373734	-282.63	283.5223	-247.544	36.80176	-198.143	275.2681	-153.031
0.2	-35.6625	-283.395	292.865	-191.084	-6.76512	-190.394	240.7696	-125.47
0.24	-65.355	-274.29	293.6294	-110.623	-44.0049	-181.274	201.7284	-101.82
0.28	-78.5967	-252.76	283.2364	-43.1305	-74.9398	-170.01	156.6114	-82.1173
0.32	-78.789	-217.907	261.2352	8.36533	-97.5541	-156.124	102.8016	-69.3289
0.36	-65.8523	-169.311	223.6933	40.85695	-112.452	-139.582	34.1633	-68.1259
0.4	-40.3707	-107.617	164.7458	48.32697	-118.044	-120.102	-43.9841	-78.3531
0.44	-10.4216	-41.1515	84.91647	32.24067	-114.048	-96.546	-120.618	-92.4552
0.48	16.35777	21.96062	-8.78027	0.110893	-103.016	-68.5503	-185.635	-102.456
0.52	36.71845	77.87449	-107.824	-38.7406	-86.7793	-36.8816	-231.443	-101.357
0.56	52.60626	127.8282	-201.758	-72.9794	-70.5178	-3.38172	-244.985	-76.0722
0.6	62.04727	167.8557	-276.044	-89.2723	-58.683	30.59967	-232.902	-33.3513
0.64	60.55063	192.5898	-306.887	-65.0625	-46.1138	64.2723	-214.378	10.33473
0.68	46.19152	203.7142	-290.585	5.273527	-25.4479	105.582	-189.646	60.97204
0.72	22.46741	207.3276	-260.191	85.67103	1.717903	150.2638	-157.733	115.0888
0.76	-4.85242	208.3837	-231.407	154.0807	31.97774	188.5659	-120.105	163.7546
0.8	-32.4003	208.7146	-204.149	206.0504	57.9639	209.4371	-85.3285	193.9288
0.84	-58.9048	208.9359	-177.633	243	81.88329	234.5023	-51.9563	225.6287
0.88	-84.5858	209.073	-151.901	267.7308	79.07813	246.9123	-45.1631	241.6261
0.92	-111.307	208.2912	-128.93	281.1207	68.44472	265.8559	-45.7251	263.2677
0.96	-142.53	204.7315	-114.808	285.724	51.70964	289.7484	-52.5984	288.906
1	-165.976	200.407	-115.663	284.504	32.2506	300.933	-66.8541	300.399

7.2.6 WRS Results Comparisons Between 28- and 12-inch Recirculation Lines

Comparison of the axial WRS fields plotted through the thickness in the weld and HAZ for the 12- and 28-inch lines are illustrated in Figure 66. It is seen that the trends between the two size lines are similar, but the magnitudes differ. Also, note that the 12-inch baseline hoop WRS fields (lower left in Figure 66) are higher near the ID compared with the 28-inch baseline case. This is consistent with prior experience in that higher stresses result in thinner pipe because the bead shrinkage induces a ring load that increases tension stresses near the ID for the latter passes due to bending although this does not affect hoop stresses. This effect is more pronounced in even thinner pipe. This ring load does not have a large effect for the thicker the pipes are since the latter pass shrinkage is far from the ID because the induced bending has less of an effect in thick pipe.

Figure 67 compares the WRS baseline results between the 12- and 28-inch lines after application of the MSIP at operation. The MSIP is effective for both thickness lines. Finally, the WRS fields after the repair are compared between the two size lines in Figure 68 at operation. The WRS in the 12-inch line is a little higher near the ID compared to the 28-inch line.

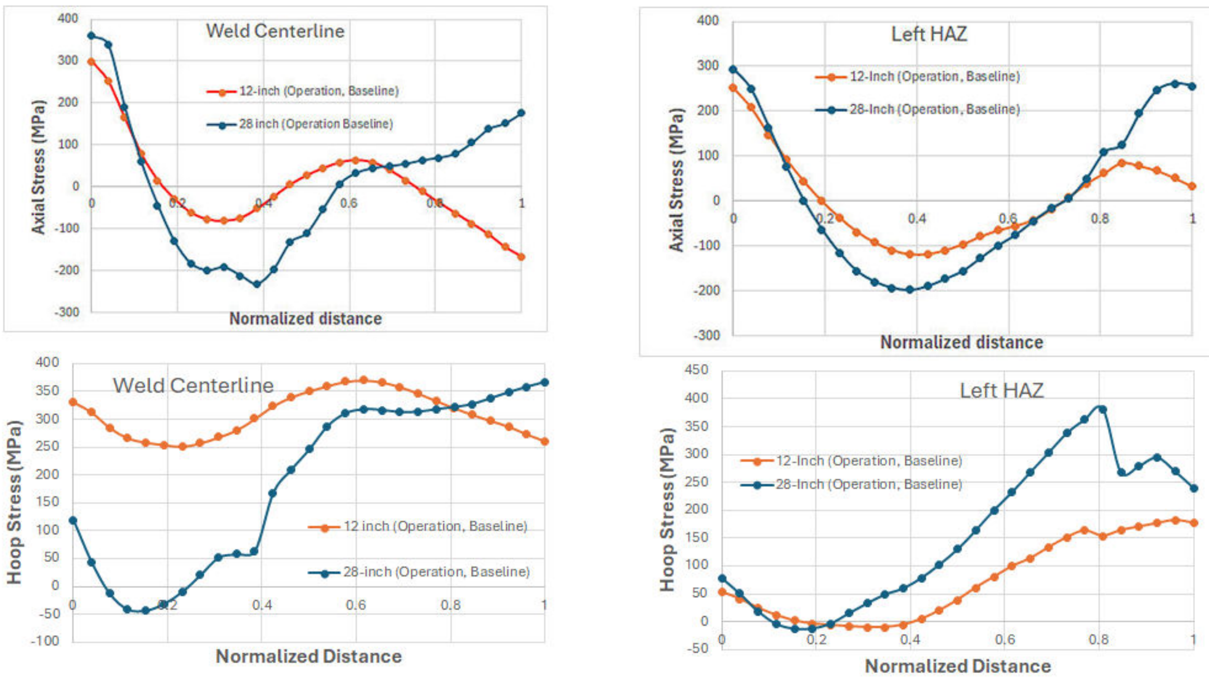

Figure 66: Comparison of baseline WRS fields at operation for 12- and 28-inch lines.

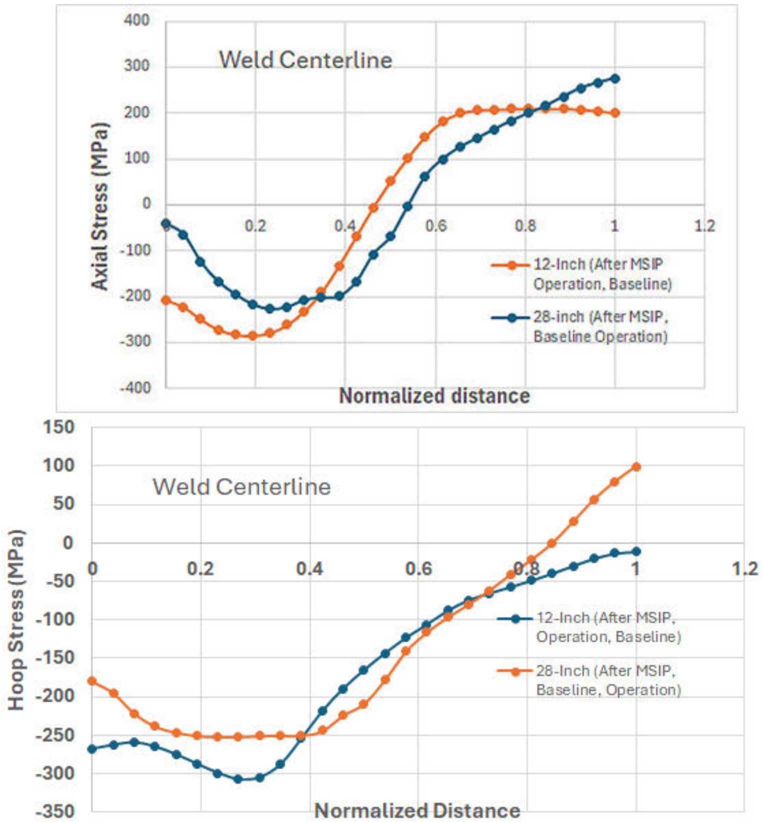

Figure 67: WRS fields at operation for 12- and 28-inch lines after MSIP application.

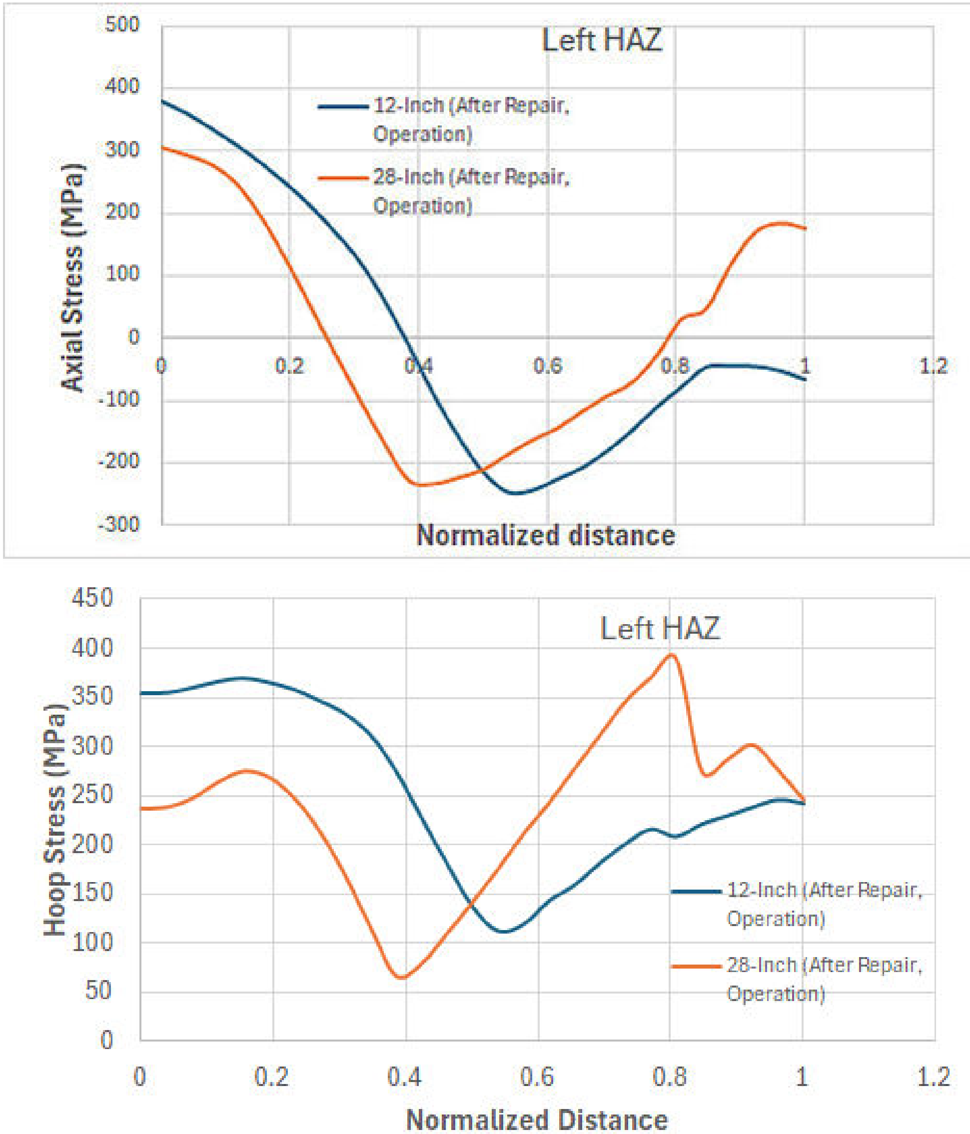

Figure 68: Comparison of WRS fields at operation for 12- and 28-inch lines after repair.

7.2.7 Summary

IGSCC became a problem in BWRs in the 1980s. At that time, the NRC and EPRI performed a number of studies to determine the WRS fields in stainless steel BWR piping. This older work included residual stress measurement work and WRS model development work. The WRS fields that were developed in the 1980s were rather crude models that represented the state of the art at the time. In addition, the WRS measurements performed at the time were developed using older cutting methods. This prior work is summarized in the ERPI report (EPRI NP-1743) and the many references cited therein [34]. Methods to reduce tensile WRS fields in the HAZ of welds, where IGSCC was occurring, were developed and implemented as mitigation measures for BWRs partially based on this work (MSIP, HSW, IHSI, and backlay welding).

Modern methods were used here to develop the WRS fields for the LOCA assessments performed in this study. The WRS analysis methods are detailed in [27] which is the technical basis document for the WRS fields that reside in the xLPR library of solutions. These procedures consist of performing analyses using isotropic and kinematic hardening and then using the average of these results. While Reference [27] shows that using this average of isotropic and kinematic hardening produces results closer to measurements, only isotropic hardening is used for a conservative estimate of faster crack growth of IGSCC.

Results are compiled at operation stresses for both a 12-inch and 28-inch BWR recirculation line for a baseline cases, after repair, and after MSIP application. These are placed within the xLPR code to permit probabilistic risk assessment of IGSCC to estimate the frequencies associated with a LOCA event. These WRS fields are considered upper bound since they were developed using isotropic hardening. Risk assessment using these WRS fields for both size lines are presented in the main body of the report.

7.3 OpE Example Calculation

The OpE analyses in Section 3 were implemented using Microsoft® Excel with two add-in programs: one for the Bayesian reliability analysis (RDAT-Plus by Precision Technologies Inc.) and one for Monte Carlo uncertainty propagation (Oracle Crystal Ball). The implementation of the Bayesian methodology is illustrated in Figure 69, which is adapted from Reference [13]. Table 47 is a summary of the application of the calculation format to Base Case PWR-1.

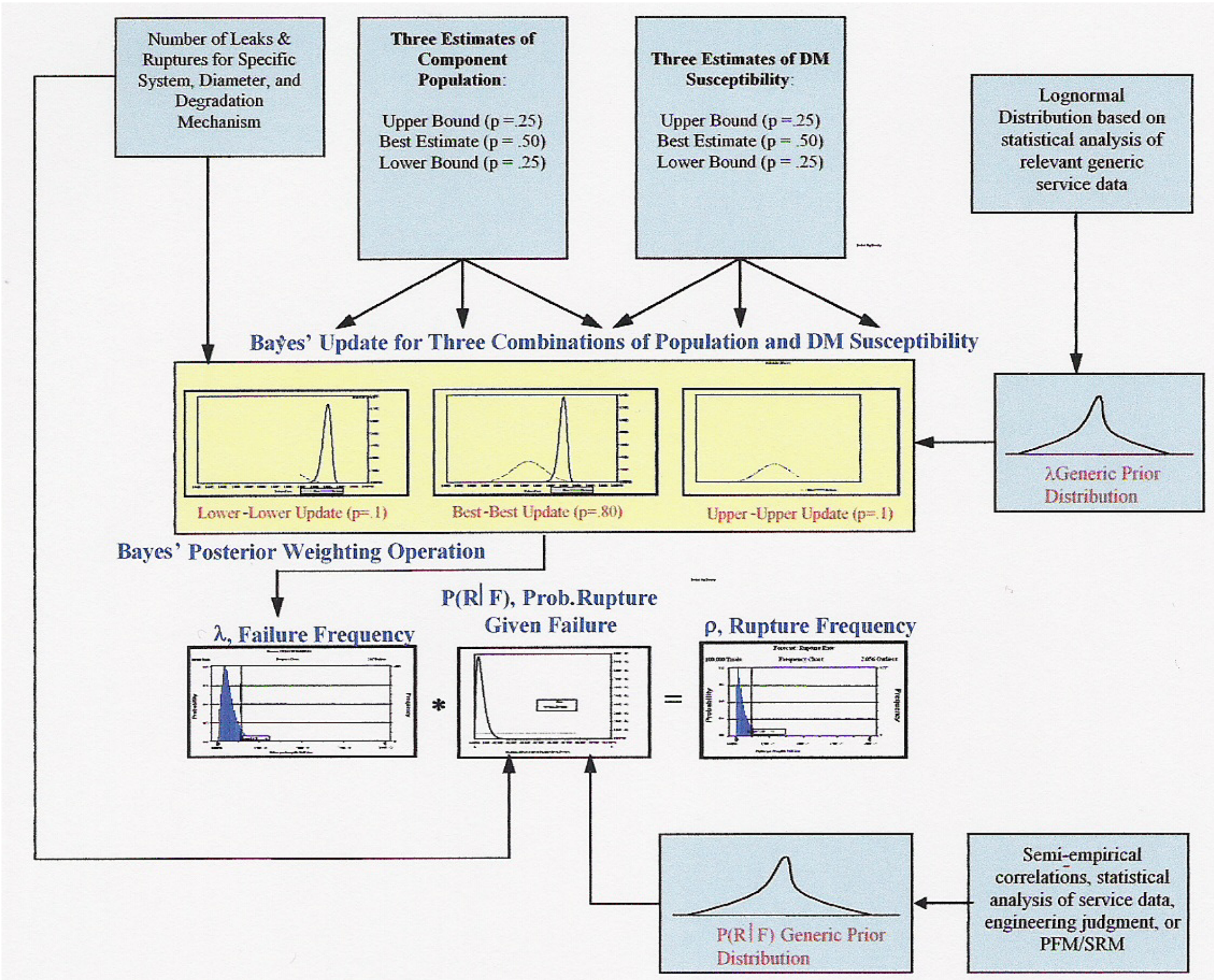

Figure 69: Flow Chart for the Bayesian Estimation Process.

The approach taken to address the uncertainty in the piping component population is to apply a Bayes' posterior weighting procedure. A set of three estimates is obtained for the susceptible component population exposure, one for the best estimate, one for an upper bound estimate and one for a lower bound estimate. For each of these three estimates the number of pipe failures and the exposure population estimate is used to perform a Bayes' update of a generic prior distribution. Then a posterior weighting procedure is applied to synthesize the results of these three Bayes' updates into a single composite uncertainty distribution for the precursor rate. An Excel spreadsheet format with the Monte Carlo simulation add-in program is used to implement the posterior weighting procedure. The precursor estimation involves the following steps:

- For each calculation case, identify the applicable prior precursor rate distribution to be applied together with the event population to be input to the Bayesian update.
- Develop the exposure term that produced the OpE event population.

- Standalone software for Bayesian reliability analysis was used to calculate precursor rates for each unique combination of pipe size, material degradation mechanism and exposure term (low-medium-high).
- In ‘R-DAT Plus’, define a project with “subsystems.” Each subsystem representing a Calculation Case serves to facilitate the precursor rate and CFP calculations. One set of precursor rate parameters per exposure term assumption (low-medium-high). A CFP posterior distribution is calculated for each of a predefined set of pipe failure consequence categories, in terms of equivalent break size (EBS).
- Export the Bayesian analysis results to an Excel workbook to facilitate the posterior weighting procedure component-specific “rupture mode” frequency calculations.
- Post-processing of results. The calculation procedure provides results in the form of pipe precursor rates by pipe size, component type and degradation mechanism. The pipe rupture frequencies are calculated in terms of rupture frequencies versus different equivalent break sizes.
- Open Excel and create linked tabs to form a workbook: 1) R-DAT-FR, 2) FR Calcs., and 3) CFP. On the 'R-DAT-FR' sheet, import the 'R-DAT' output-file. The calculation procedure addresses the uncertainties in the failure population data as well as in the exposure term data. The Oracle Crystal Ball add-in software facilitates the posterior weighting process and through Monte Carlo simulation generates a single composite distribution for the pipe precursor rate. A Monte Carlo “merge” technique is used to develop a distribution that has a mean value equal to a weighted average of the three (low - medium - high), while maintaining the full range of values representing the three input distributions.

Table 47: Application of Calculation Format to Base Case PWR-1 (RVON).

Precursor Analysis of Reactor Vessel Outlet Nozzle Dissimilar Metal Weld (RCS Hot Leg)		
1.1	Determine component and weld types	Dissimilar metal (ASME XI Category B-F) weld
1.2	Perform data query domestic OpE for failure counts, n_{fail}	1 through-wall (TW) weld flaw (V.C. Summer)
1.3	Estimate component exposure, *T,* in terms of reactor operating years. Develop uncertainty distributions to account for plant-to-plant weld population variability. Using engineering judgment, assign a 50% probability that the best estimate of weld population is the correct value, 25% probability that the lower estimate is correct, and 25% that the upper estimate is correct.	One B-F-RVON weld per loop. The exposure term corresponds to the number of reactor operating years for 2-loop, 3-loop and 4-loop Westinghouse plants, Section 3.1.3. Note that the OpE does not apply to Babcock & Wilcox or Combustion Engineering PWR plants. There is no plant-to-plant variability for this calculation case.
1.4	Develop component informed precursor rate (λ) prior distributions for each degradation mechanism (DM), 1970 to 2004 OpE analysis. Characterize the uncertainty using a constrained noninformative prior (CNID) prior distribution.	1 through-wall (TW) weld flaw (V.C. Summer) in 7163 weld-years
1.5	Perform Bayes' update for each exposure case (combination of weld count case and DM susceptibility (DMS) case) to account for the 2005 to 2024 OpE	0 TW weld flaws in 3371 weld years. Perform Bayesian update using the 1970-2004 OpE as the prior state of knowledge
1.6	Develop mixture distribution to combine results for different exposure hypotheses to yield conditional precursor rate distributions given plant-specific DM analysis results from RI-ISI program	An underlying assumption for the prior precursor rate is that all plants were equally susceptible to primary water stress corrosion cracking. Therefore, a mixture distribution was not developed.
1.7	Calculate total precursor rate over all applicable degradation mechanisms	Not needed for Base Case PWR-1
RVON Conditional Failure Probability (CFP) Analysis		

2.1	Select component evaluation boundaries to define conditional rupture probability (CRP) model categories. Differentiate ASME XI Category B-F from Category B-J welds	NUREG-1829, Volume 1, Section 3.5.1.1, “Piping Base Case Definition”
2.2	Obtain NUREG-1829 Expert Elicitation LOCA distributions from the “PWR Piping Raw Data” files, NRC ADAMS Accession No. ML080560011.	Review Panelists’ response to “Reactor Coolant Piping Hot Leg”. Nine-of-twelve provided “plant-level” LOCA frequencies @ 25 years.
2.3	Determine geometric mean of expert distributions from Step 2.2 (lognormal). Obtain a single lognormal distribution for each system case and LOCA category by taking the geometric mean of the medians of the experts’ lognormal distributions as the composite distribution median, and the geometric means of the range factors of the experts’ lognormal distributions as the composite distribution range factor.	Results are given in Section 3.1.3, Table 19
2.4	Determine precursor rate distribution for the Base Case Analysis in NUREG-1829, fit to lognormal distribution	The precursor rate as defined in NUREG-1829, Volume 2, Appendix D is used.
2.5	Apply formulas to calculate CFP distributions to be used as prior distributions for each valid combination of CFP category and component	Results are given in Section 3.1.3, Table 22.